C 55.13: ERL 401 - APCL 43

NOAA Technical Report ERL 401-APCL 43

PENNSYLVANIA STATE UNIVERSITY
MAY 25 1979
DOCUMENTS COLLECTION

Meteorological Analysis of the Johnstown, Pennsylvania, Flash Flood, 19-20 July 1977

L. Ray Hoxit, Robert A. Maddox, Charles F. Chappell, Fred L. Zuckerberg, H. Michael Mogil, Ike Jones, Douglas R. Greene, Robert E. Saffle, and Roderick A. Scofield

October 1978

U. S. DEPARTMENT OF COMMERCE
National Oceanic and Atmospheric Administration
Environmental Research Laboratories

NOAA Technical Report ERL 401-APCL 43

Meteorological Analysis of the Johnstown, Pennsylvania, Flash Flood, 19-20 July 1977

L. Ray Hoxit, Robert A. Maddox, Charles F. Chappell, Fred L. Zuckerberg, H. Michael Mogil, and Ike Jones

With appendices by Douglas R. Greene and Robert E. Saffle, and Roderick A. Scofield

Atmospheric Physics and Chemistry Laboratory
Boulder, Colorado

October 1978

U. S. DEPARTMENT OF COMMERCE
Juanita Kreps, Secretary

National Oceanic and Atmospheric Administration
Richard A. Frank, Administrator

Environmental Research Laboratories
Wilmot Hess, Director

For sale by the Superintendent of Documents, U.S. Government Printing Office, Washington, D.C. 20402
Stock Number 003-017-00445-17

1

3

CONTENTS

	Page
Abstract	1
1. Introduction	1
2. Large-Scale Meteorological Conditions	3
3. Mesoscale Analysis	14
4. Distribution of Rainfall	31
5. Discussion and Summary	44
6. References	45
Appendix A. Upper-Air Analyses and Comparable GOES-1 Visible Imagery	47
Appendix B. D/RADEX Rainfall Estimates	61
Appendix C. Using Satellite Imagery to Estimate Convective Rainfall	65

Examples of the damage in and near Johnstown, Pa., following the intense rainfall of July 19–20, 1977. (Photographs courtesy of the U. S. Geological Survey, Harrisburg, Pa.)

1. Geistown, Pa.
2. Laurel Run Dam.
3. Below Laurel Run Dam.

Digitized by the Internet Archive
in 2013

http://archive.org/details/meteorologicalan00atmo

METEOROLOGICAL ANALYSIS OF THE JOHNSTOWN, PENNSYLVANIA, FLASH FLOOD OF 19–20 JULY 1977

L. Ray Hoxit, Robert A. Maddox, Charles F. Chappell, Fred L. Zuckerberg,[1] H. Michael Mogil,[2] and Ike Jones[3]

ABSTRACT. Synoptic and mesoscale analyses of the meteorological conditions that produced disastrous flash flooding in the Johnstown, Pa., region on July 19–20, 1977, are presented. Detailed rainfall analyses based on surface rain gauges, National Weather Service (NWS) radar, and satellite rainfall estimation techniques are also shown. Dynamic processes associated with a weak short-wave trough triggered and maintained widespread thunderstorm activity over Pennsylvania and New York during the afternoon and evening of July 19. Two major squall lines moved across Pennsylvania. The western extension of the outflow boundary produced by the second squall line became quasi-stationary in western Pennsylvania, and appeared to be the primary feature that focused the heavy rainfall over a relatively small region. Warm, moist air was lifted over the rain-cooled air lying north and east of the boundary, triggering new storms in the same general region. The storms repeatedly moved southeastward over the Conemaugh River Basin, producing 8- to 9-h rainfalls of up to 12 in.

1. INTRODUCTION

During the evening and early morning of July 19–20, 1977, a series of thunderstorms moved over the mountainous areas of southwest Pennsylvania. Parts of Indiana and Cambria Counties received 8- to 12-in of rain over a 8- to 9-h period. Major flash flooding occurred, especially along the Conemaugh River and its tributaries. Seventy-seven casualties and more than $200 million in property damage have been attributed to the storm (NOAA, 1977). At the time of this publication several persons are still missing although the disaster occurred more than a year ago. Seven earthen and rock-fill dams failed completely and another four were partially destroyed during the early morning hours of July 20. Of these, the Laurel Run and Sandy Run dams were the largest. These failures compounded the stream flooding and accounted for approximately 44 of the 77 total casualties.

The storms and flash floods centered on a region already famous for its floods; indeed the name "Johnstown" has become synonymous with major flood disasters. Table 1 provides a brief summary of the major floods affecting the Johnstown area since 1889.

Table 1. Major Floods in Johnstown, Pa.

Date	Description	Casualties	Est. Damage
May 31, 1889	Heavy rains, dam break	2,209	$ 12,000,000*
Mar. 17, 1936 (St. Patrick's Day)	Heavy rains, melting snow	25	$ 80,000,000*
July 19–20, 1977	Heavy, localized thunderstorms during an 8- to 9-h period, 11 dam breaks	77	$200,000,000

*Not adjusted for the present value of the dollar.

[1]National Weather Service, NOAA, Eastern Region Headquarters, Garden City, New York
[2]National Weather Service Headquarters, NOAA, Disaster Preparedness Staff, Silver Spring, Maryland
[3]National Weather Service, NOAA, Weather Service Forecast Office, Pittsburgh, Pennsylvania

Figure 1. Locations and geographical features surrounding Johnstown, Pa., flood area.

More than 2,200 lives were lost in the 1889 flood. This tragic event ranks third after the Galveston, Tex., hurricane, and the San Francisco, Calif., earthquake in the number of casualties resulting from natural disasters in the United States.

This report focuses on the large-scale and mesoscale meteorological processes that contributed to the localized and intense rainfall. Mesoanalyses were performed using techniques mainly developed in severe storm research and forecasting. Many of the techniques are currently used at the National Severe Storms Forecast Center in Kansas City, Mo., and the Air Force Global Weather Center in Omaha, Neb. All available data are utilized, including those from satellite and radar. Special attention is given to the sequence of events recorded in hourly and special surface observations. A complete and thorough text on mesoanalysis is not available. However, examples of mesoanalyses and techniques can be found in many articles on severe local storms (e.g., Fujita et al., 1956, and Magor, 1959). Figure 1 shows the region surrounding the flood area and identifies many of the cities and geographical features referred to in the discussion.

2. LARGE-SCALE METEOROLOGICAL CONDITIONS

The evolution of larger-scale processes, before and during the intense rainfalls over southwest Pennsylvania, is shown in the map series beginning at 1200 GMT July 19 and extending through 1200 GMT July 20. These standard meteorological analyses provide a general setting and background for the detailed mesoscale analyses presented in Section 3.

Surface and 500 mb map analyses are presented in Figs. 2 and 3, respectively, and show the major pressure systems and their changes through the 24-h period. (A complete set of upper-air analyses including the 850, 700, 500, and 300 mb analyses is included in Appendix A.)

Most of the eastern United States was under general anticyclonic flow around a

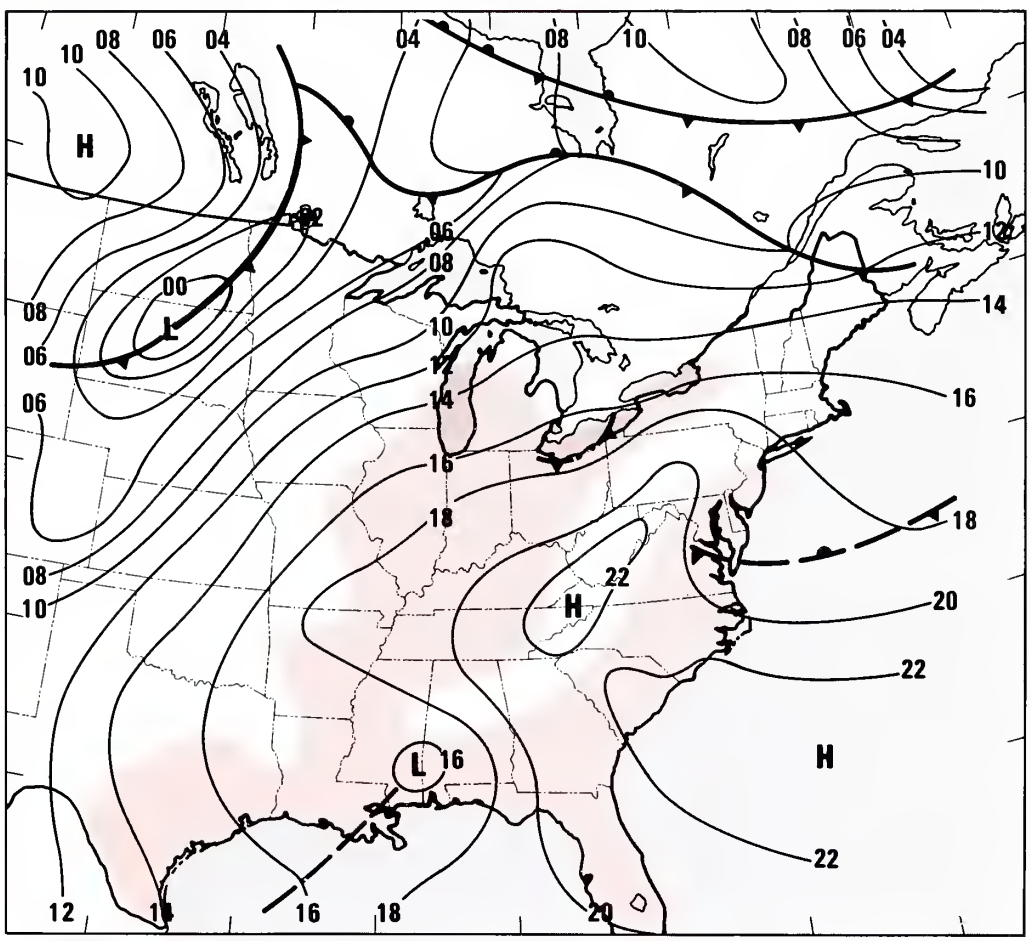

Figure 2a. Surface analysis for 1200 GMT, July 19, 1977. Frontal positions, outflow boundaries, pressure centers, and isobars for 2 mb intervals (16 = 1016 mb) are shown in black. Frontal symbols are added to conventional squall line notation to indicate whether cool thunderstorm outflow or warmer environmental air is advancing. Region with dew points ≥ 70°F is shaded orange.

large subtropical high located in the western Atlantic—a fairly typical midsummer pattern. The major storm track was across central Canada, and associated frontal systems lay across east-central Canada southwestward into the northern high plains of the United States. Early on July 19, a weak surface trough, associated with an upper-level low pressure area, extended northeastward through Louisiana and Mississippi. This low pressure area moved slowly northwestward to the Arkansas region by 1200 GMT on July 20. A small, separate, high pressure area persisted during this period along the western slopes of the Appalachian Mountains in West Virginia and eastern Kentucky. Dew point temperatures of 70°F or greater extended northward into the Great Lakes region and into a small portion of southeastern Canada, and low-level moisture flux into the Pennsylvania region was from the southwest.

Major thunderstorm outflow boundaries were generated in the Lake Erie region and moved southeastward across the mid-Atlantic states. A mesoscale high pressure system ("bubble high") was evident at both 0000 GMT and 1200 GMT on July 20. This mesoscale high pressure system and associated outflow boundary are discussed in more detail in Section 3.

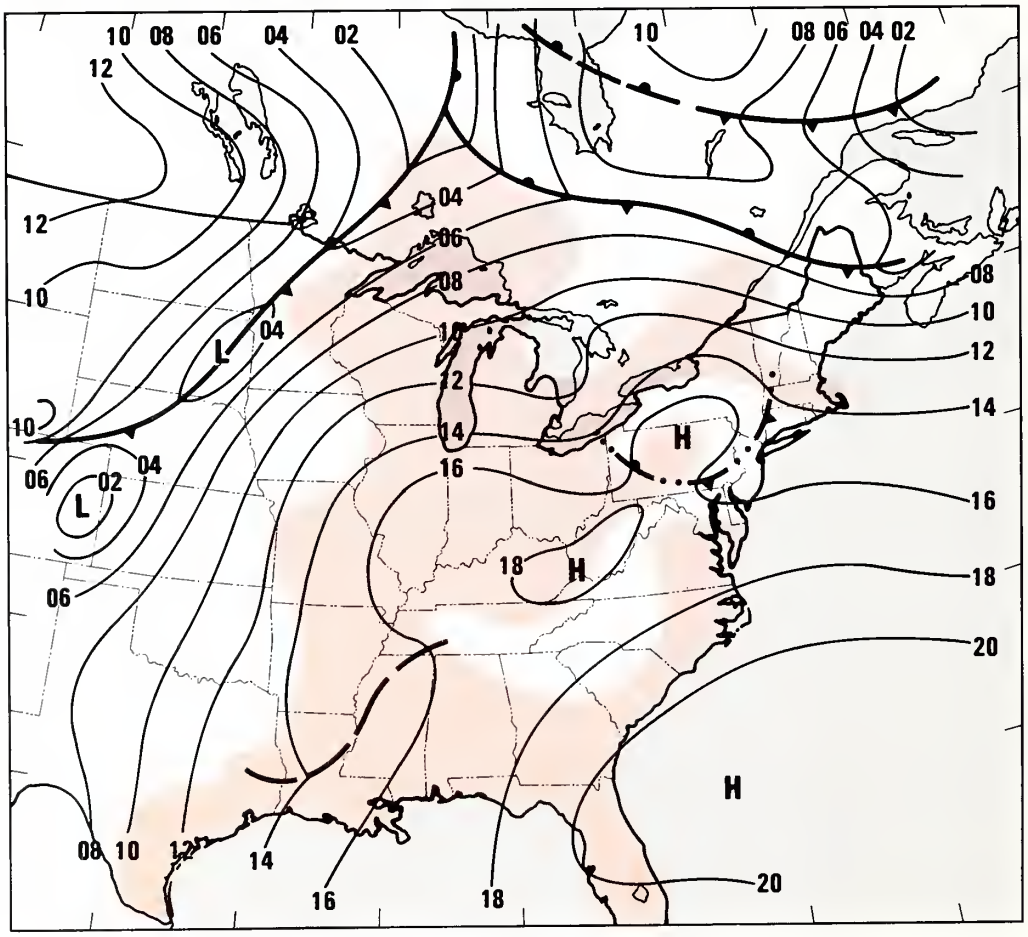

Figure 2b. Surface analysis for 0000 GMT, July 20, 1977.

The flow pattern in the middle troposphere (500 mb) was again fairly typical for mid-summer (Figs. 3a–3c). At 1200 GMT on July 19, a broad, large-scale ridge existed over the central and eastern United States. A weak, closed, low pressure area over the southern Mississippi Valley and a short-wave trough (meso-α scale) over the eastern Great Lakes region constituted smaller perturbations in this mean pattern. A moderately strong westerly current extended across southern Canada.

The short-wave trough over the Lake Huron and Lake Erie region at 1200 GMT on July 19 played a key role in the development of the flash flood. The trough moved east-southeast at 15 to 20 kt across Pennsylvania and southern New York during the next 24 hours, and a small 500 mb closed circulation developed over eastern Pennsylvania by the end of the period. The trough axis remained positively tilted (from northeast to southwest) throughout this period. Strong, warm advection in the lower troposphere was indicated to the west and northwest of the short-wave trough (see the 850 mb analysis in Appendix A). As warmer air moved under the relatively cool air aloft, the atmosphere became more unstable. This flow regime was somewhat uncharacteristic, since low-level

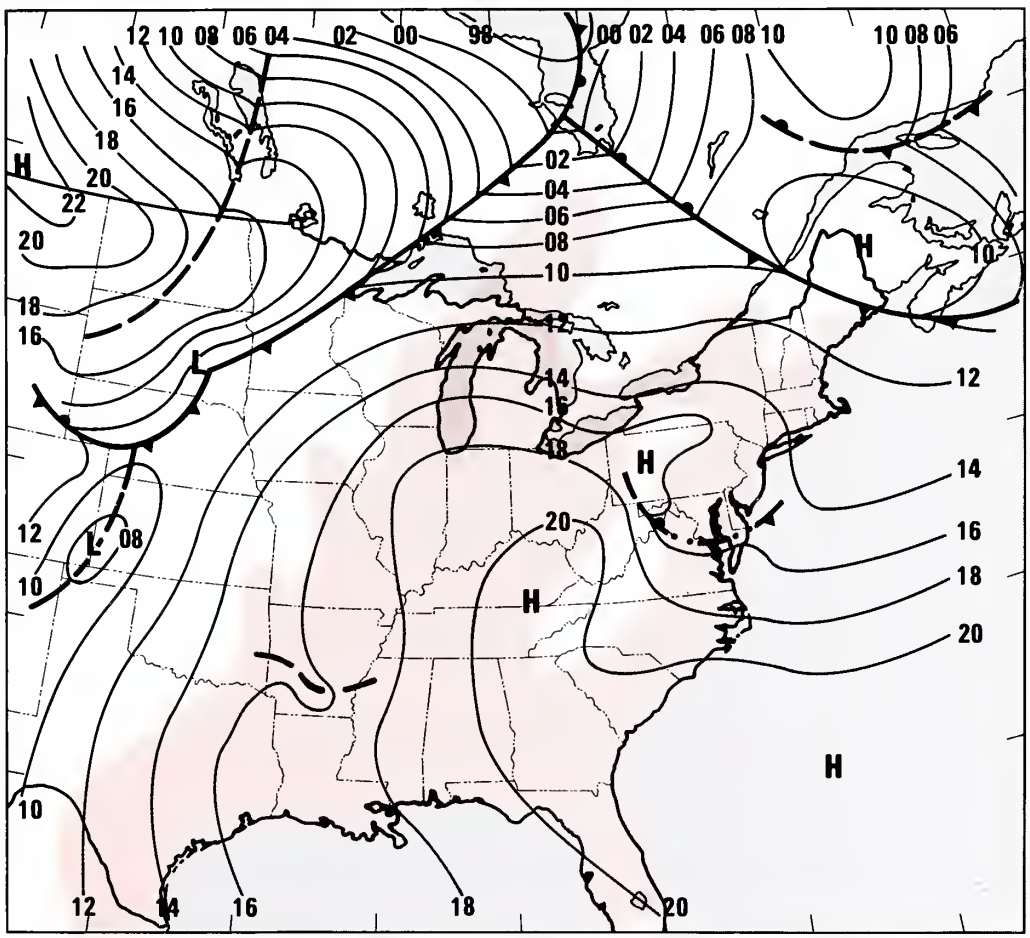

Figure 2c. Surface analysis for 1200 GMT, July 20, 1977.

warm advection typically occurs in advance (east) of short-wave troughs embedded in westerly flow. At the same time, the upward vertical motion in advance of the trough axis acted to further destabilize the atmosphere and trigger widespread convection during the afternoon and evening of July 19.

Analyses of stability indices computed from standard rawinsonde data (Fig. 4) show the development of a very unstable air mass ahead of the advancing short-wave trough. By 0000 GMT on July 20, the air mass over western Pennsylvania was characterized by Lifted Index values of −4 or less and K Index values ≥ 36. These values are comparable with those associated with major, severe thunderstorm outbreaks.

Precipitable water in the surface to 500 mb layer was substantially greater than climatological mean values along and ahead of the upper-level trough axis (Fig. 5). High precipitable water values developed southeastward and increased in areal coverage during July 19. Values greater than 4.4 cm were found over a wide area extending from northeastern Kentucky through much of New York by 0000 GMT on July 20. The 4.6 cm measured at Pittsburgh at 0000 GMT was approximately 172 percent of the July average documented by Lott (1976).

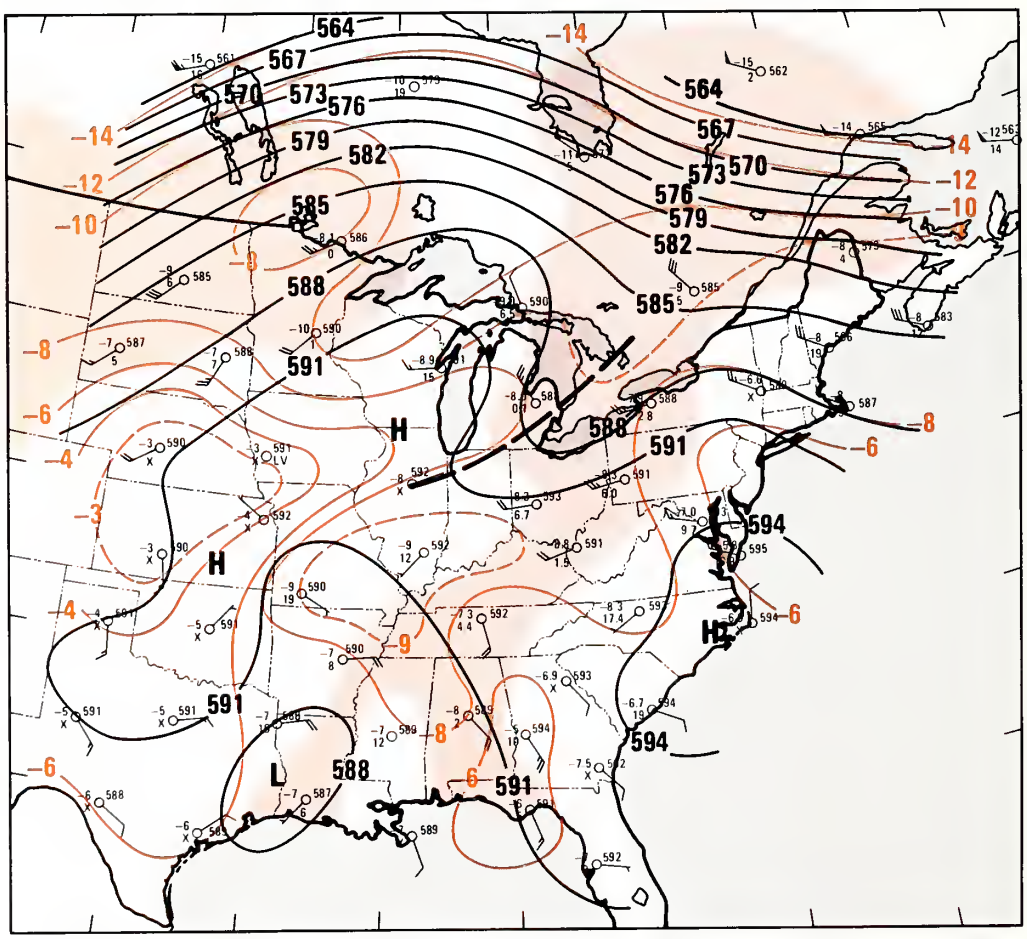

Figure 3a. 500 mb analysis for 1200 GMT, July 19, 1977. Height centers, trough lines, and height contours at 30-m intervals (591 = 5910 m) are shown in black. Isotherms for 2°C intervals are in orange; moist regions with $T-T_d \leq 6$°C are shaded orange.

Data from three upper-air soundings, taken at Pittsburgh during this 24-h period, are shown in Fig. 6. Note that the winds shifted in the 850 to 400 mb layer from west-southwest to northwest and north as the short-wave trough passed. Abundant moisture up to almost 500 mb was also evident in the 0000 GMT sounding (Fig. 6b). The surface inversion evident in the temperature and moisture profiles at 0000 GMT resulted from earlier thunderstorm activity and was topped by strong westerly winds immediately above. Strongest winds are in the 700 to 950 mb layer with weak wind shear present from the top of the inversion to nearly 300 mb.

Profiles of equivalent potential temperature at Pittsburgh (Fig. 7) show further the unstable environment over western Pennsylvania. Equivalent potential temperatures of more than 360 K are characteristic of a tropical boundary layer. The 0000 GMT sounding indicated a value of 362 K at the top of the surface inversion.

A conditionally unstable atmosphere, unusually high moisture content, and the slow moving short-wave trough all contributed to thunderstorm development over a rather large area on the afternoon and evening of July 19, 1977. This area included most of

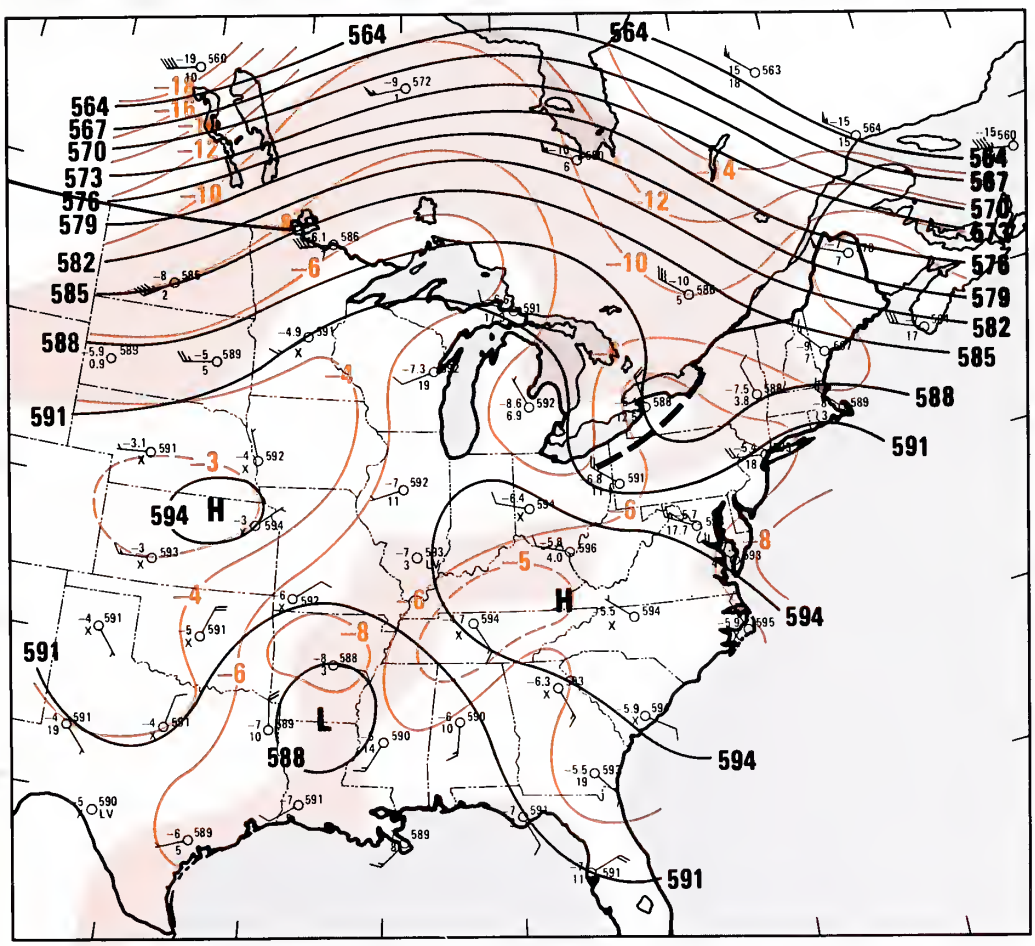

Figure 3b. 500 mb analysis for 0000 GMT, July 20, 1977.

Pennsylvania and portions of several surrounding states. However, the atmospheric structure over this region differed from that usually associated with a major tornado outbreak in the following ways: (a) moisture content was relatively high up to nearly 500 mb, which contrasts with the strong inversion with dry air above often observed between 700 and 850 mb in the pre-tornado environment, and (b) wind shear was small in the convective cloud layer (cloud base to nearly 300 mb). The precipitation efficiency of convective clouds in this environment is higher than for clouds embedded in the highly sheared environment usually associated with tornadoes, strong surface winds, and large hail (Maurwitz, 1972); that is, a greater percentage of the water vapor condensed in the updrafts eventually reaches the ground as precipitation.

Two important questions cannot be answered by the synoptic scale analyses just presented:

> Why did the convective processes focus on such a small area around Johnstown?
>
> What distinguished this region from the surrounding region which apparently had the same general potential for heavy thunderstorms?

The answer to these questions may lie in the evolution of mesoscale weather processes preceding and during the storm event.

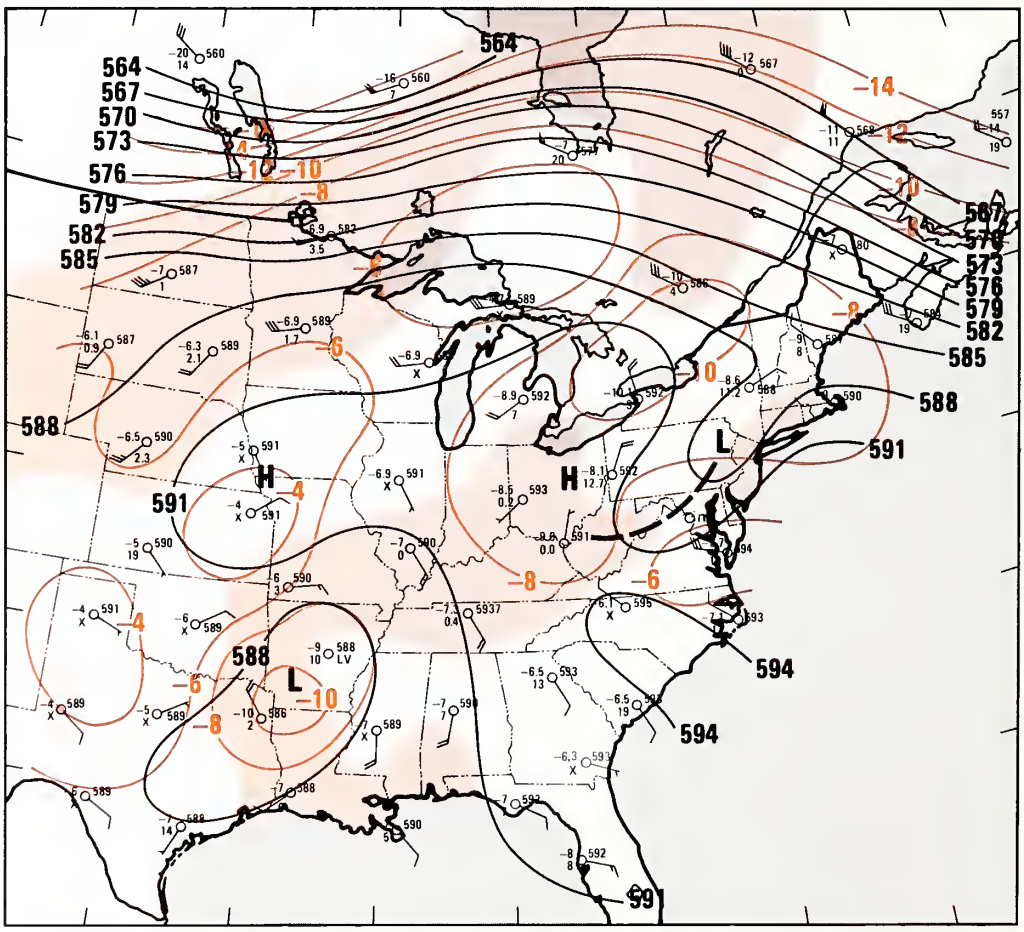

Figure 3c. 500 mb analysis for 1200 GMT, July 20, 1977.

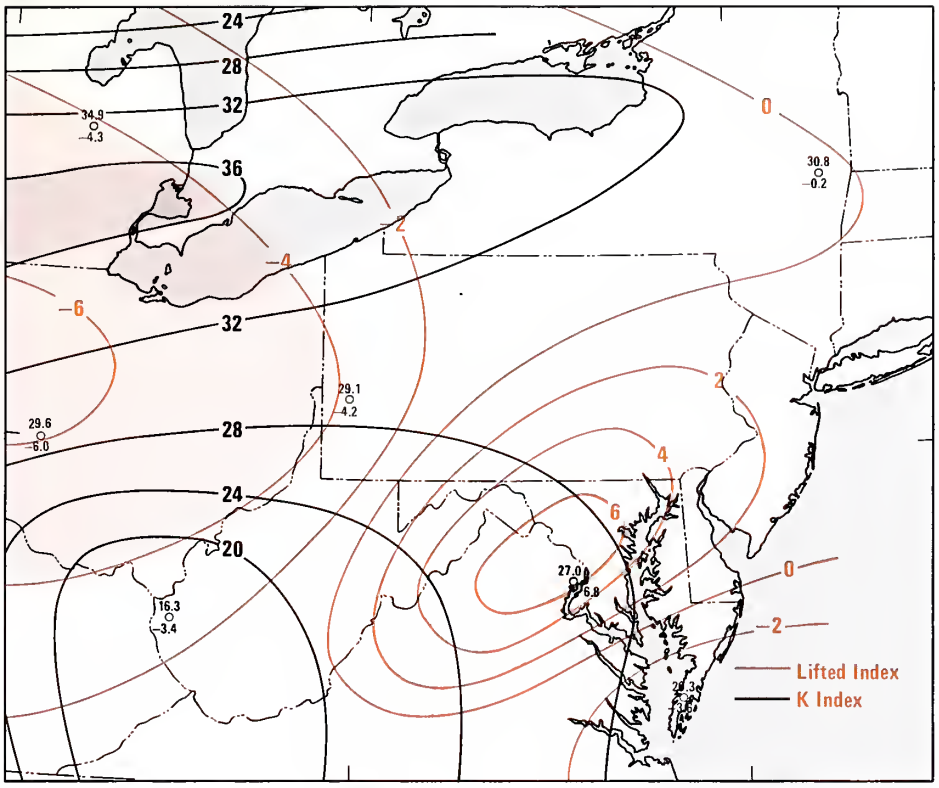

Figure 4a. Stability chart for 1200 GMT, July 19, 1977. Unstable regions with Lifted Index values ≤ −4 are shaded orange. Regions with K Index values ≥ 36 are shaded gray.

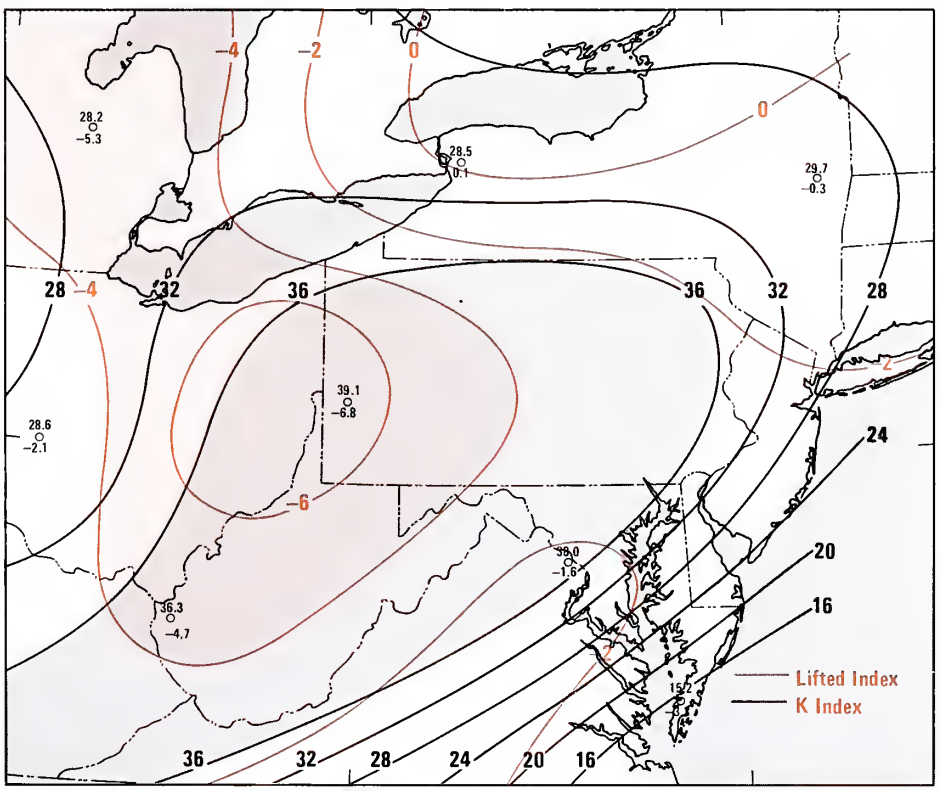

Figure 4b. Stability chart for 0000 GMT, July 20, 1977.

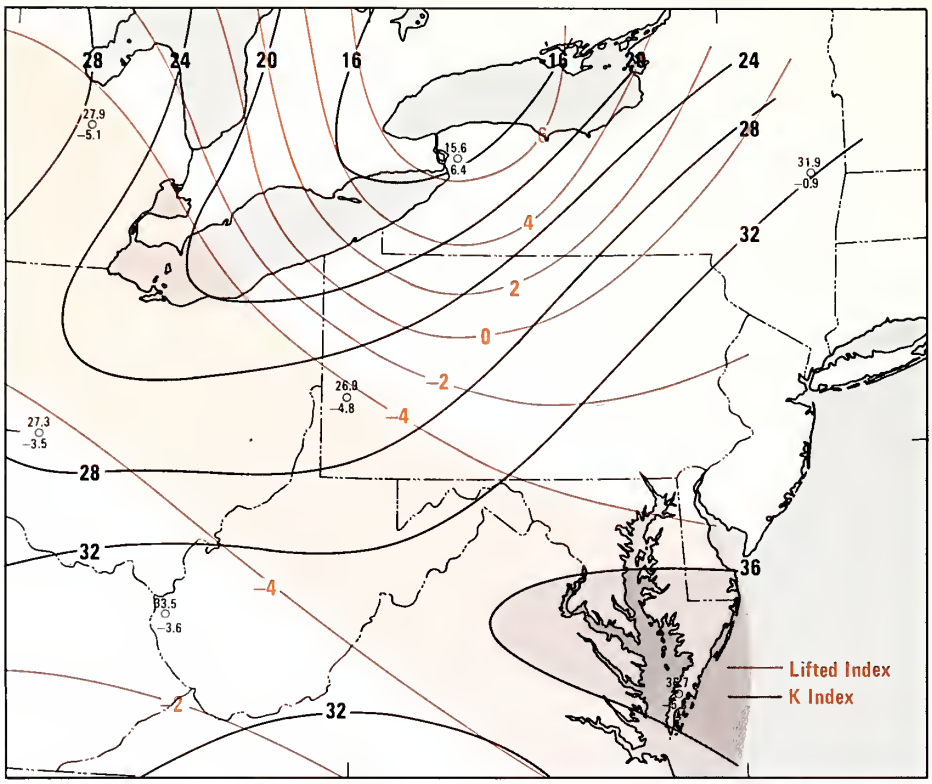

Figure 4c. Stability chart for 1200 GMT, July 20, 1977.

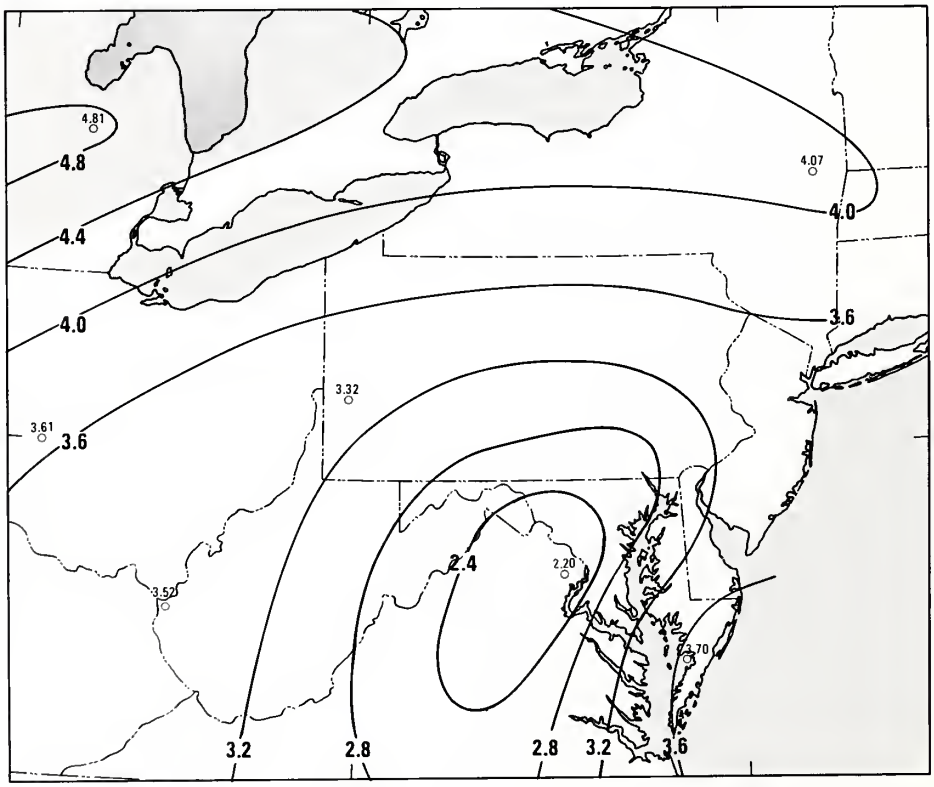

Figure 5a. Precipitable water analysis in cm (surface to 500-mb layer) for 1200 GMT, July 19, 1977. Regions with more than 4.4 cm are shaded gray.

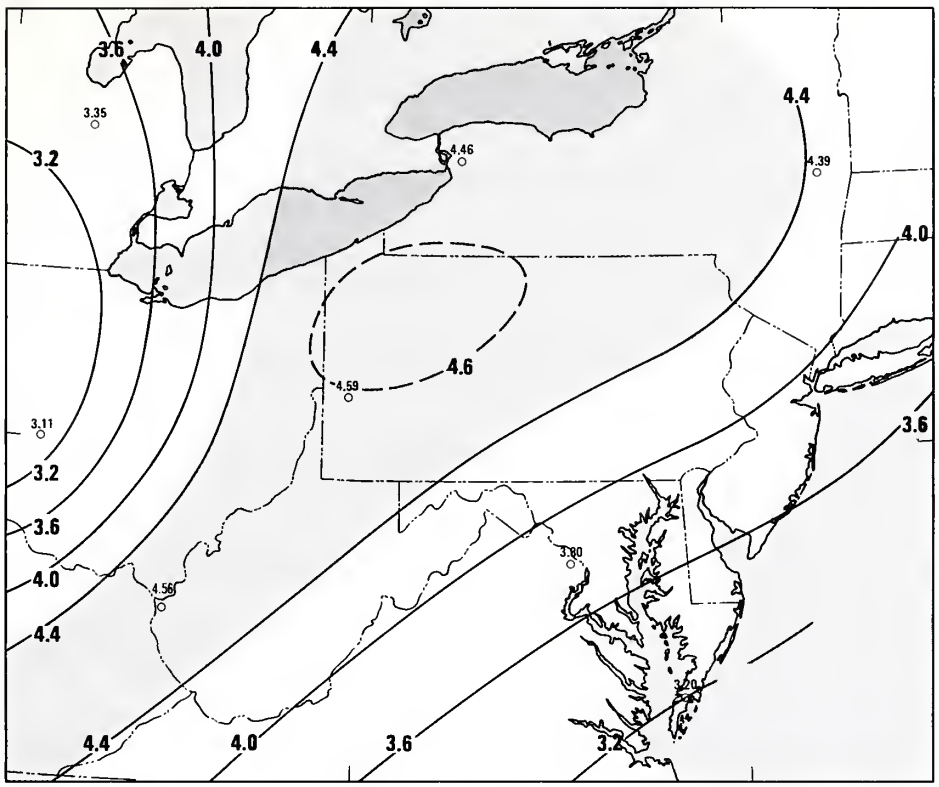

Figure 5b. Precipitable water analysis for 0000 GMT, July 20, 1977.

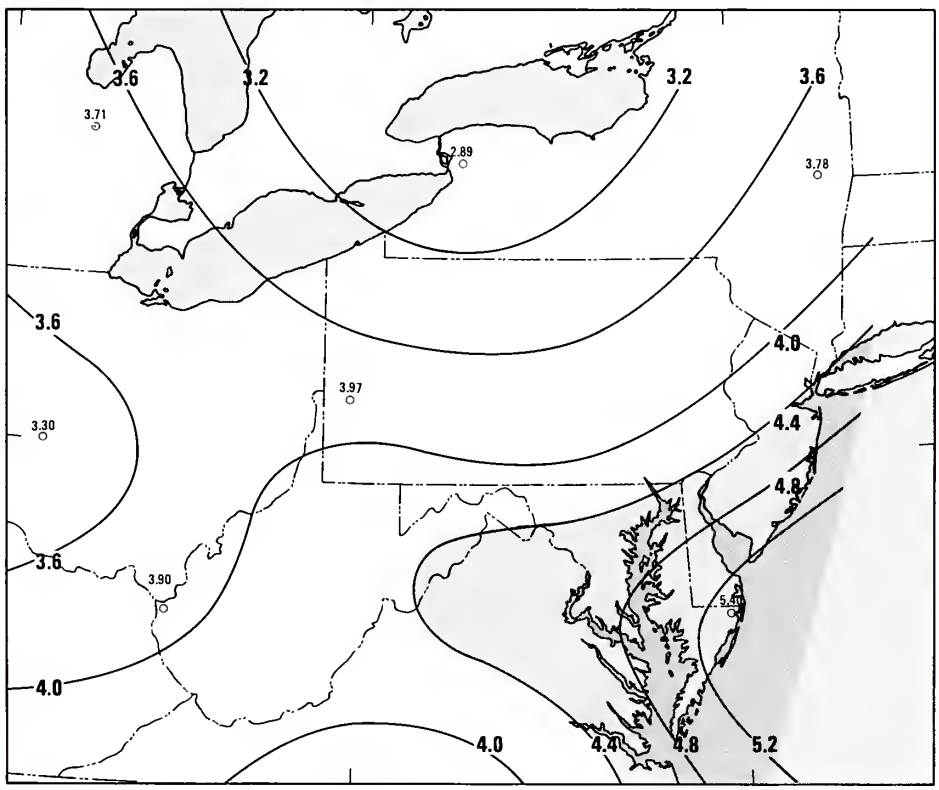

Figure 5c. Precipitable water analysis for 1200 GMT, July 20, 1977.

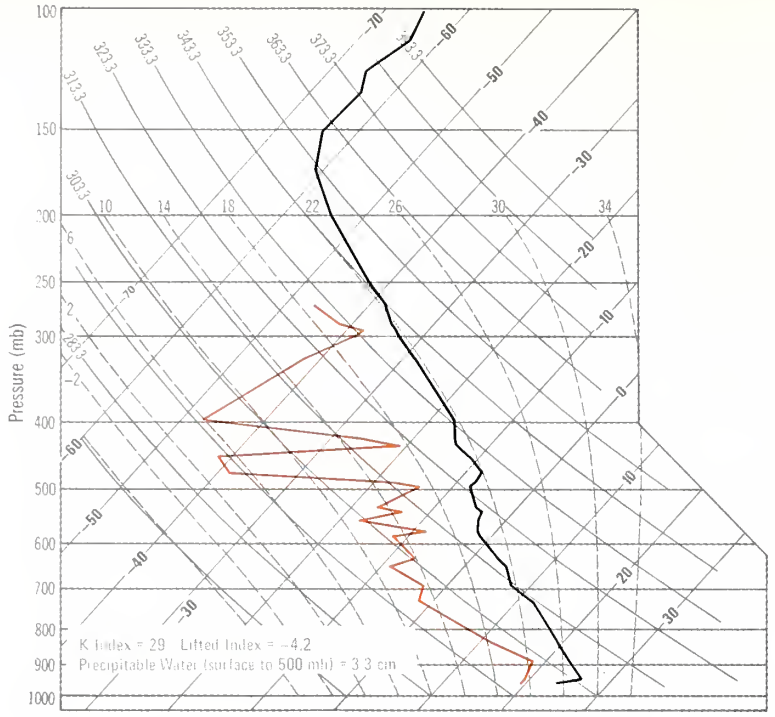

Figure 6a. Skew T/LogP plot of Pittsburgh upper-air sounding for 1200 GMT, July 19, 1977. Temperature profile is shown in black. Wind and dew point temperature profiles are shown in orange.

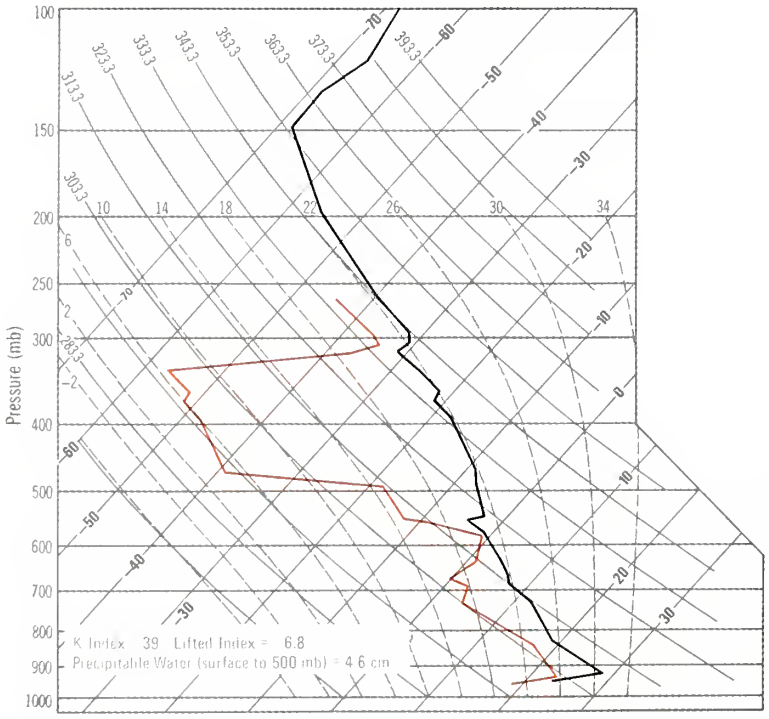

Figure 6b. Pittsburgh upper-air sounding for 0000 GMT, July 20, 1977.

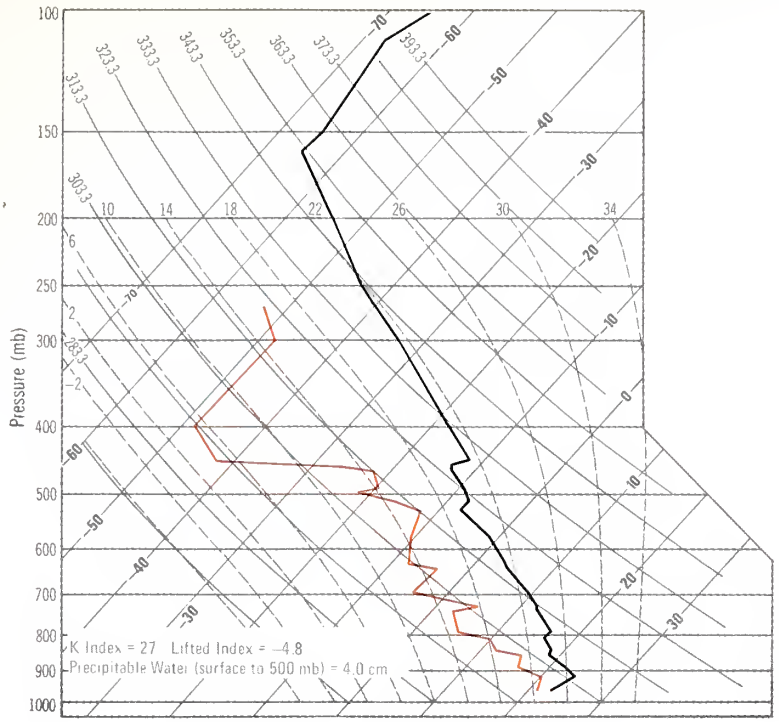

Figure 6c. Pittsburgh upper-air sounding for 1200 GMT, July 20, 1977.

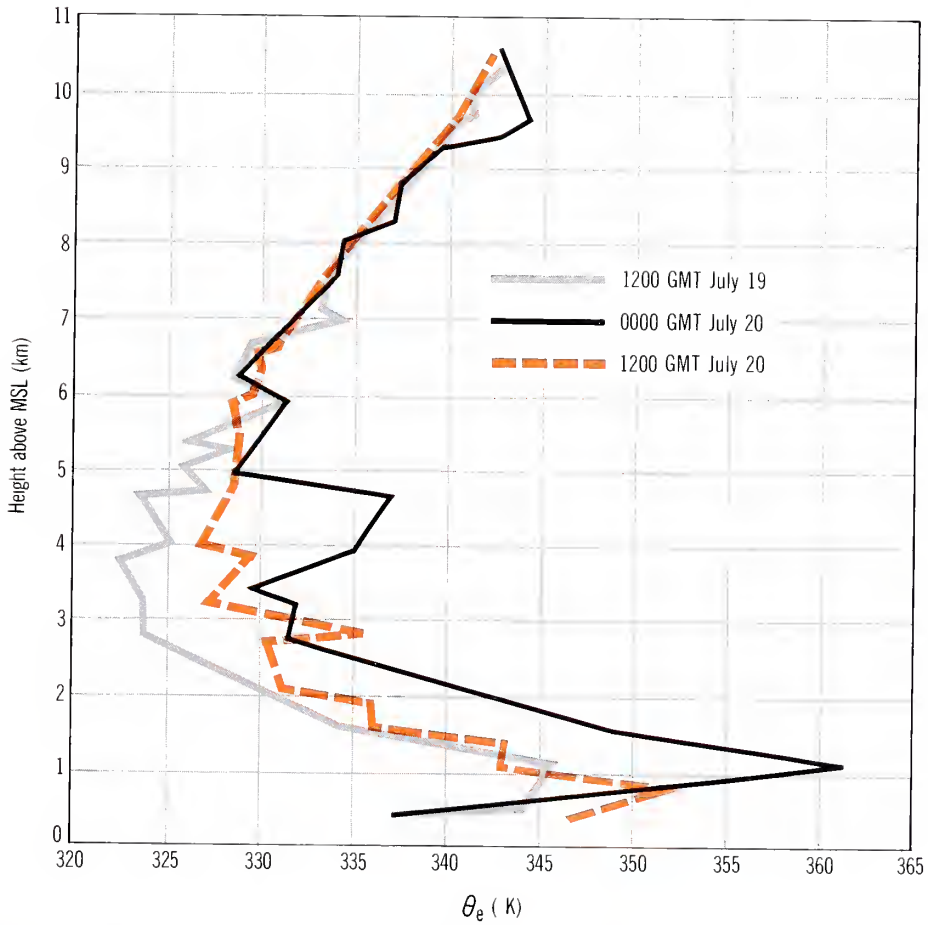

Figure 7. Vertical profiles of equivalent potential temperature from the Pittsburgh upper-air soundings.

3. MESOSCALE ANALYSIS

Hourly surface and radar charts for the period 1800 GMT July 19 to 0900 GMT July 20 are given in Fig. 8. Analyses of the pressure fields (altimeter settings) and the main thunderstorm outflow boundaries were based on surface observations, both hourly and special, radar data, and satellite photographs. Small systematic errors in the altimeter settings were suspected at several stations (e.g., Bradford, Pa., and Binghamton, N.Y.). However, no corrections were made so that analyses would be based as closely as possible on information available under operational conditions.

Radar analyses are composites prepared from radarscope photographs taken at NWS WSR-57 radar sites at Pittsburgh, Pa., Buffalo, N.Y., New York City, N.Y., Atlantic City, N.J., and Patuxent, Md. A small region in central Pennsylvania and southern New York was not covered by any of the 125-nmi range scopes.

Geostationary Operational Environmental Satellite (GOES) imagery for the same general time period is shown in Fig. 9. Routine maintenance procedures were underway during the period 0430 to 0730 GMT July 20, and satellite imagery was not available. Visible imagery is given through 2300 GMT July 19; the remainder of the satellite data are enhanced infrared imagery.

By early afternoon (1800 GMT) convective activity was already organized and widespread over northwestern Pennsylvania and southern New York (Figs. 8a and 9a). Thunderstorm activity which had been located along the southern shore of Lake Erie in the morning (Fig. 2a) had spread east-southeastward and expanded into a squall line, extending from close to Johnstown into south-central New York. In Johnstown, however, only a few hundredths of an inch of precipitation were recorded as this line moved through the area.

The cool outflow attending the first squall line extended in two arcs from near Lake Ontario southwestward to a meso-low pressure center over north-central Pennsylvania, then southwestward to near Johnstown before curving northwestward to near Youngstown, Ohio. An elongated meso- or "bubble" high pressure area was located north of the outflow boundary while an area of light precipitation was developing in extreme northwestern Pennsylvania, southwestern New York, and northeastern Ohio.

During the afternoon the first line of convective storms, and their associated cool outflow boundary, continued to move eastward at about 30 to 40 kt (Fig. 10a). By 2300 GMT, the leading edge of cooler air extended from southwestern Vermont through extreme southeastern New York to the eastern Pennsylvania border. The southwestern portion of the outflow boundary moved back toward the northeast and assumed the characteristics of a shallow, mesoscale warm front.

At about 2000 GMT a thunderstorm developed just west of Pittsburgh. This storm moved east-southeastward at about 50 kt, affected the Pittsburgh region from 2100 to 2200 GMT, and dropped about ½ inch of precipitation on the city of Johnstown between 2200 and 2300 GMT. At 2300 GMT, the small meso-high produced by this storm had reached the area just west of Johnstown and the storm was now dissipating.

Meanwhile, clouds and precipitation over northwestern Pennsylvania had moved slowly southeastward and organized into a second major squall line. Several strong cells were indicated by Pittsburgh radar (Figs. 8c-8f), and the late afternoon satellite imagery indicated several overshooting tops embedded in the line (Figs. 9c-9f). By 2300 GMT this activity had progressed to just north of the Conemaugh River Basin.

The behavior of the second squall line differed from the first in several important ways. It propagated toward the southeast (instead of east) and at a slower speed than the first line. The western section of the outflow boundary was nearly stationary along the Ohio–Pennsylvania border. The quasi-stationary character of this outflow boundary northeast of Pittsburgh continued during the remaining hourly analyses (Figs. 8g–8p).

By 0300 GMT, the first series of intense thunderstorms had moved across the Johnstown region (Fig. 8j). A well defined meso-high attending these storms was located just northwest of Johnstown, while the associated outflow boundary (second of the series) was oriented along the southern Pennsylvania border northwestward to just east of Pittsburgh and Youngstown, Ohio. This boundary, produced by the cool downdrafts from the thunderstorm activity, remained quasi-stationary and nearly perpendicular to the low-level flow of moist air streaming into western Pennsylvania from Ohio. Also a mesoscale "wake" low had formed in east-central Pennsylvania.

The hourly analyses and satellite photos (Figs. 8i–8p and Figs. 9i–9n), along with the summary analyses presented in Fig. 10b, illustrate the quasi-stationary and concentrated nature of the Johnstown flood-producing rainstorms. As the warm, unstable air from the west was lifted over the cool outflow boundary, new thunderstorms were triggered. Once these storms formed, they moved with the mean mid-tropospheric flow southeastward over the Conemaugh River Basin.

Maddox and Chappell (1978) and Mogil and Groper (1976) have found that quasi-stationary thunderstorm outflow boundaries contribute to many flash flood situations. These boundaries, as in the Johnstown instance, focus the thunderstorm development and resulting heavy rains over relatively small regions. The portion of these boundaries most likely to become stationary is that section which is parallel to the mid-tropospheric winds.

The thunderstorm cells moved roughly parallel to the outflow boundary and nearly perpendicular to the western slopes of the Appalachian (Allegheny) Mountains. Orographic lift probably enhanced storm intensities and helped concentrate the heavy rains in the hills north and east of Johnstown. However, orography was probably not as important in triggering these thunderstorms as in the Big Thompson and Rapid City floods (Maddox et al., 1978a).

Radar indicated that 12 separate thunderstorm cells moved over the Johnstown area between 0000 and 0900 GMT, July 20 (Greene and Saffle, 1978). The downdrafts and cool outflow from each successive cell reinforced and helped maintain the thermal and wind discontinuities along the outflow boundary.

As the short-wave trough moved to the east of Johnstown, drier, subsiding mid-tropospheric air moved into the region. Convective activity was suppressed, and the meso-high moved toward the southeast and slowly dissipated. Shortly after 0900 GMT the heavy rain in Johnstown ended abruptly.

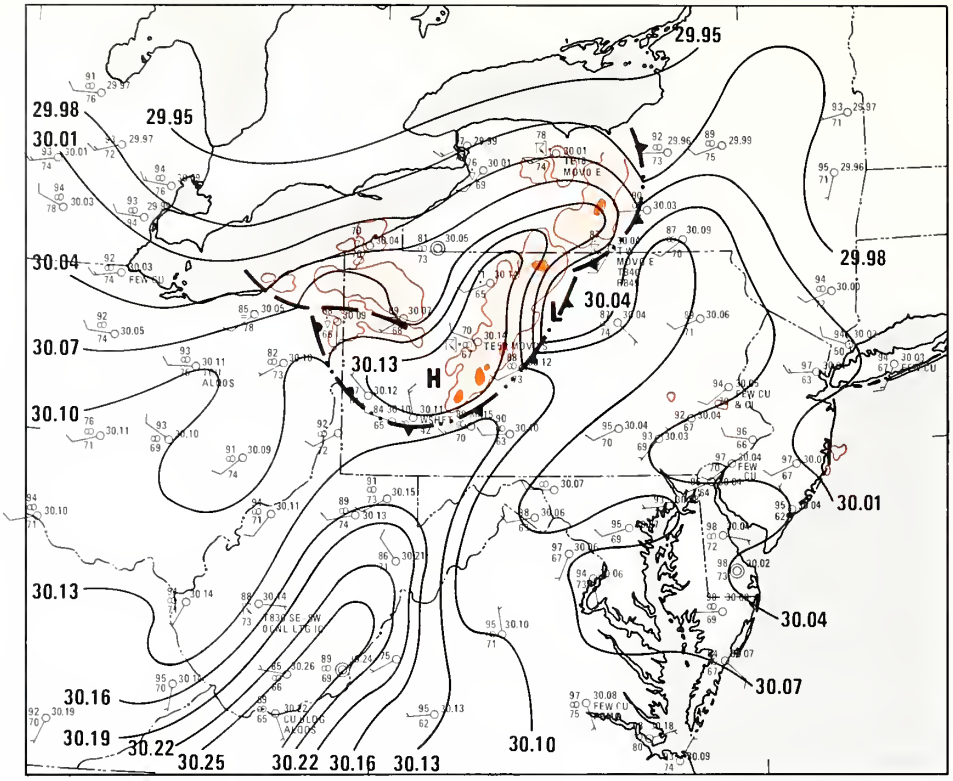

Figure 8a. Regional mesoscale analysis for 1800 GMT, July 19, 1977. Outflow boundaries, pressure centers, pressure troughs and pressure analysis (altimeter settings in intervals of 0.03 in) are in black. Orange shading indicates areas covered by radar echoes (light shading VIP level 1 or greater and dark shading VIP level 3 or greater).

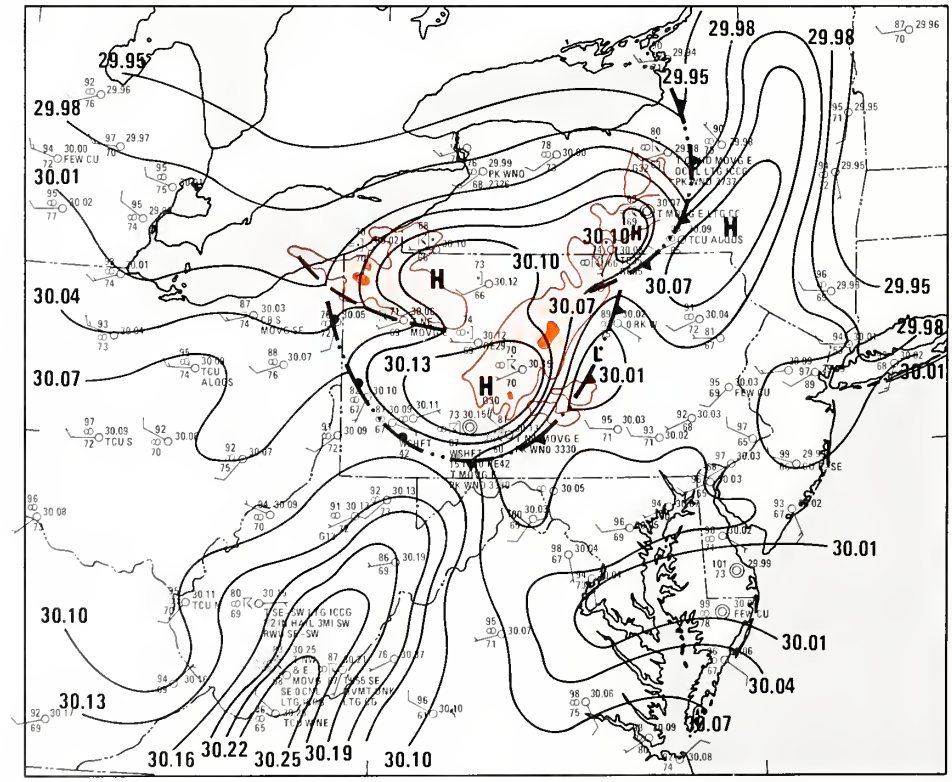

Figure 8b. Regional mesoscale analysis for 1900 GMT, July 19, 1977.

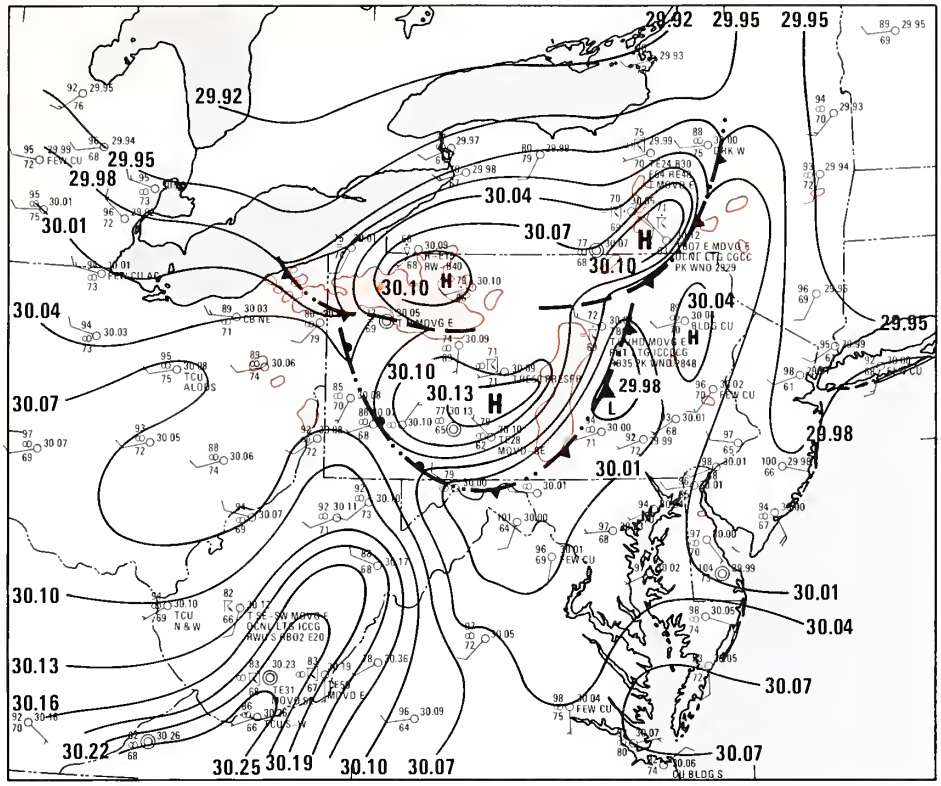

Figure 8c. Regional mesoscale analysis for 2000 GMT, July 19, 1977.

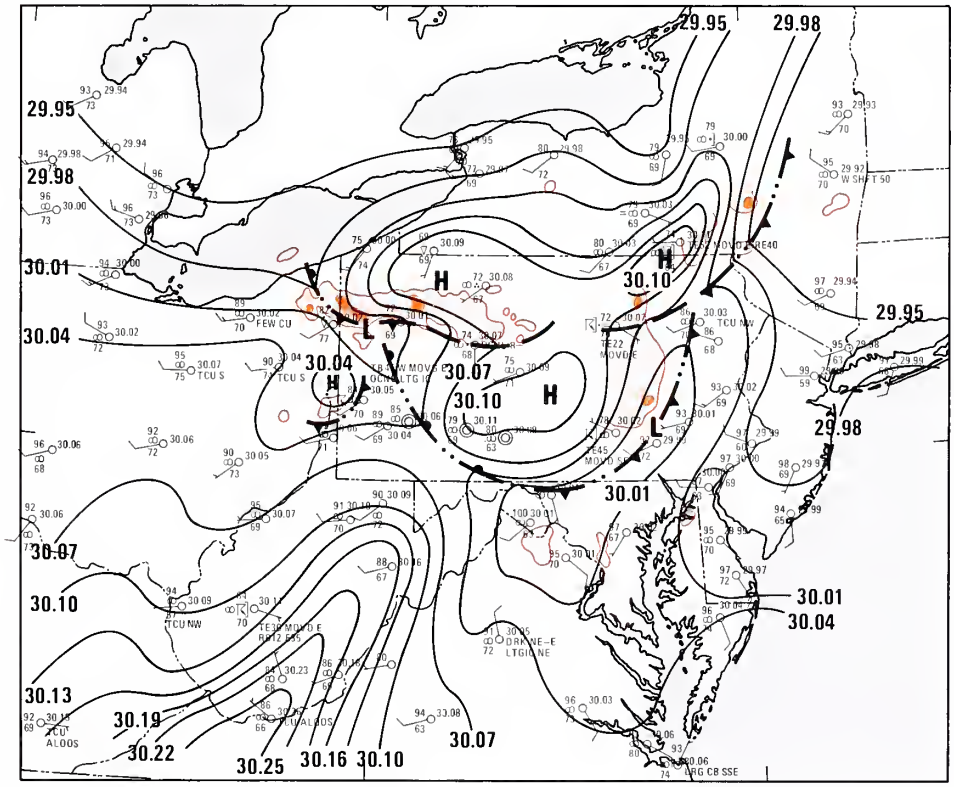

Figure 8d. Regional mesoscale analysis for 2100 GMT, July 19, 1977.

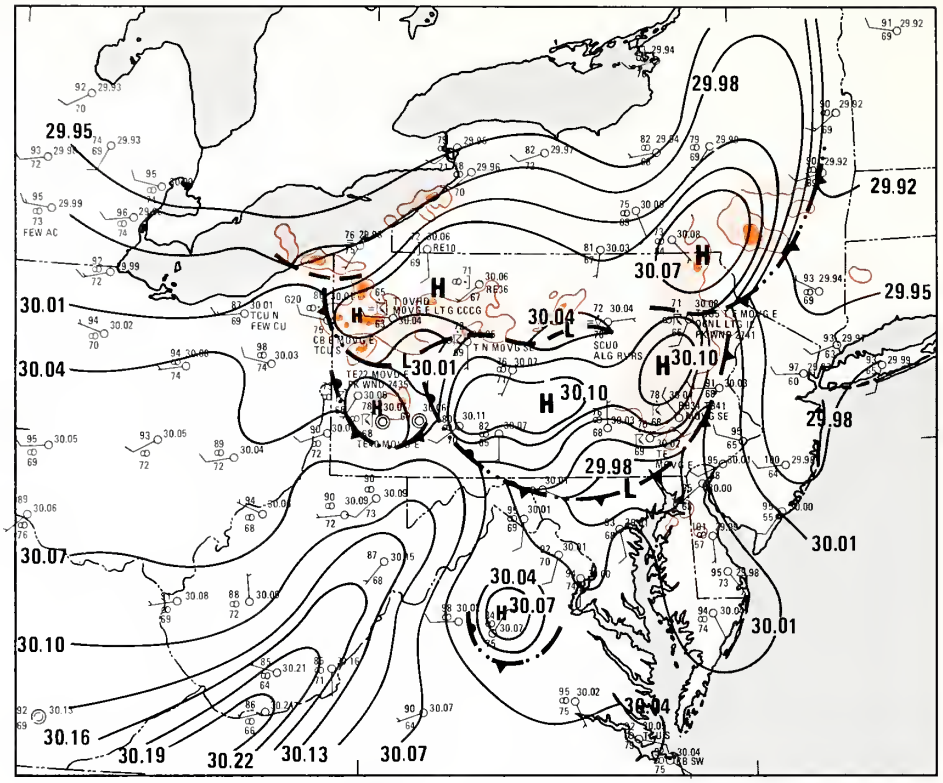

Figure 8e. Regional mesoscale analysis for 2200 GMT, July 19, 1977.

Figure 8f. Regional mesoscale analysis for 2300 GMT, July 19, 1977.

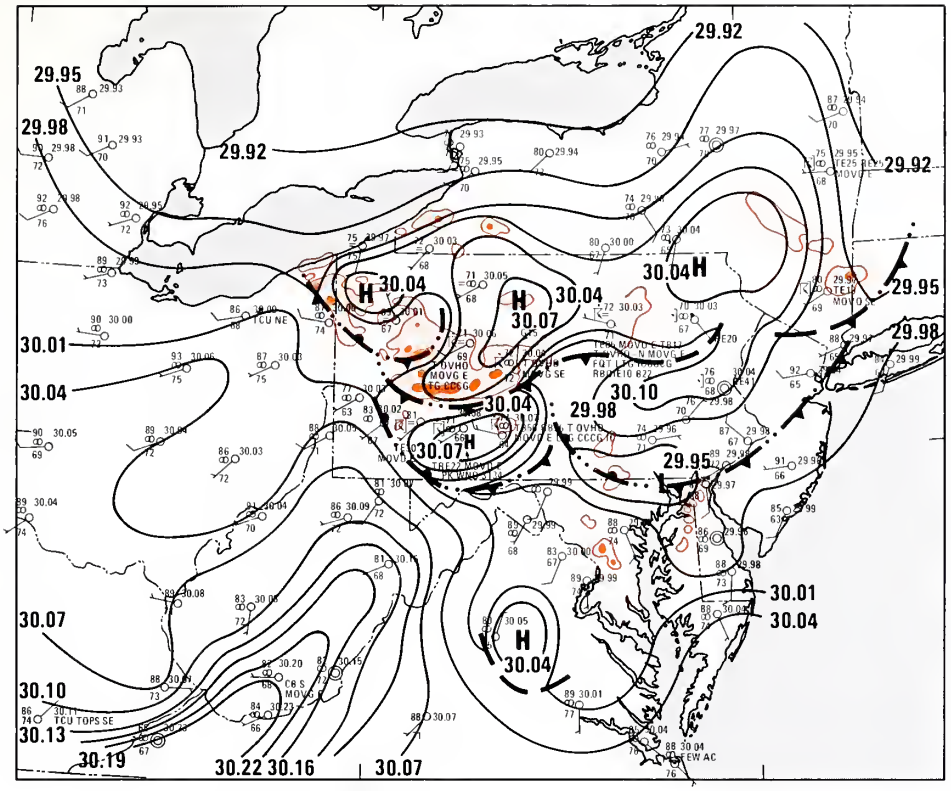

Figure 8g. Regional mesoscale analysis for 0000 GMT, July 20, 1977.

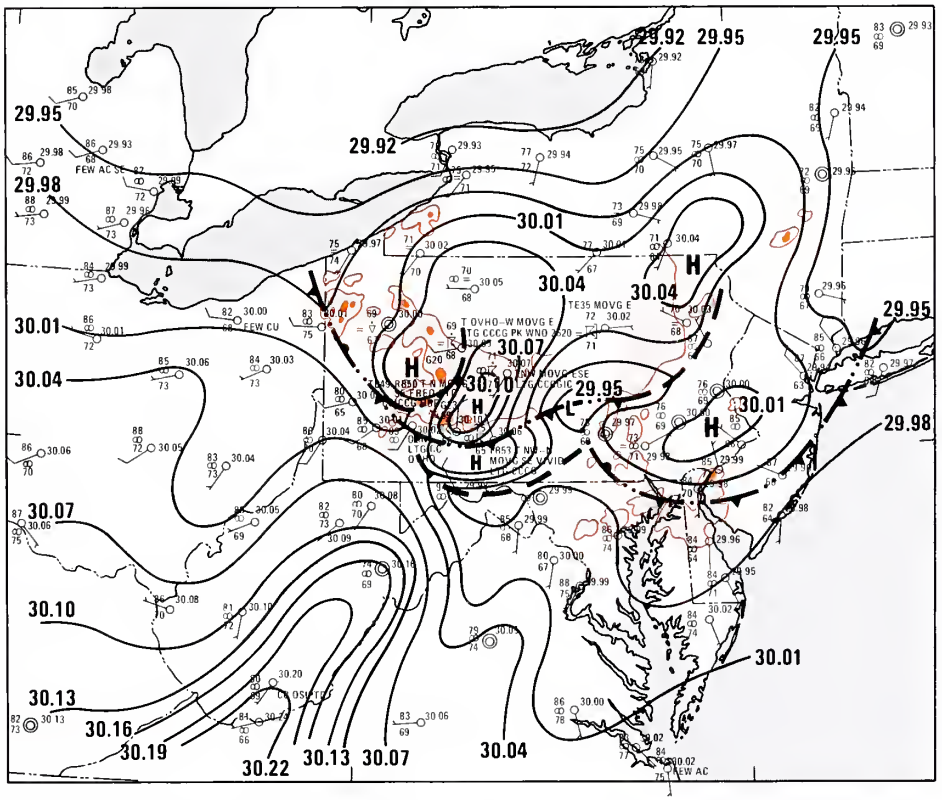

Figure 8h. Regional mesoscale analysis for 0100 GMT, July 20, 1977.

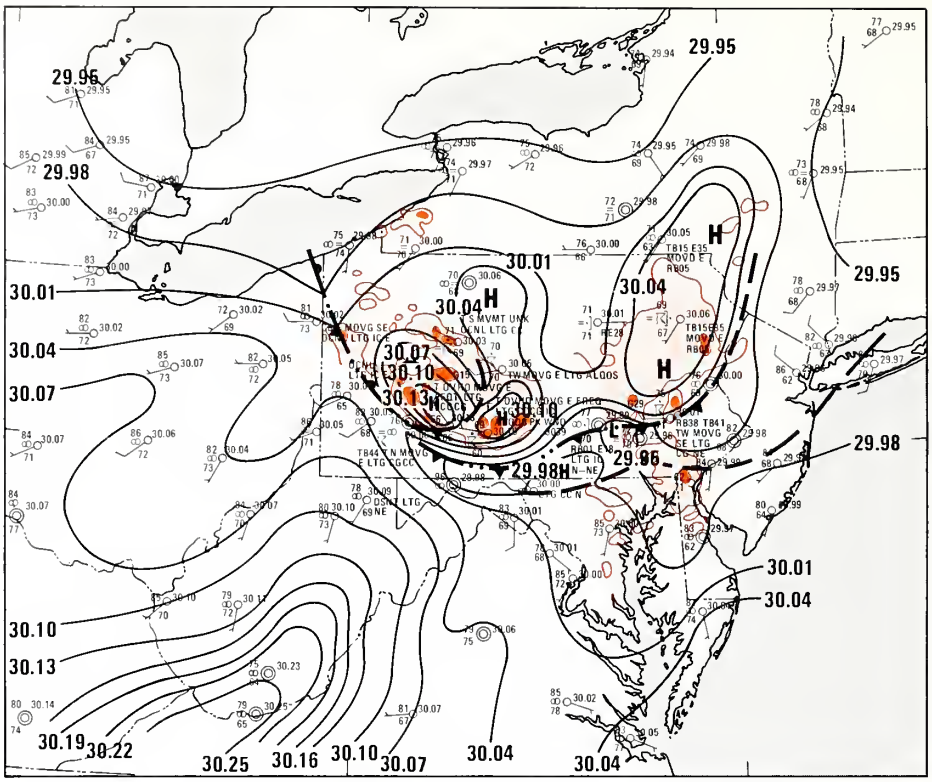

Figure 8i. Regional mesoscale analysis for 0200 GMT, July 20, 1977.

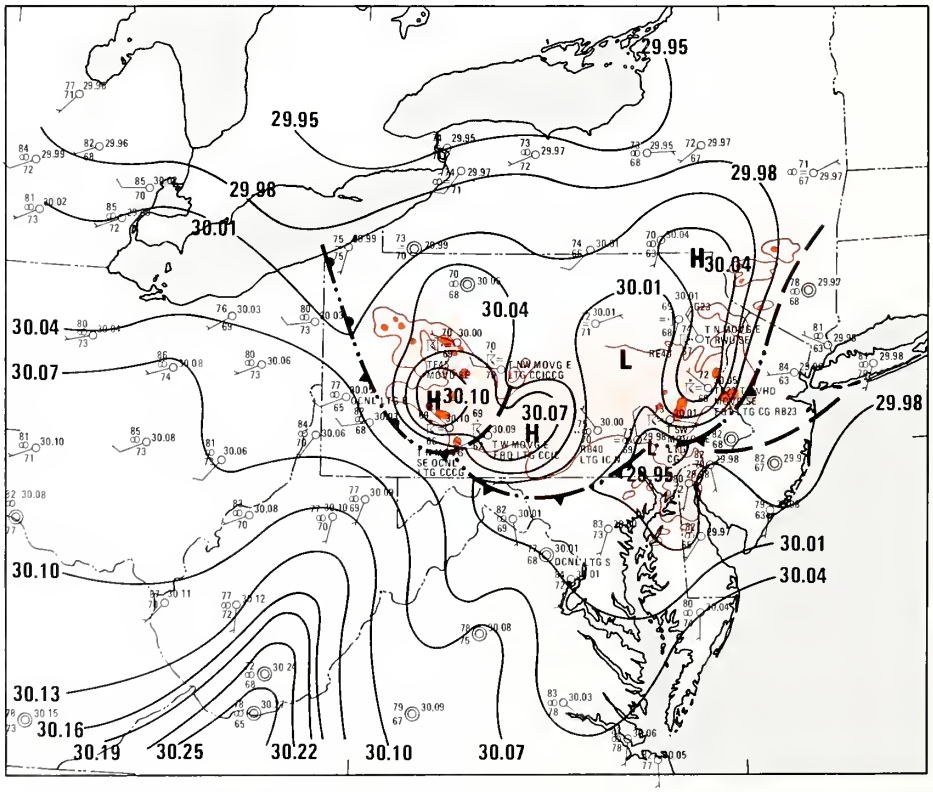

Figure 8j. Regional mesoscale analysis for 0300 GMT, July 20, 1977.

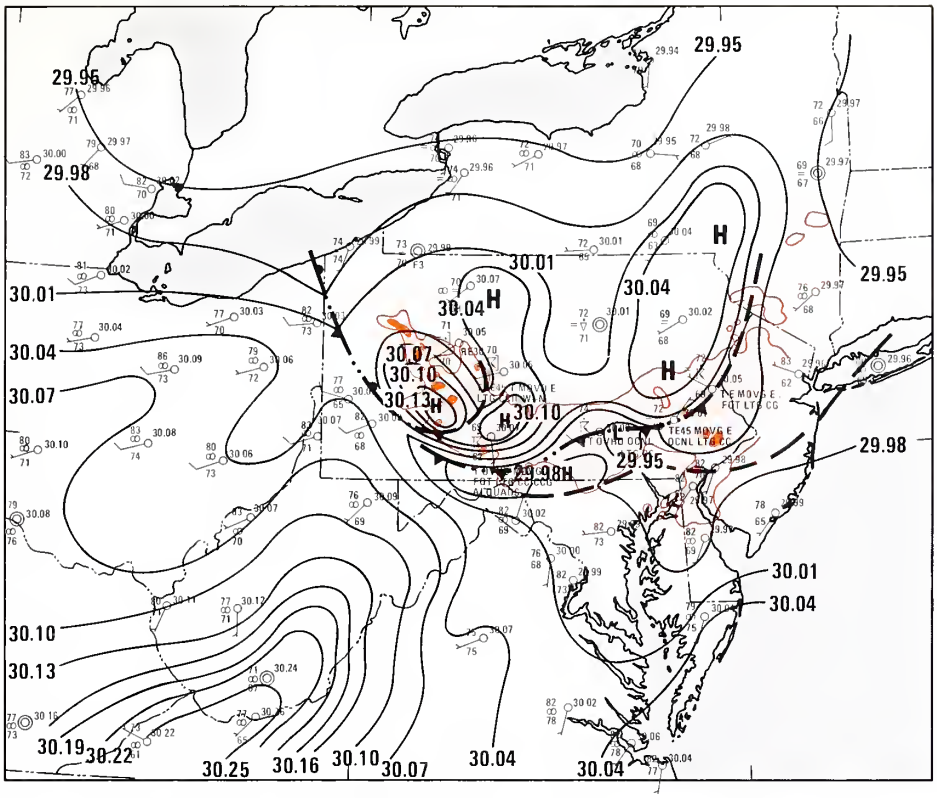

Figure 8k. Regional mesoscale analysis for 0400 GMT, July 20, 1977.

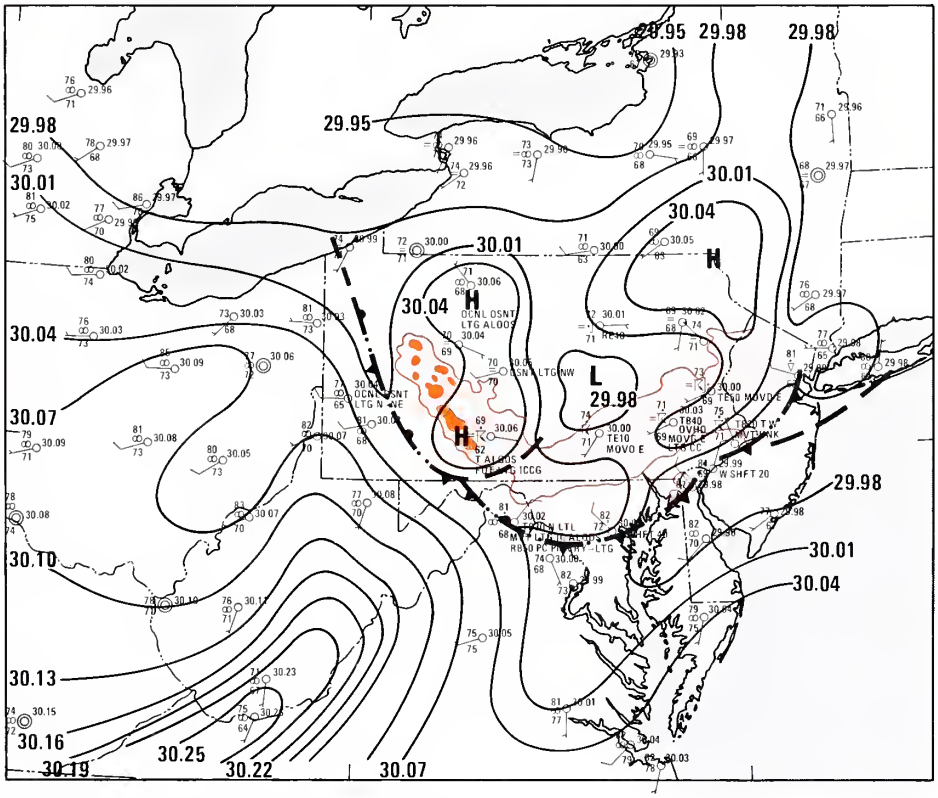

Figure 8l. Regional mesoscale analysis for 0500 GMT, July 20, 1977.

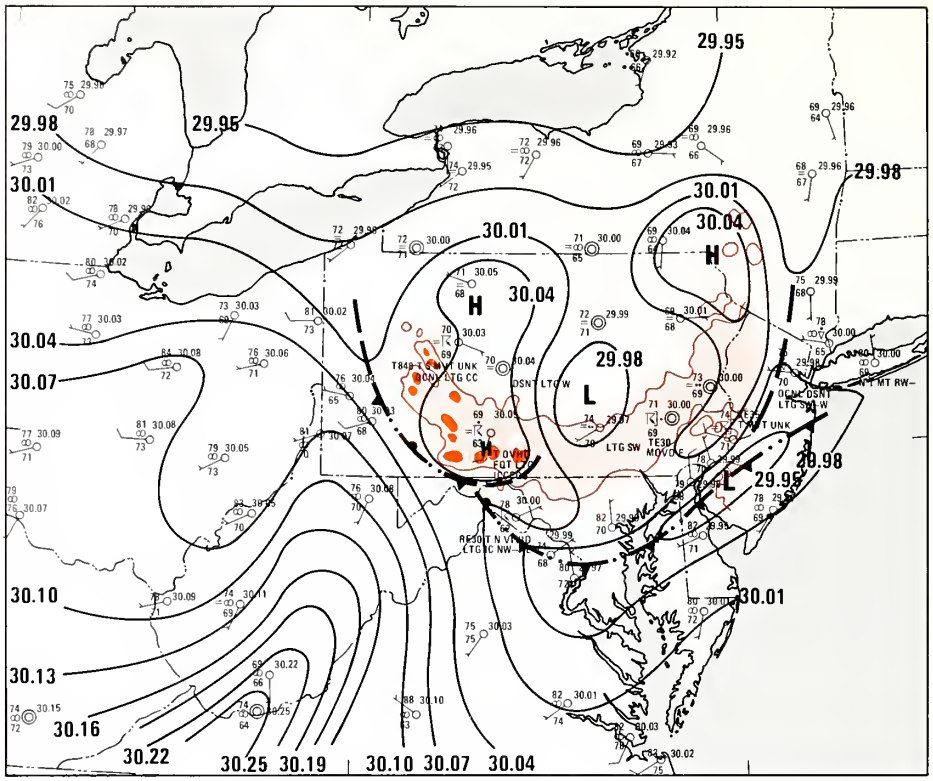

Figure 8m. Regional mesoscale analysis for 0600 GMT, July 20, 1977.

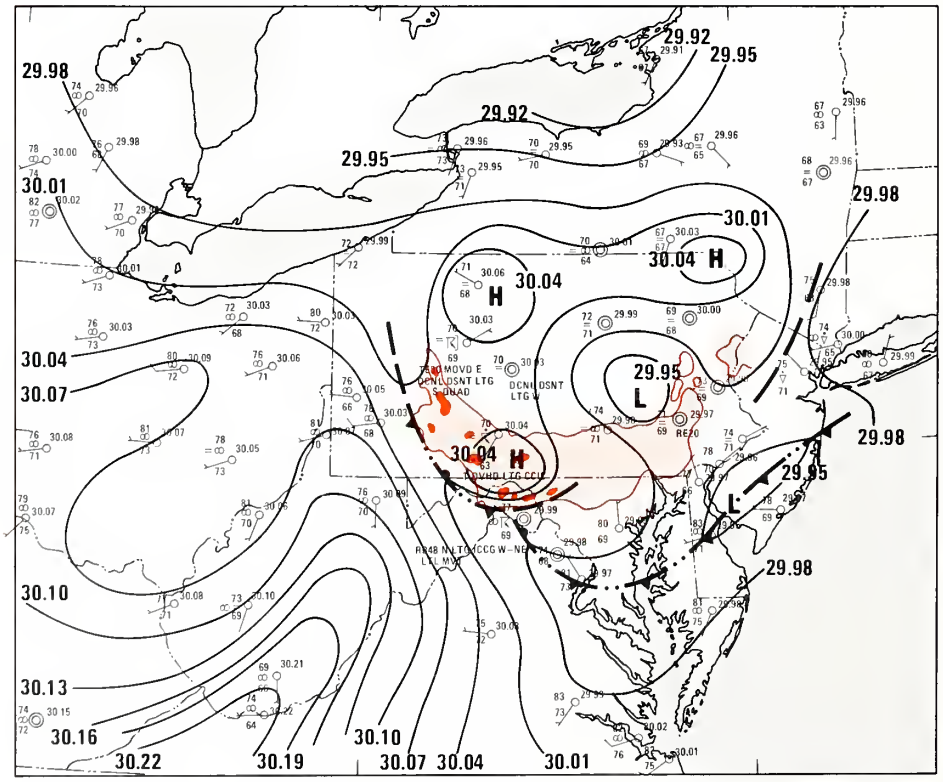

Figure 8n. Regional mesoscale analysis for 0700 GMT, July 20, 1977.

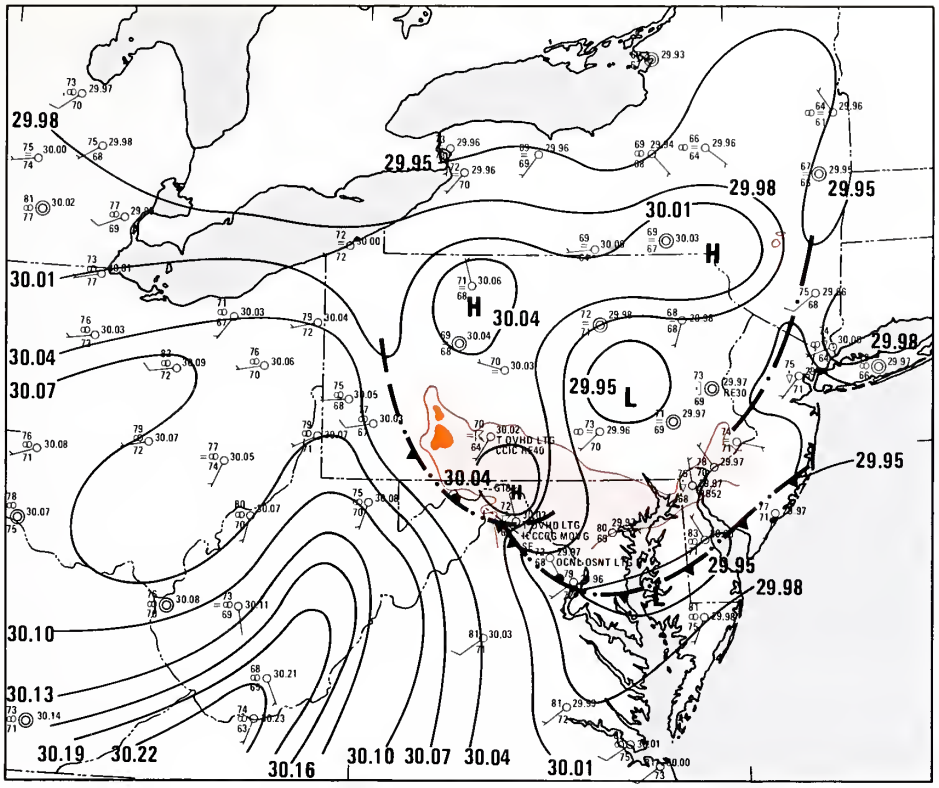

Figure 8o. Regional mesoscale analysis for 0800 GMT, July 20, 1977.

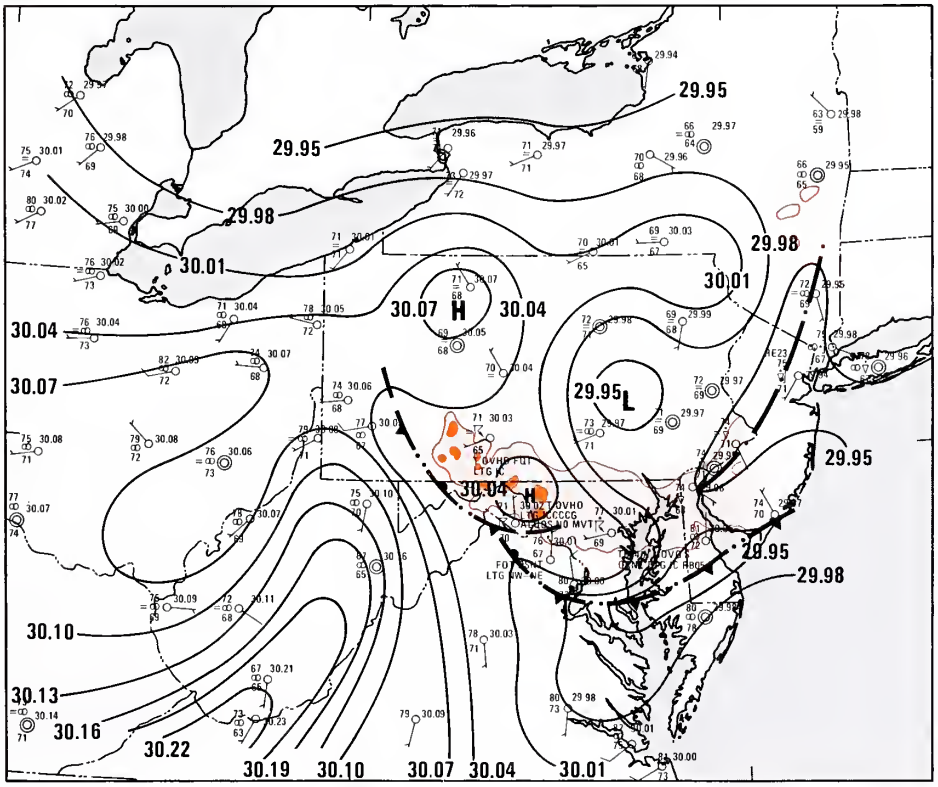

Figure 8p. Regional mesoscale analysis for 0900 GMT, July 20, 1977.

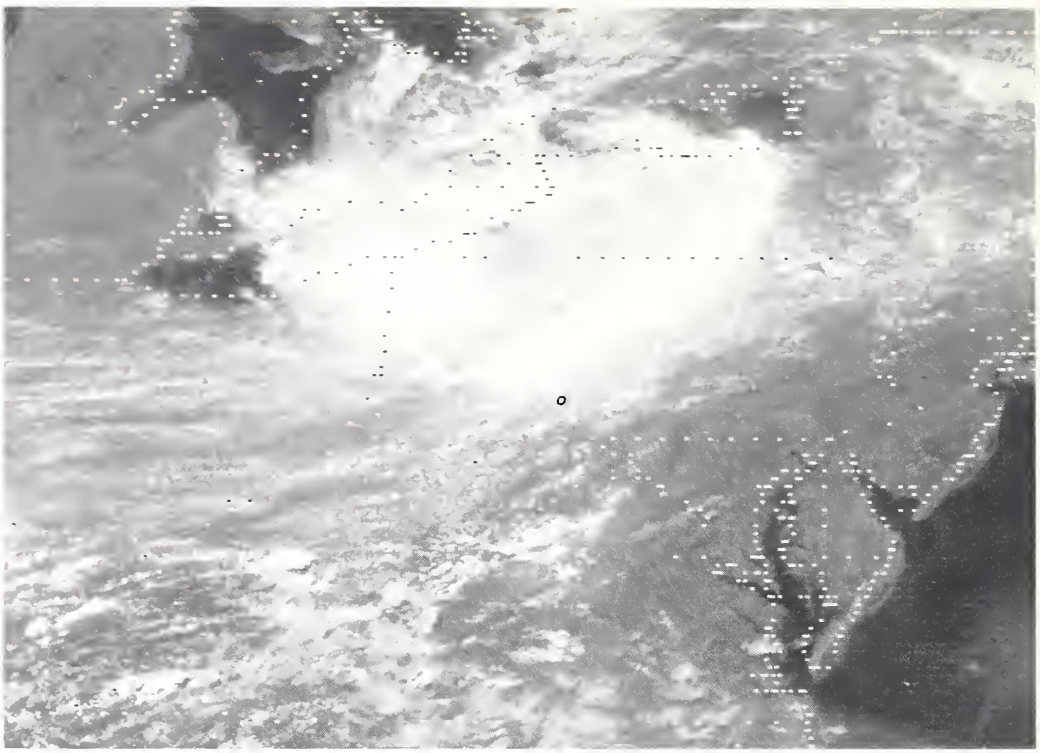

Figure 9a. GOES-1 photograph for 1800 GMT, July 19, 1977. Visible imagery 1800 to 2300 GMT, July 19 (1 km resolution at satellite subpoint). Enhanced infrared imagery 0000 to 0900 GMT, July 20 (2 km equivalent resolution at satellite subpoint).

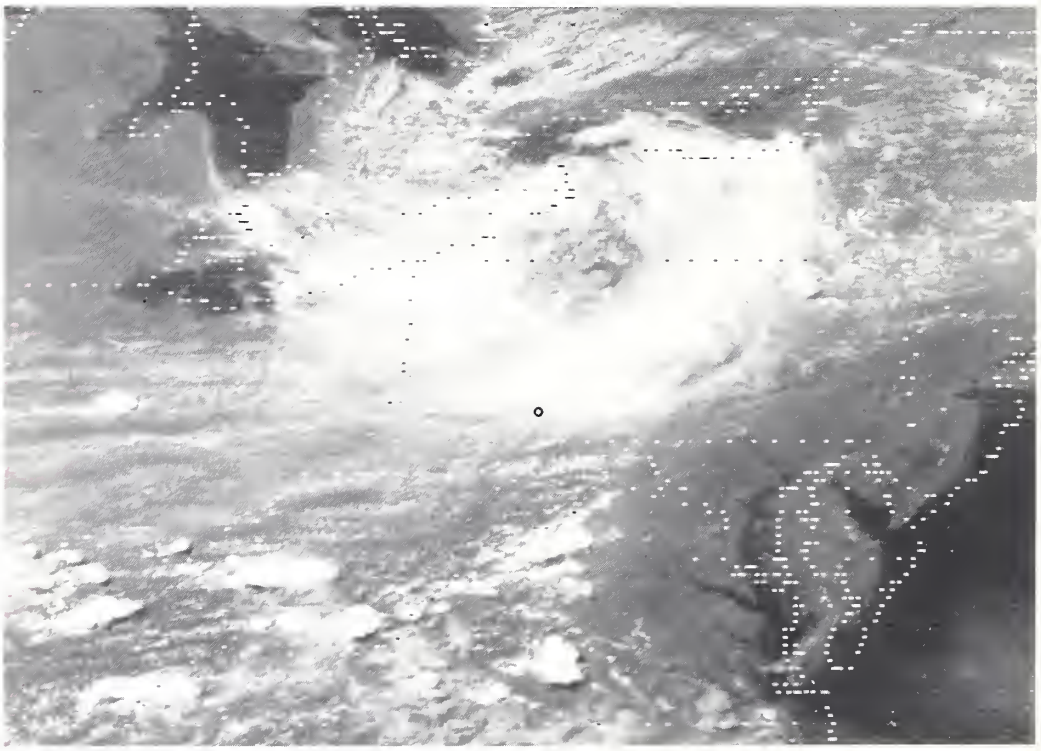

Figure 9b. GOES-1 photo for 1900 GMT, July 19, 1977.

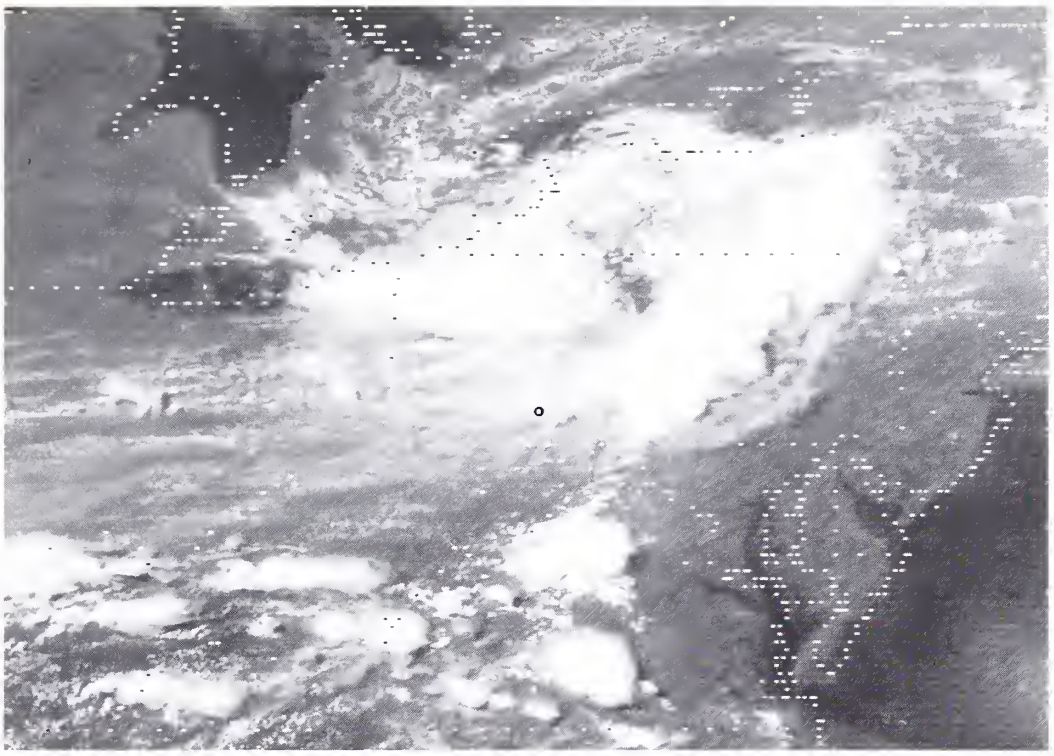

Figure 9c. GOES-1 photo for 2000 GMT, July 19, 1977.

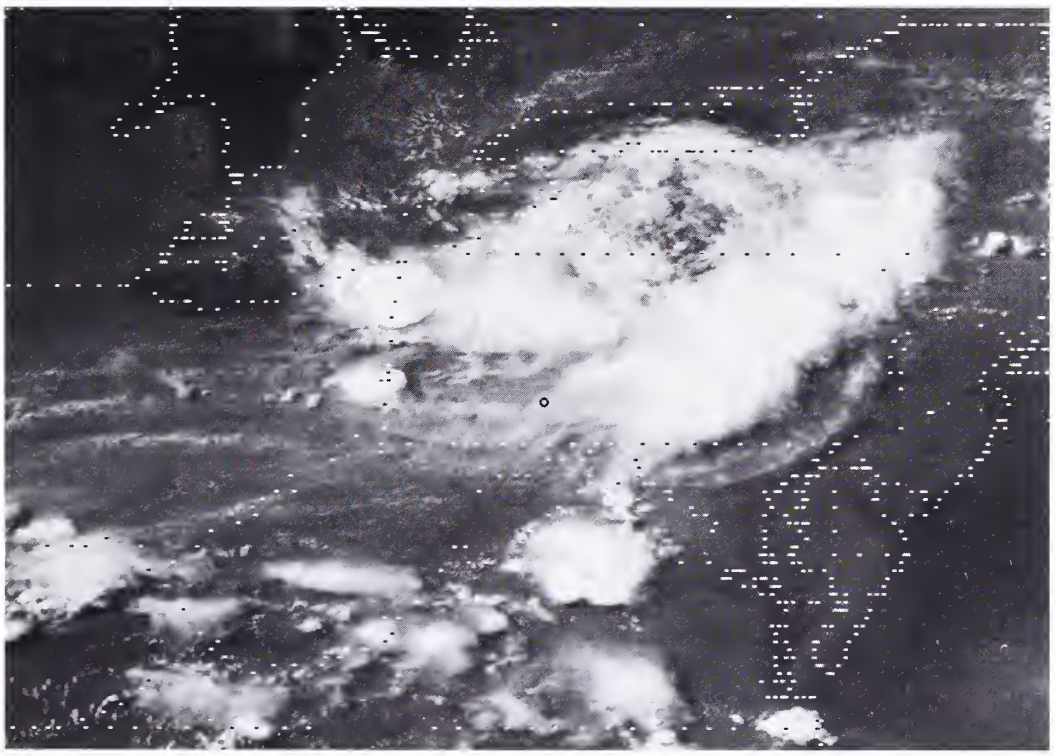

Figure 9d. GOES-1 photo for 2100 GMT, July 19, 1977.

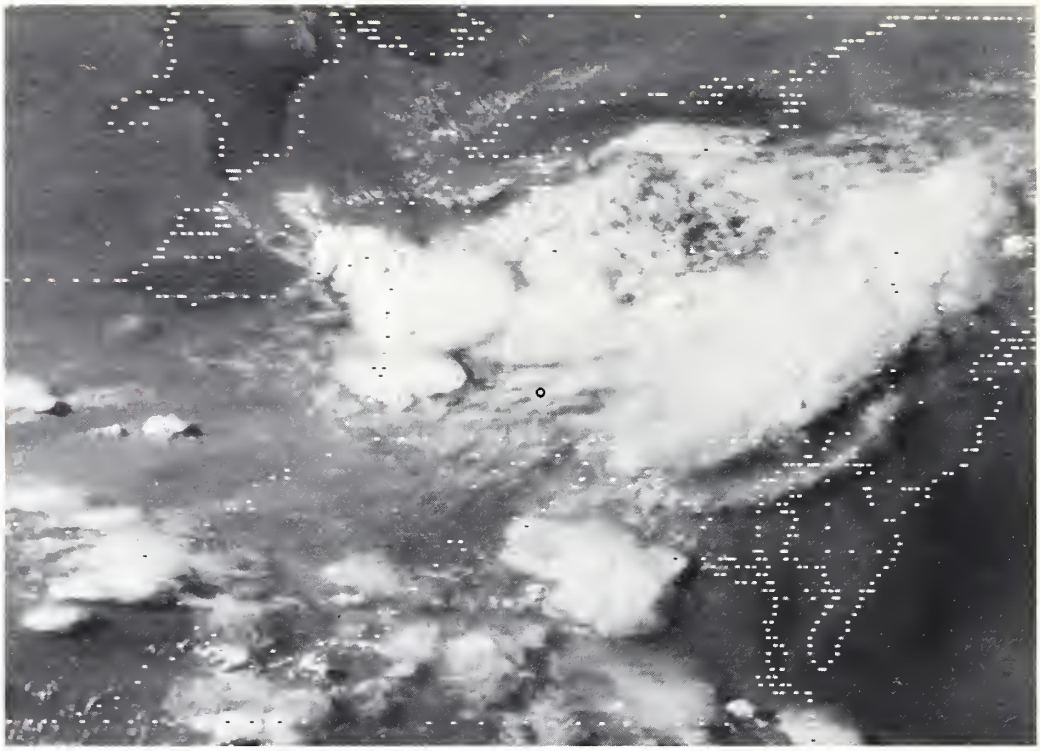

Figure 9e. GOES-1 photo for 2200 GMT, July 19, 1977.

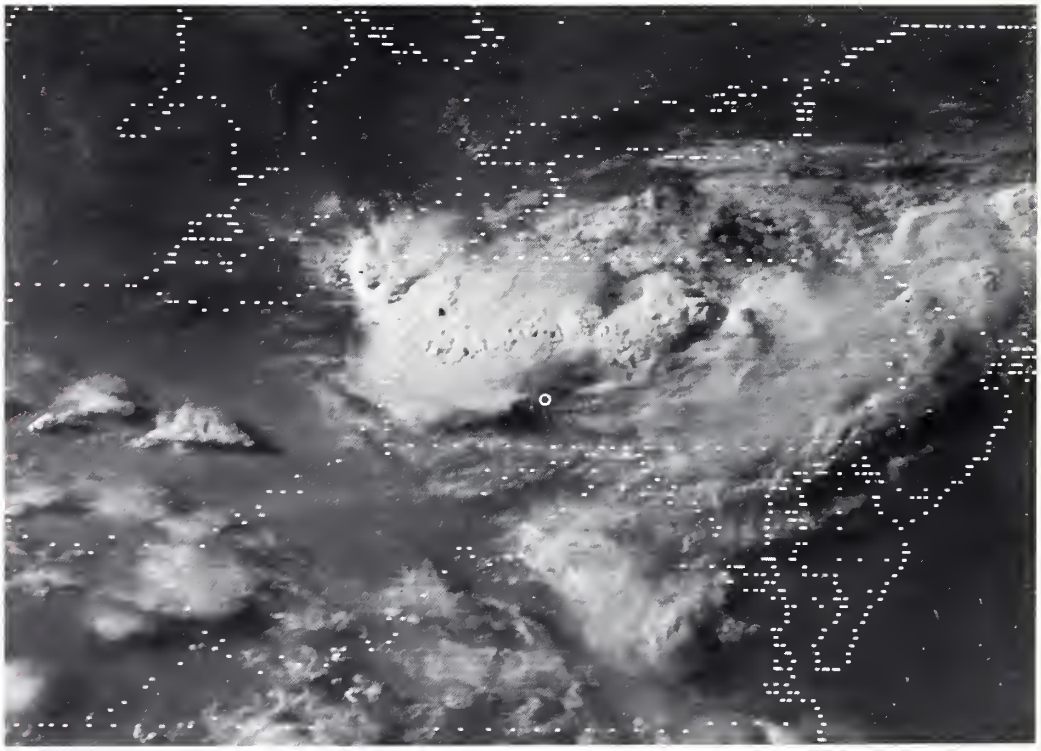

Figure 9f. GOES-1 photo for 2300 GMT, July 19, 1977.

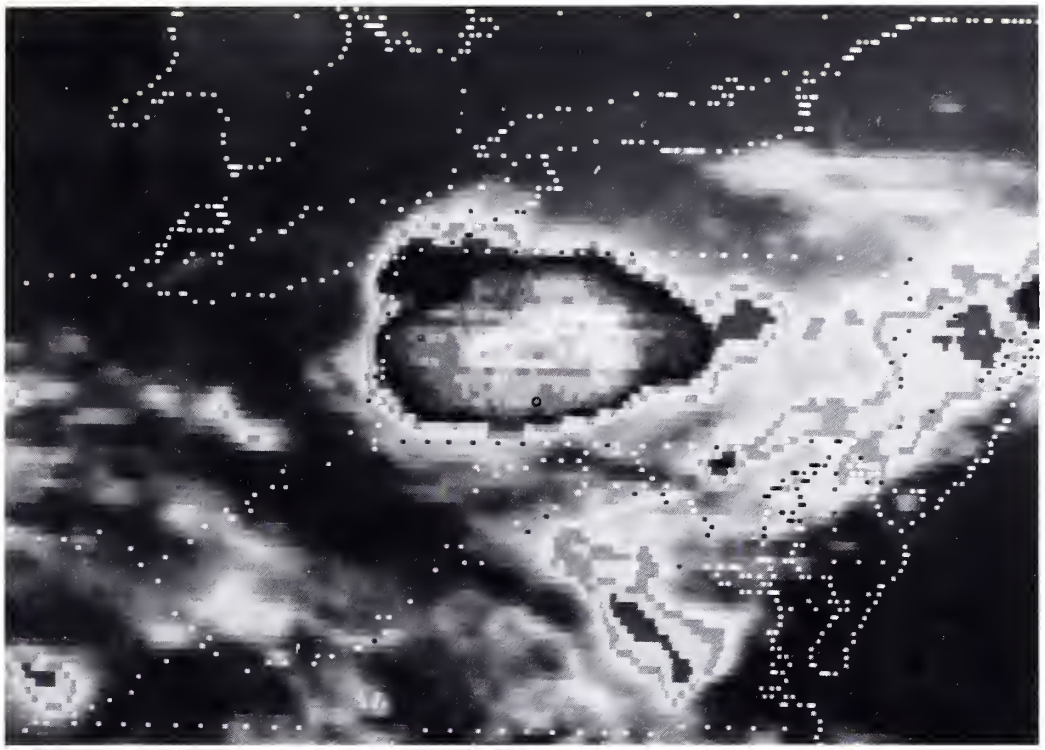

Figure 9g. GOES-1 photo for 0000 GMT, July 20, 1977.

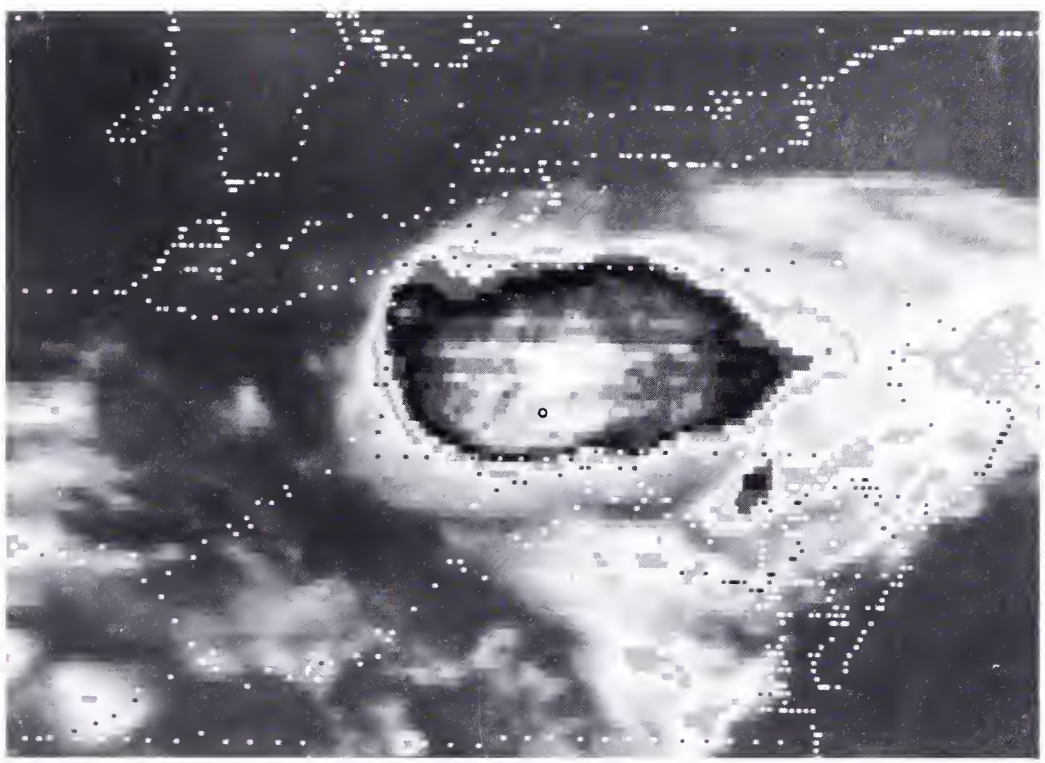

Figure 9h. GOES-1 photo for 0100 GMT, July 20, 1977.

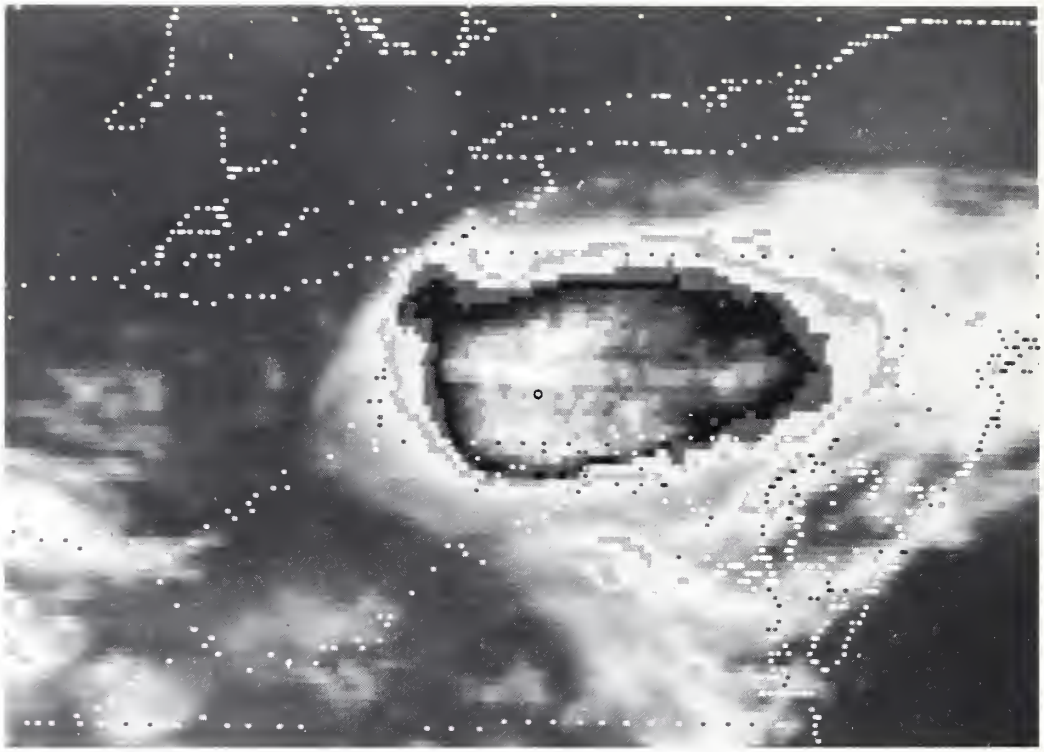

Figure 9i. GOES-1 photo for 0200 GMT, July 20, 1977.

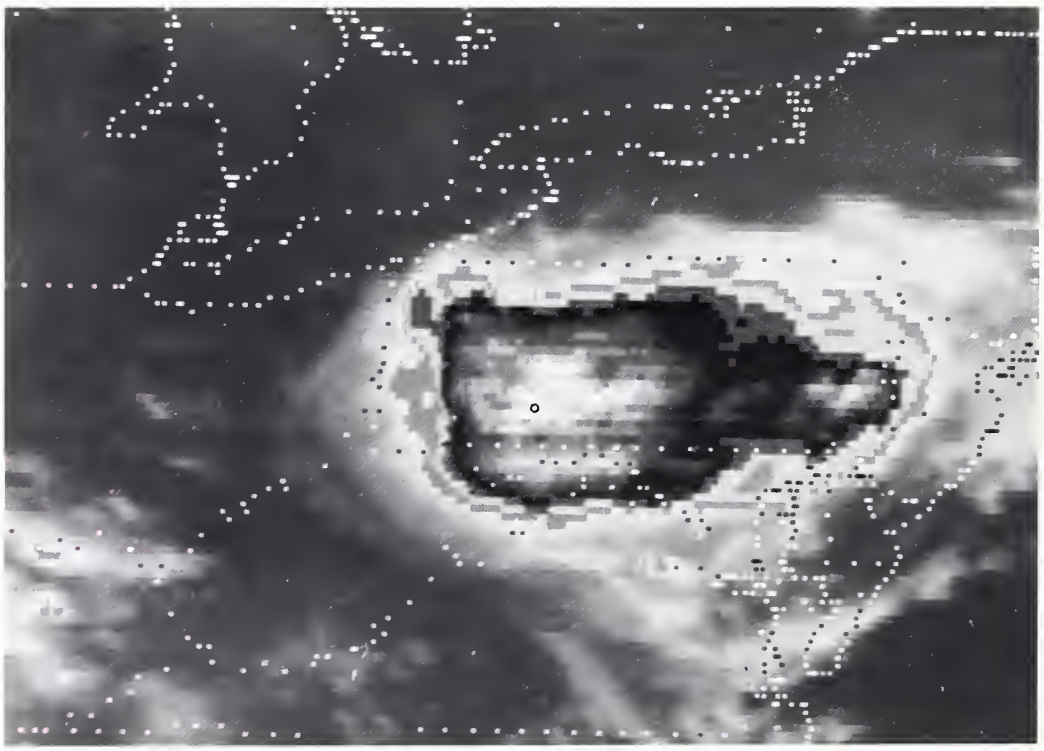

Figure 9j. GOES-1 photo for 0300 GMT, July 20, 1977.

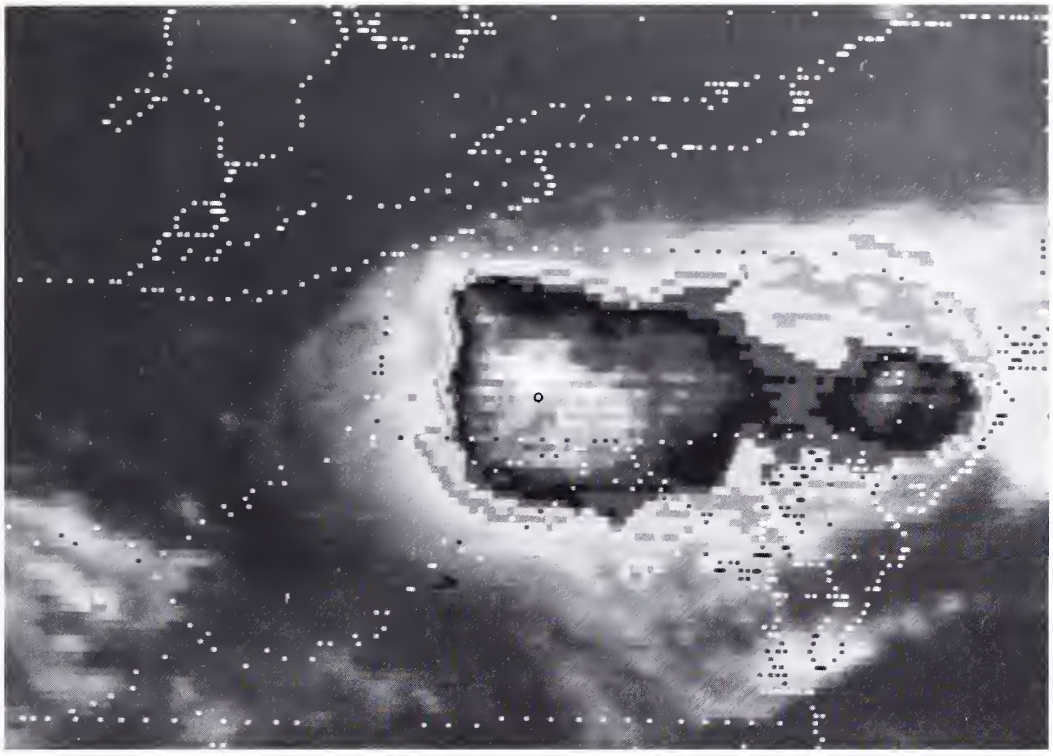

Figure 9k. GOES-1 photo for 0400 GMT, July 20, 1977.

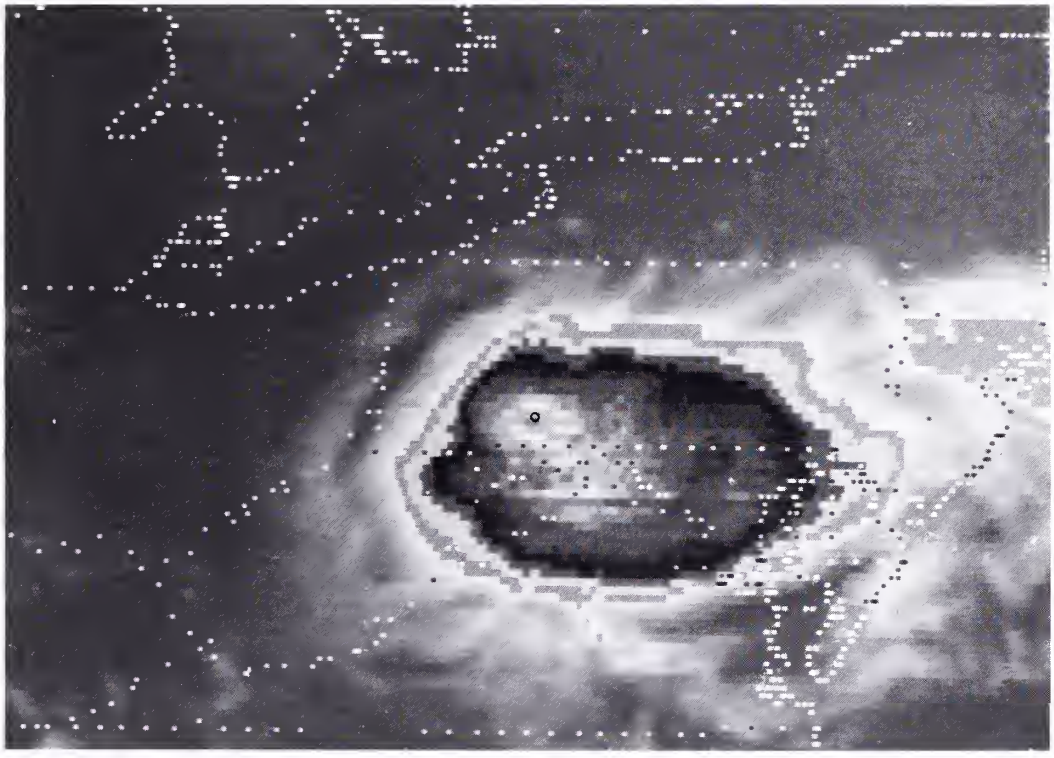

Figure 9l. GOES-1 photo for 0800 GMT, July 20, 1977.

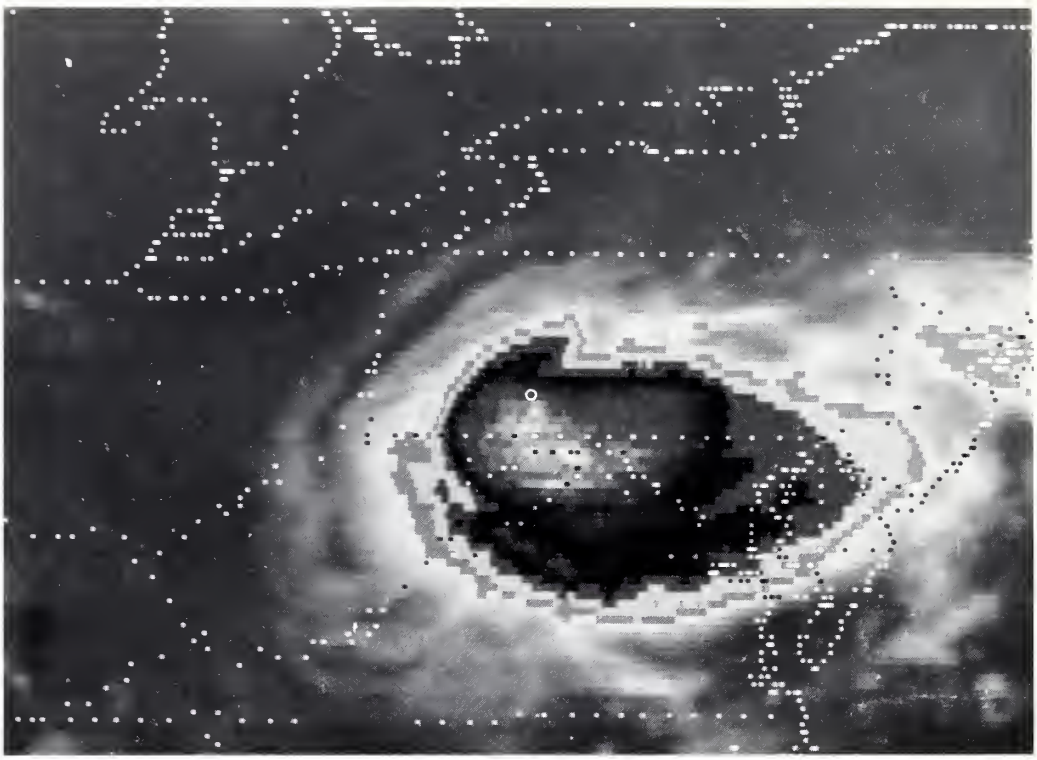

Figure 9m. GOES-1 photo for 0900 GMT, July 20, 1977.

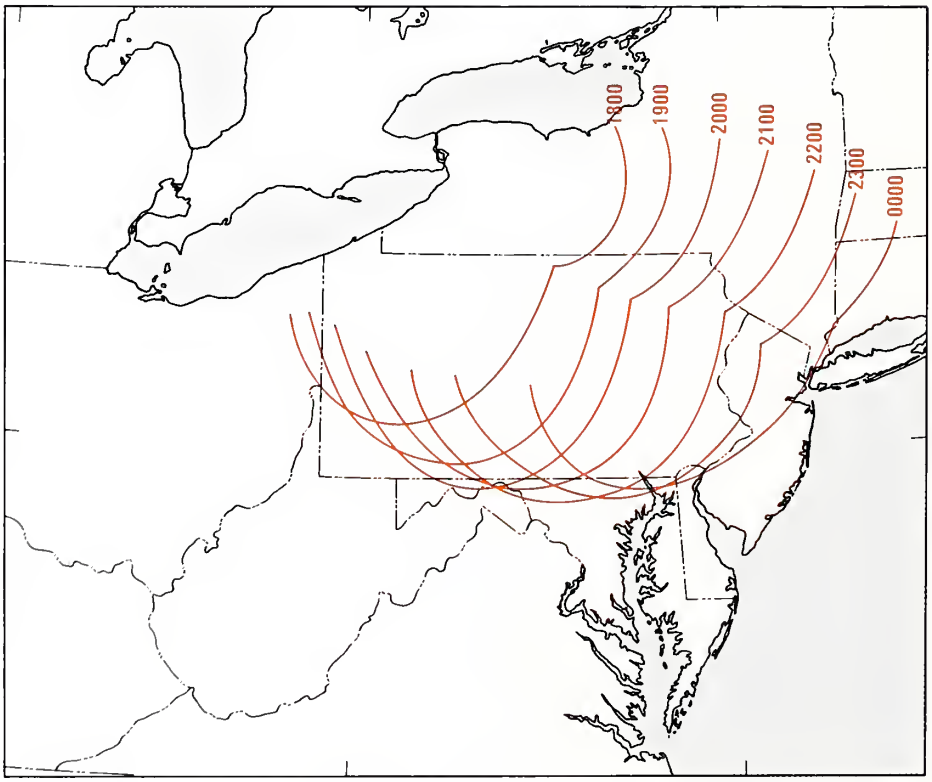

Figure 10a. Hourly positions of first thunderstorm outflow boundary, from 1800 GMT, July 19, 1977 to 0000 GMT, July 20, 1977.

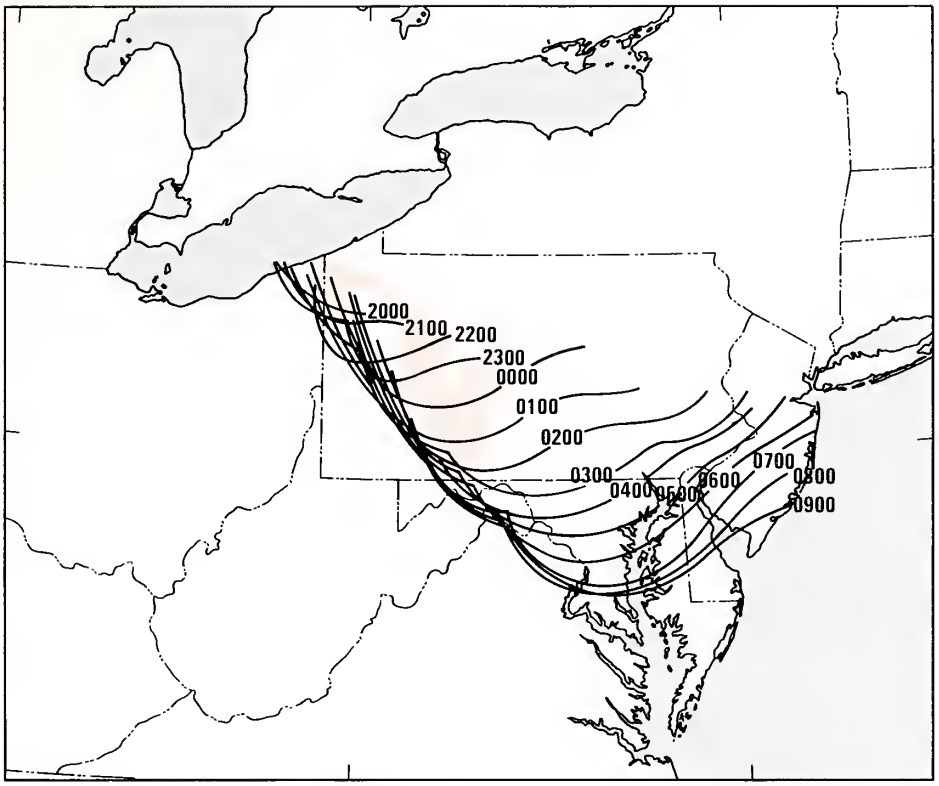

Figure 10b. Hourly positions of second thunderstorm outflow boundary, from 2000 GMT, July 19, 1977 to 0900 GMT, July 20, 1977. Orange shading defines the region with 24-h rainfalls in excess of 2 inches.

4. DISTRIBUTION OF RAINFALL

Temporal and spatial distributions of the rainfall over western Pennsylvania before and during the major flooding are now examined. Hourly and daily rainfall totals from the rain gauge network are shown, as well as rainfall estimates from the D/RADEX radar facility at Pittsburgh (Greene and Saffle, 1978) and satellite derived rainfall amounts from the method developed by Scofield and Oliver (1977a,b). D/RADEX values were computed and available during the storm. Many surface observations of rainfall were not available until after the flood. Satellite estimates of rainfall were computed by the National Environmental Satellite Service after the flood to examine the potential of this technique for future real-time application to major rainfall events of this type. Appendix B contains a brief description of how the D/RADEX system works, and Appendix C presents a discussion of the procedures used in the satellite rainfall estimation technique.

Analyses of the hourly rainfalls, obtained from D/RADEX for the period 1800 GMT, July 19, until 1000 GMT, July 20, are presented in Fig. 11. Satellite derived rainfall estimates are presented for the period from 2100 to 0900 GMT. Since data were not available from 0430 to 0730 GMT, satellite estimates shown for the periods 0400 to 0500 GMT and 0700 to 0800 GMT are only 30-min accumulations. Hourly rainfalls observed at stations in and surrounding the Conemaugh River Basin are plotted for the period 2200 to 1000 GMT.

During the afternoon, the hourly

D/RADEX totals clearly show the eastward movement of the first squall line out of western Pennsylvania and the development and eastward extension of the second line over northwestern Pennsylvania.

As the second line moved into the Johnstown area during the late afternoon and early evening, agreement between the hourly rainfall, estimated by satellite and radar, and observed amounts is reasonably good. In general, the satellite analyses are not as smooth as the radar analyses and often show rainfall covering a larger area than the radar analyses. Maximum values from the satellite analysis are somewhat higher than those from D/RADEX during the early evening period and are in better agreement with the maximum observed values. Hourly rainfall totals at three stations (Fig. 12) indicate that the bulk of the rainfall occurred in a 6- to 9-h period.

A comparison of 24-h rainfall amounts from D/RADEX data with an isohyetal analysis of surface rain gauge data is shown in Figs. 13 and 14. The pattern of heavy rainfall is very similar in both analyses. However, observed maximum totals are more than 12 in, although the maximum radar accumulation is slightly more than 8 in. Figures 11 and 12 indicate that radar estimates were somewhat low during the early evening but compare more favorably with the observed values in the 0500 to 1000 GMT July 20 time period.

Analyses in Figs. 12 and 14 show the intensity of the rain during the 6- to 9-h period and the very localized nature of the rainfall. For example, Nanty Glo about 10 mi north of Johnstown received about 12 inches of rain during the 24-h period whereas locations 30 mi to the southwest received little or none.

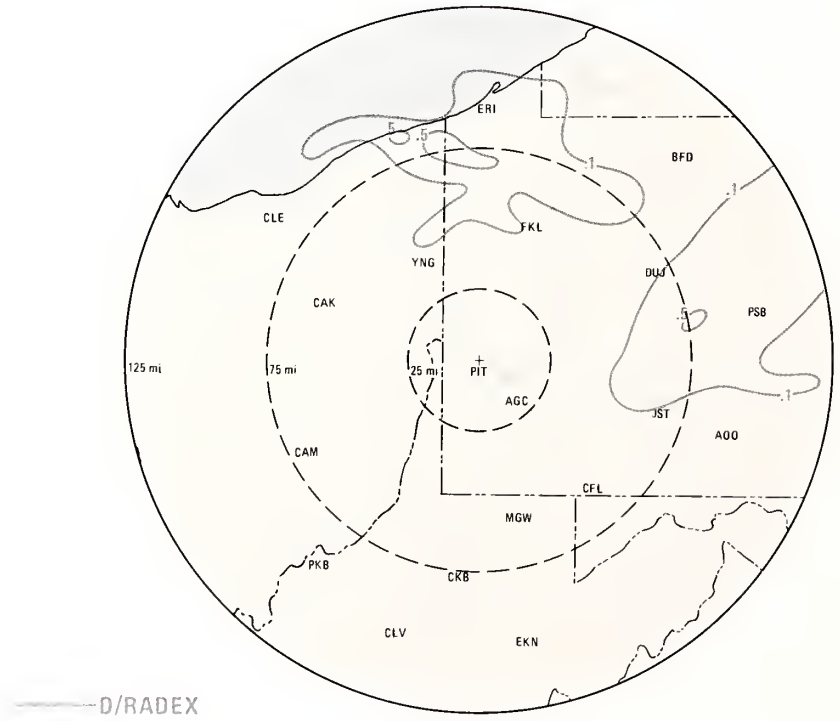

Figure 11a. Hourly rainfall analyses in inches for 1800 to 1900 GMT, July 19, 1977. D/RADEX rainfall accumulations in gray. Rainfall estimates from satellite using Scofield-Oliver technique are in orange. Plotted numbers in black are observed hourly rainfall.

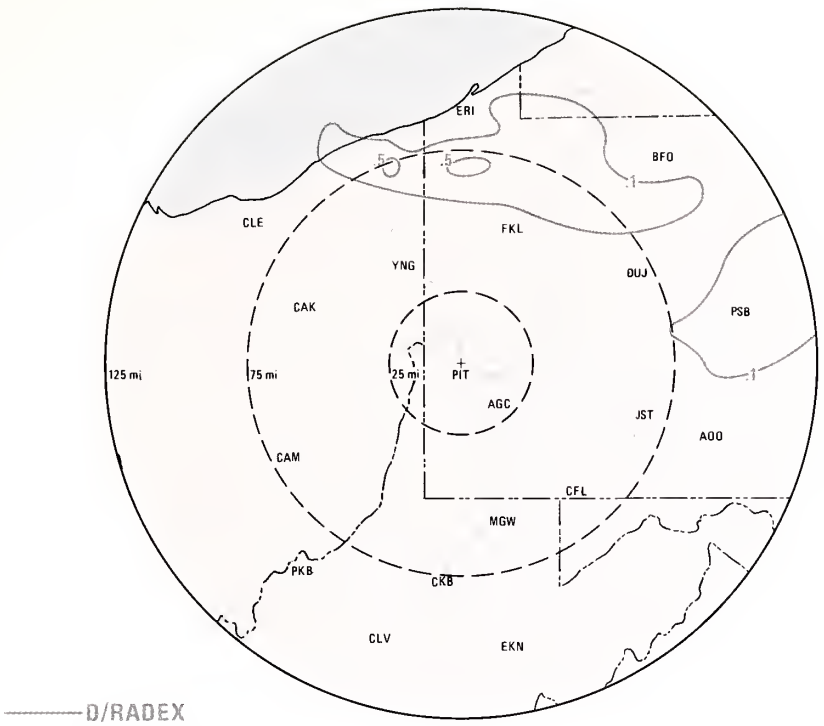

Figure 11b. Hourly rainfall analyses for 1900–2000 GMT, July 19, 1977.

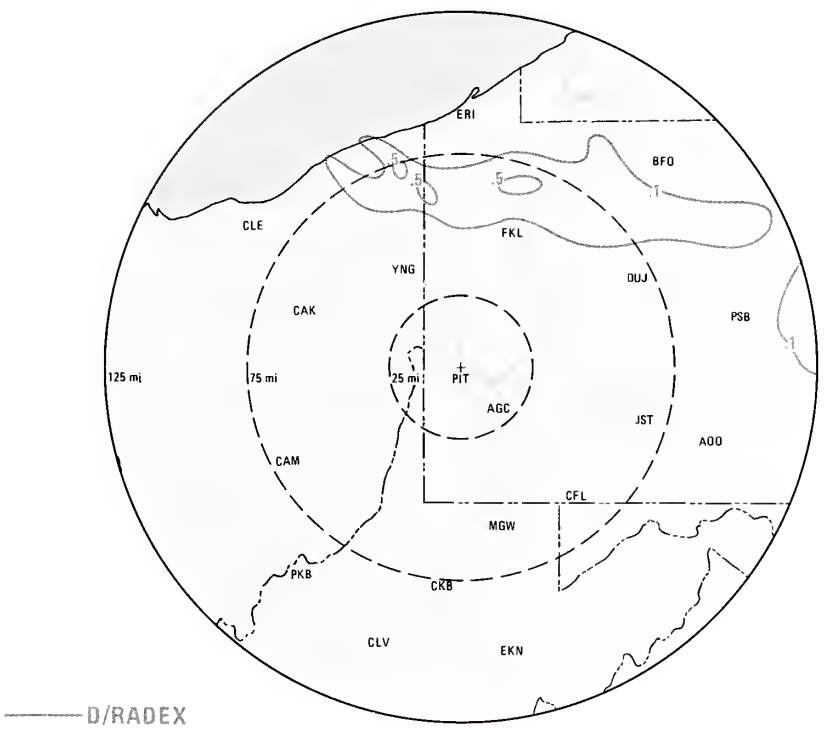

Figure 11c. Hourly rainfall analyses for 2000–2100 GMT, July 19, 1977.

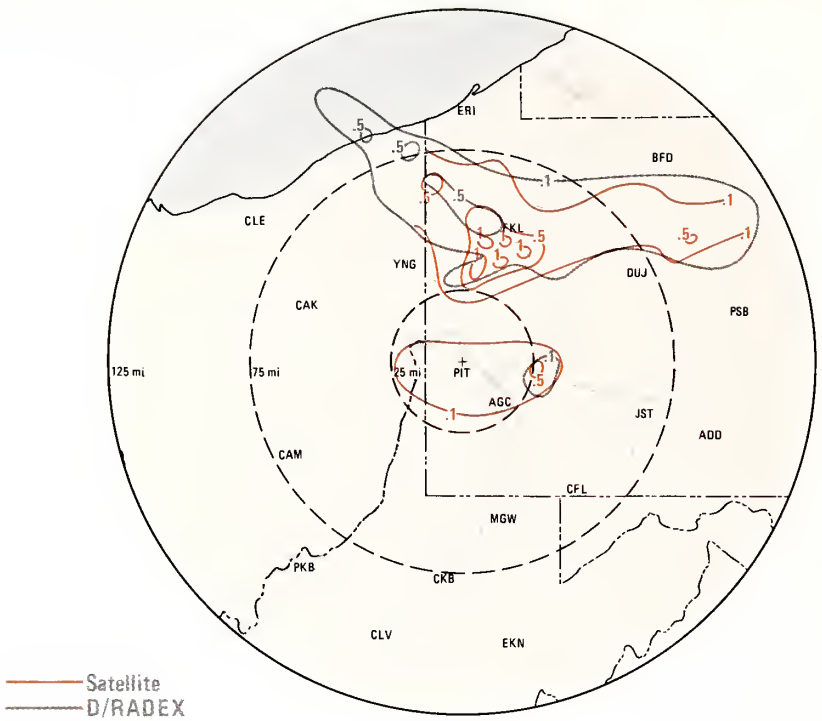

Figure 11d. Hourly rainfall analyses for 2100–2200 GMT, July 19, 1977.

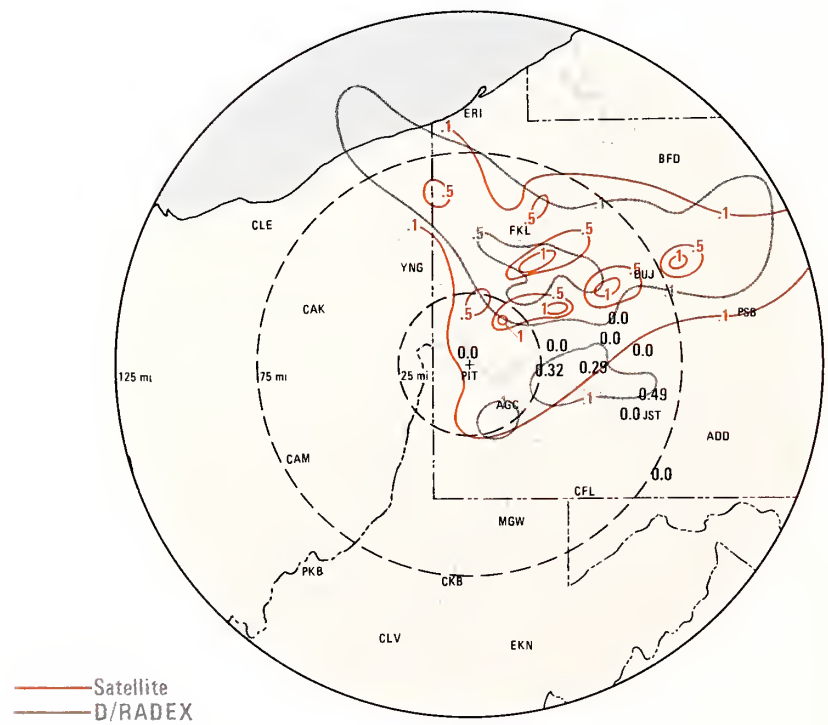

Figure 11e. Hourly rainfall analyses for 2200–2300 GMT, July 19, 1977.

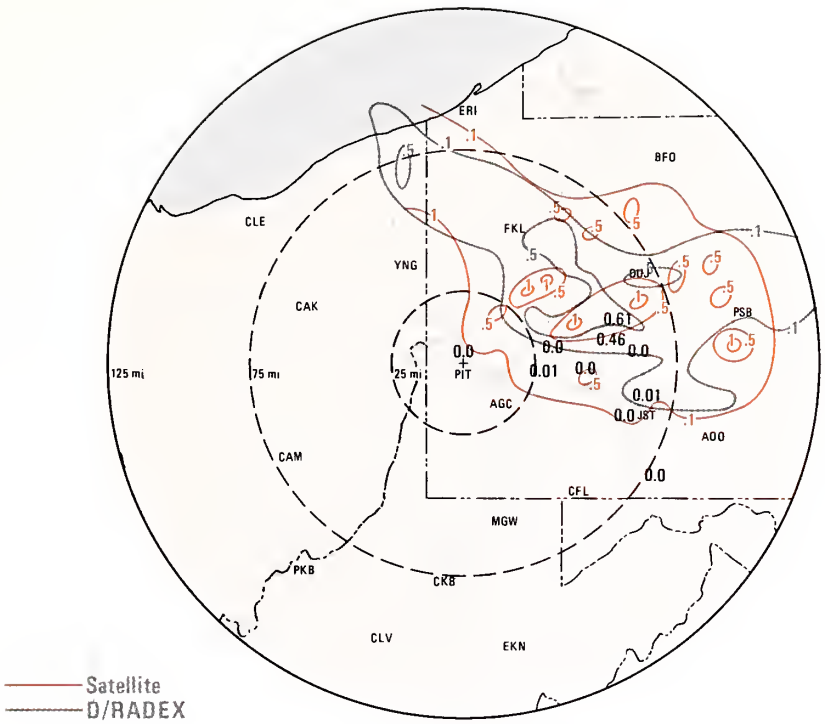

Figure 11f. Hourly rainfall analyses for 2300-2400 GMT, July 19, 1977.

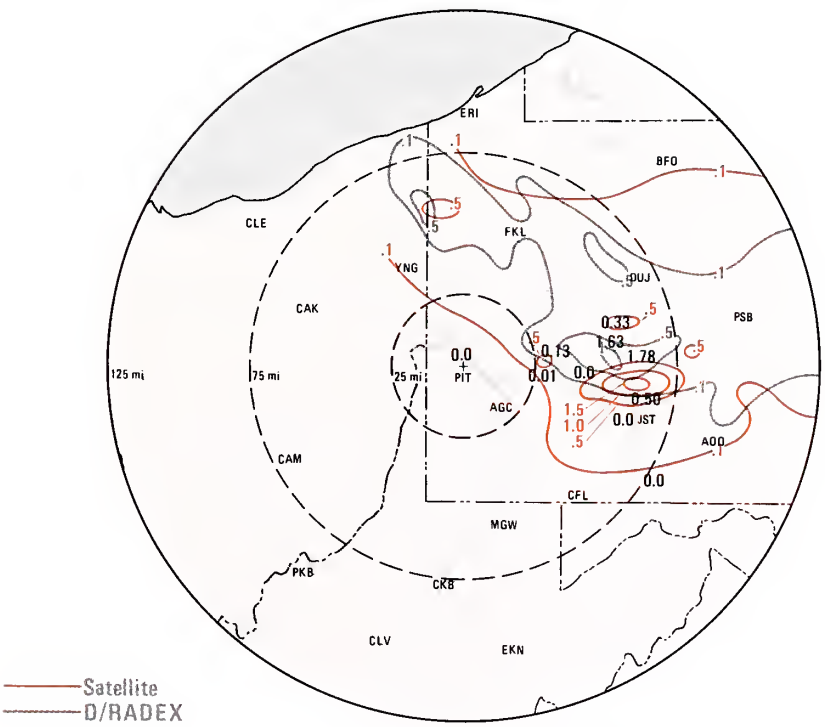

Figure 11g. Hourly rainfall analyses for 0000-0100 GMT, July 20, 1977.

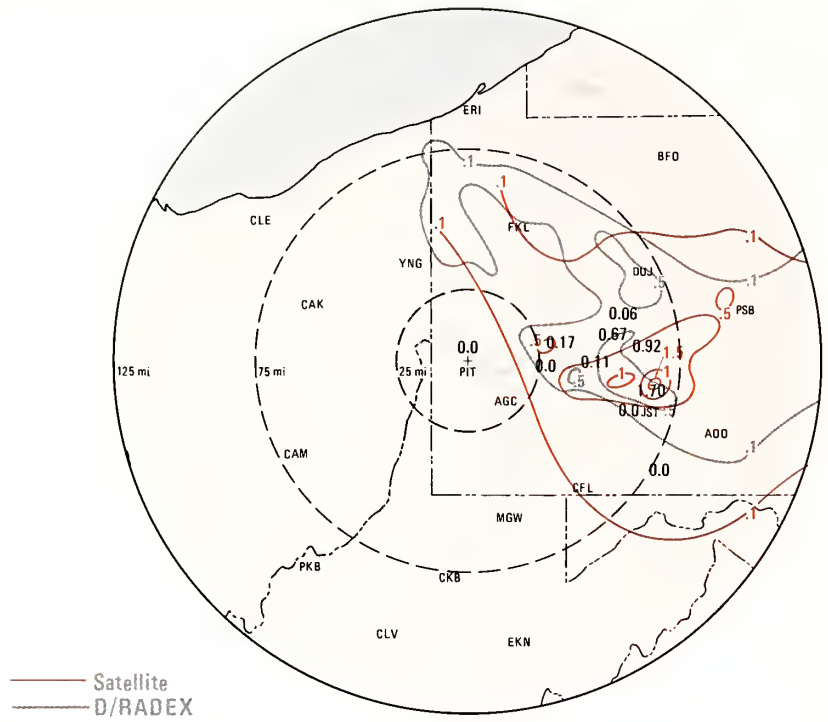

Figure 11h. Hourly rainfall analyses for 0100–0200 GMT, July 20, 1977.

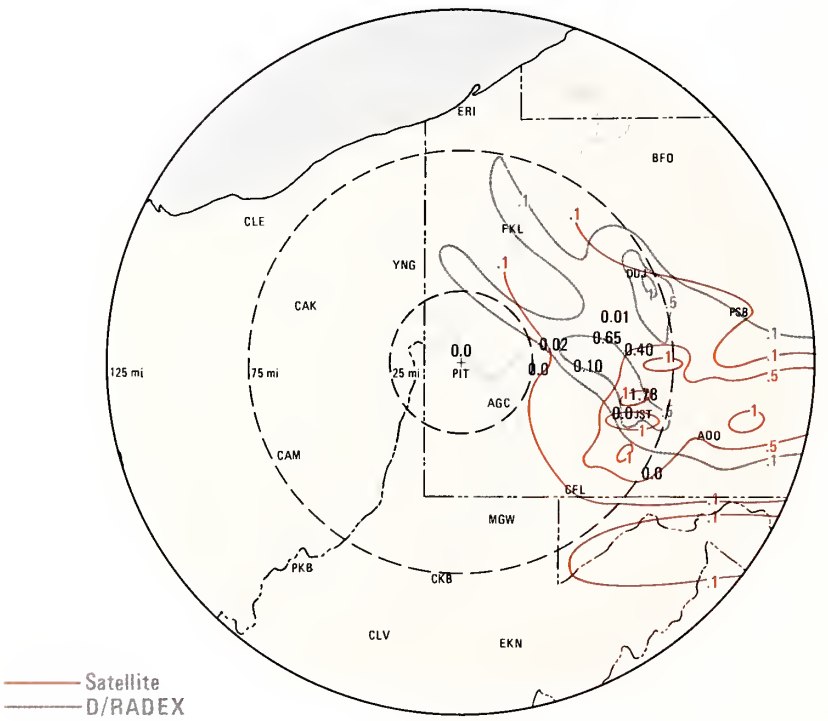

Figure 11i. Hourly rainfall analyses for 0200–0300 GMT, July 20, 1977.

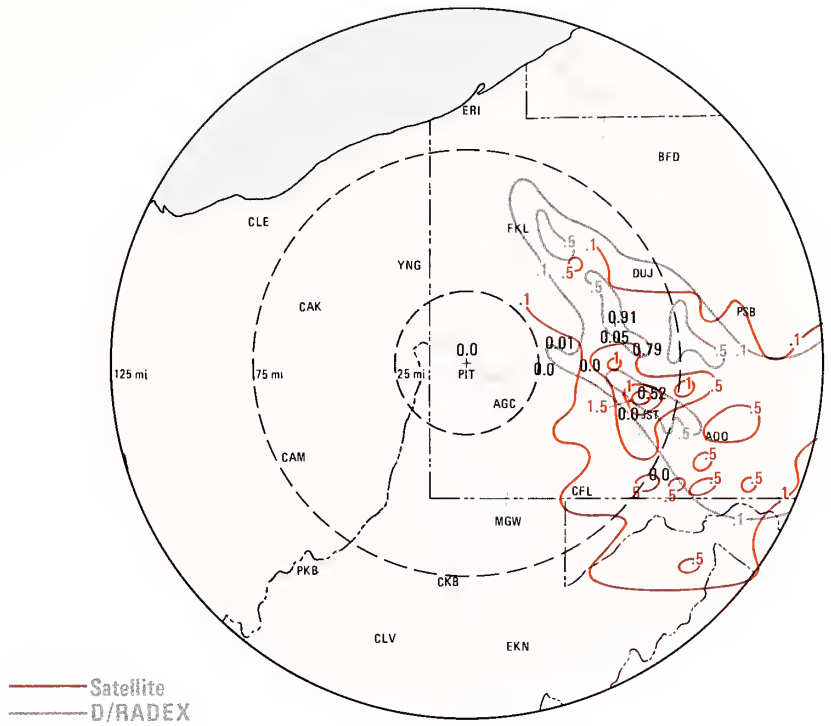

Figure 11j. Hourly rainfall analyses for 0300-0400 GMT, July 20, 1977.

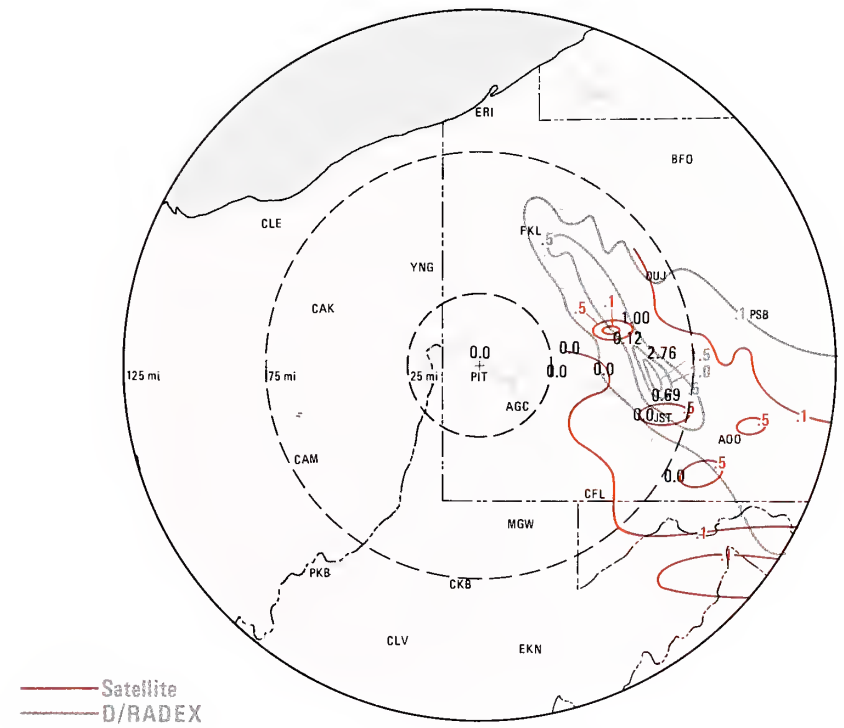

Figure 11k. Hourly rainfall analyses for 0400-0500 GMT, July 20, 1977. Note that the satellite analysis is for a 30-min period from 0400 to 0430 GMT.

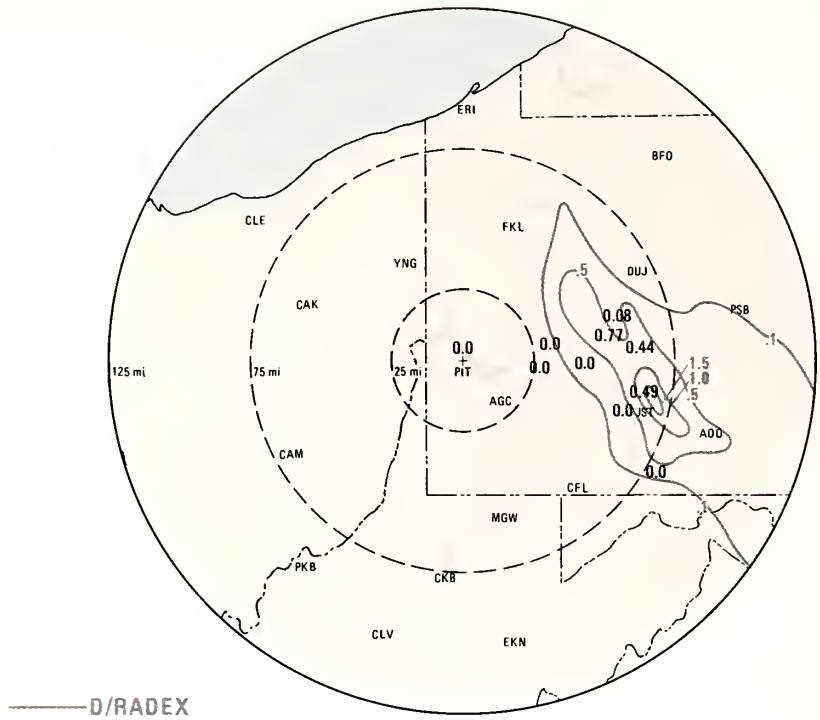

Figure 11l. Hourly rainfall analyses for 0500–0600 GMT, July 20, 1977.

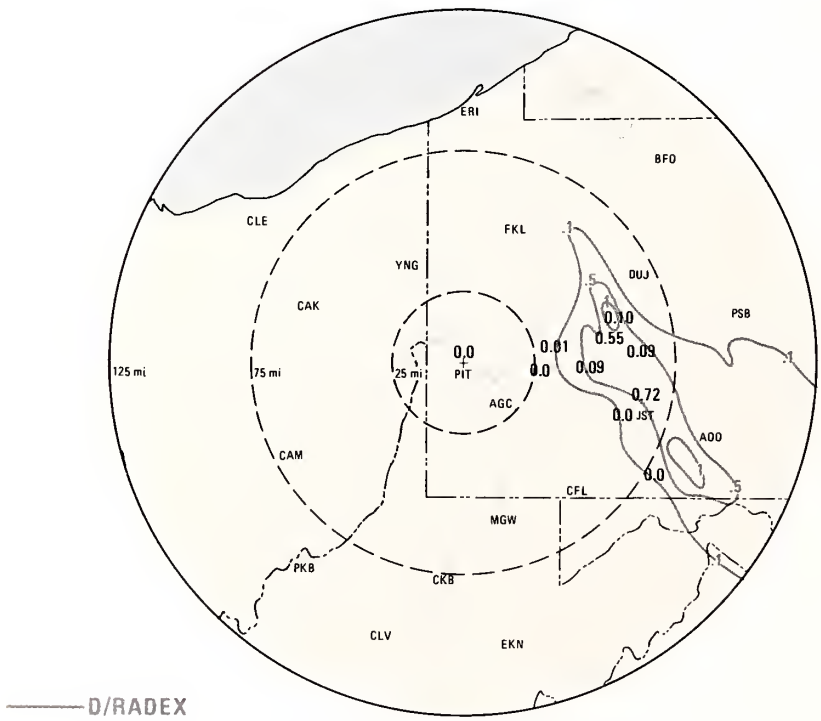

Figure 11m. Hourly rainfall analyses for 0600–0700 GMT, July 20, 1977.

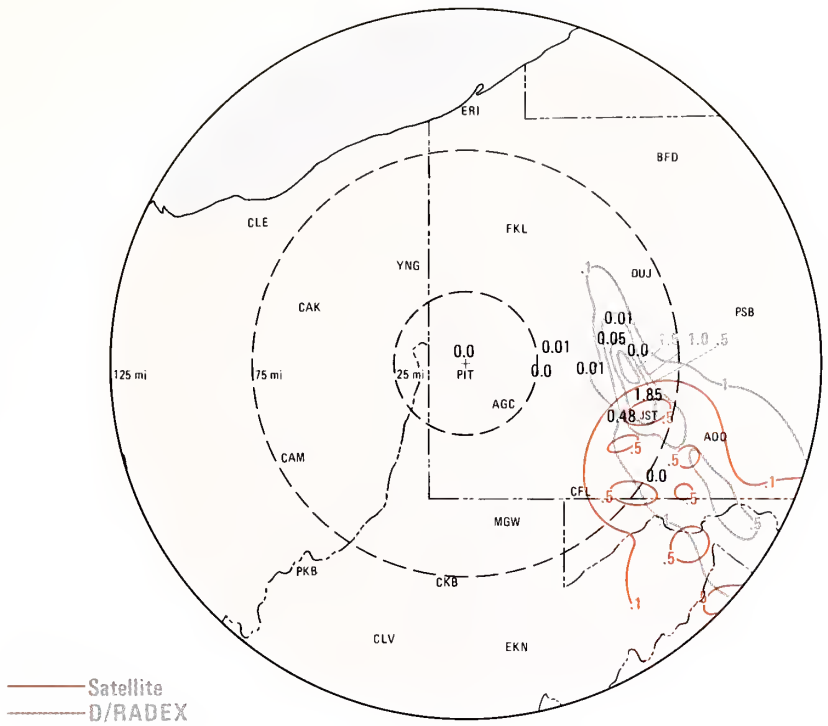

Figure 11n. Hourly rainfall in inches for 0700–0800 GMT, July 20, 1977. Note that the satellite analysis is for a 30-min period from 0730 to 0800 GMT.

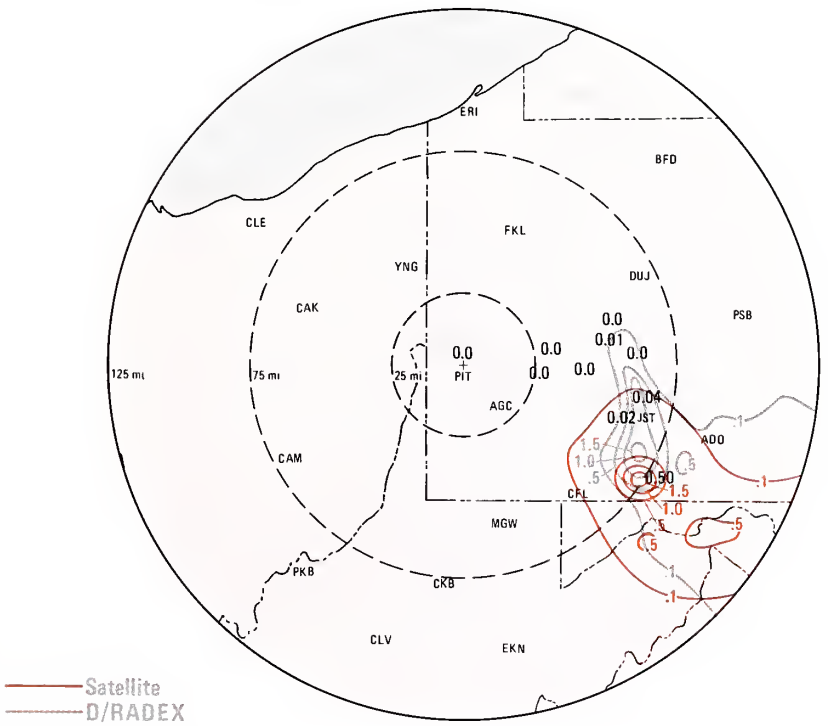

Figure 11o. Hourly rainfall analyses for 0800–0900 GMT, July 20, 1977.

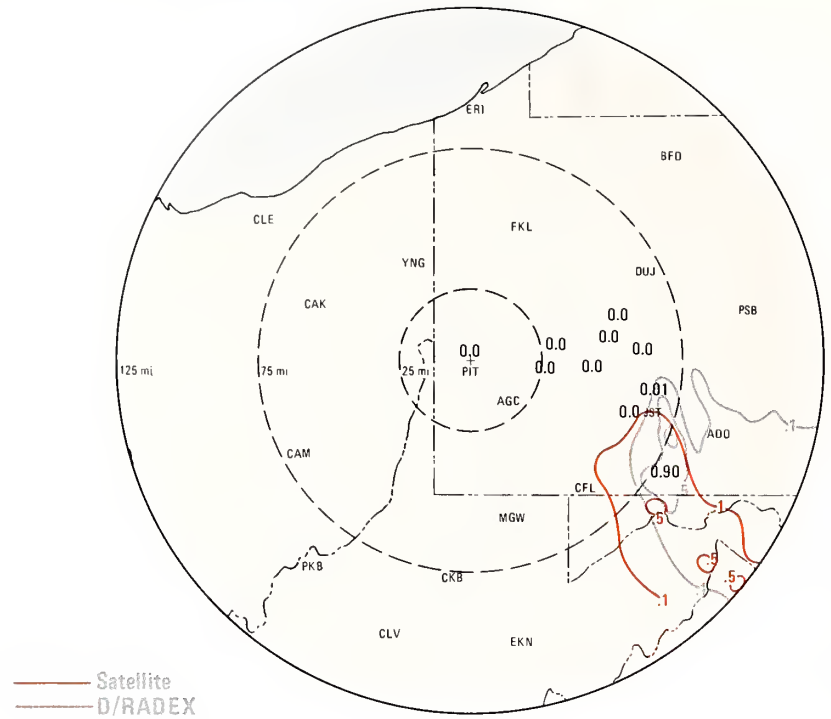

Figure 11p. Hourly rainfall analyses for 0900–1000 GMT, July 20, 1977.

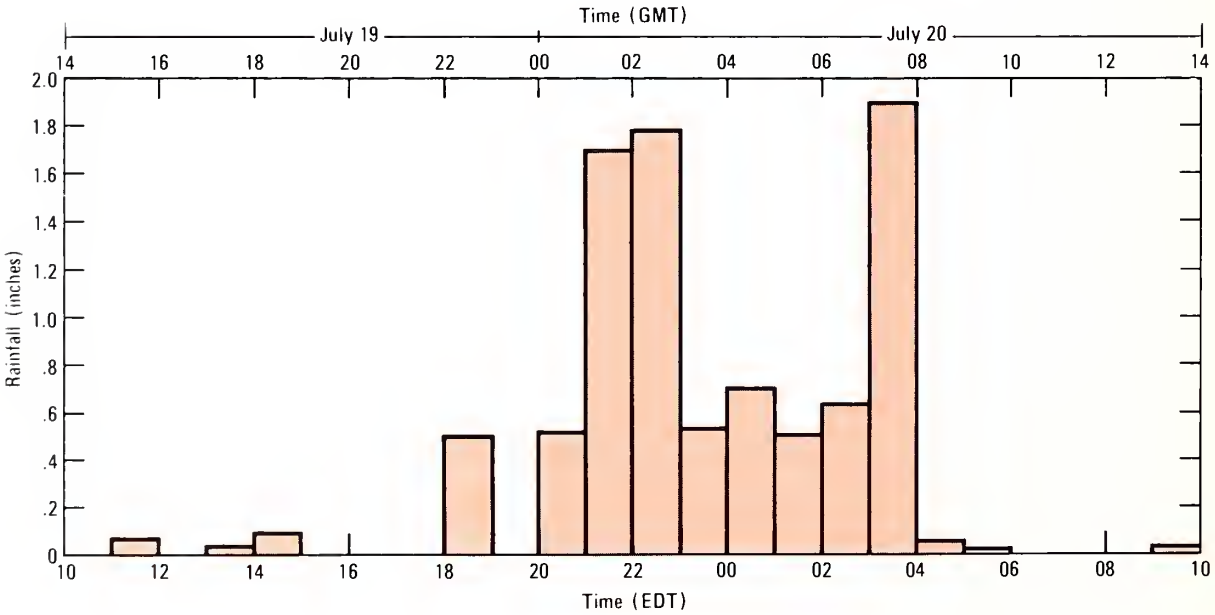

Figure 12a. Observed hourly rainfall at the Public Safety Building, Johnstown, Pa.

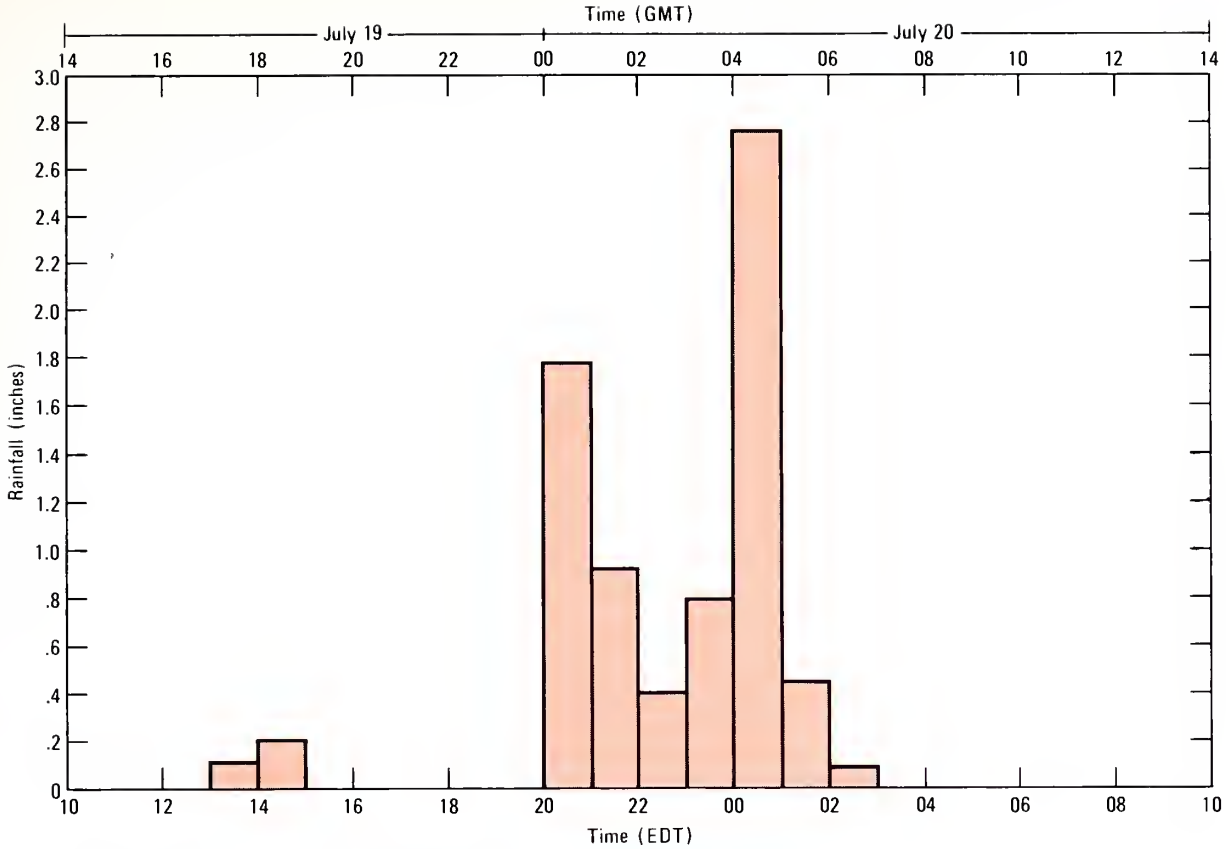

Figure 12b. Observed hourly rainfall at Strongstown, Pa.

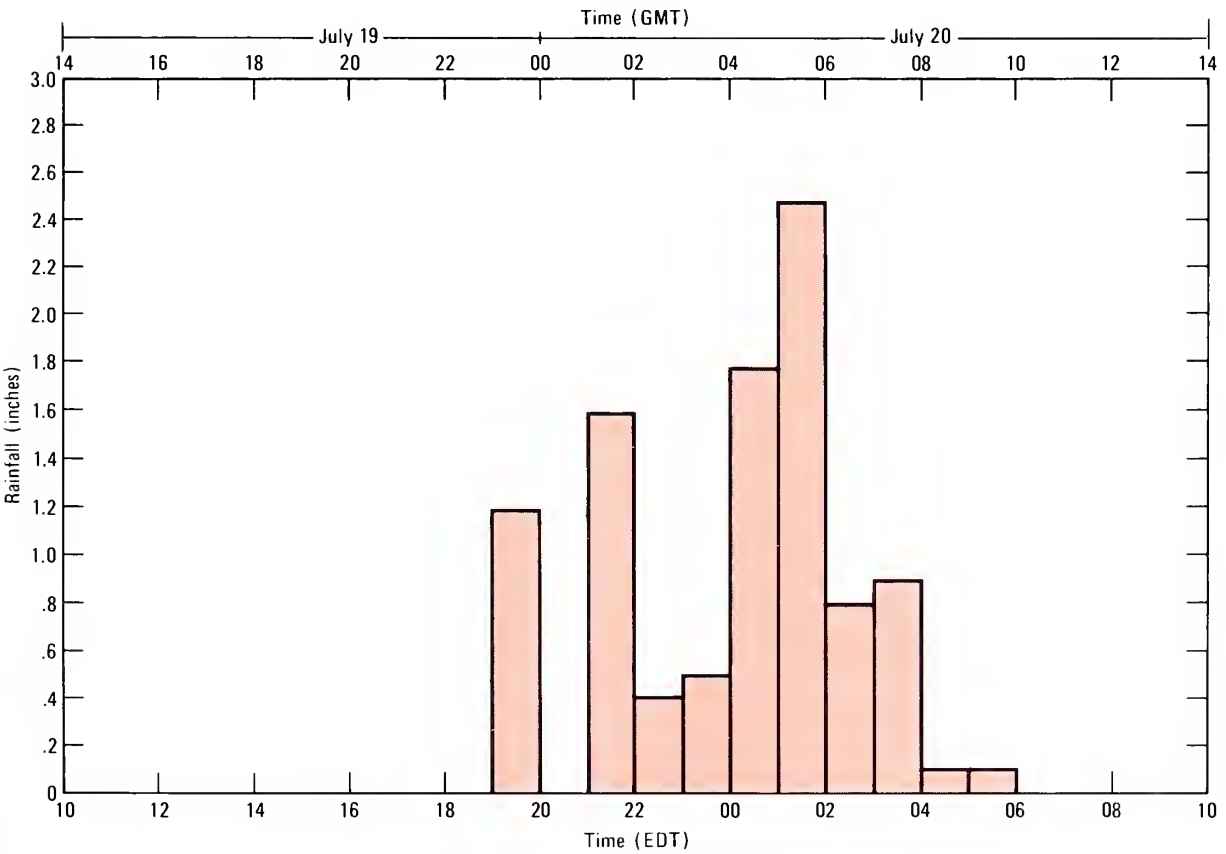

Figure 12c. Observed hourly rainfall at Dunlo, Pa.

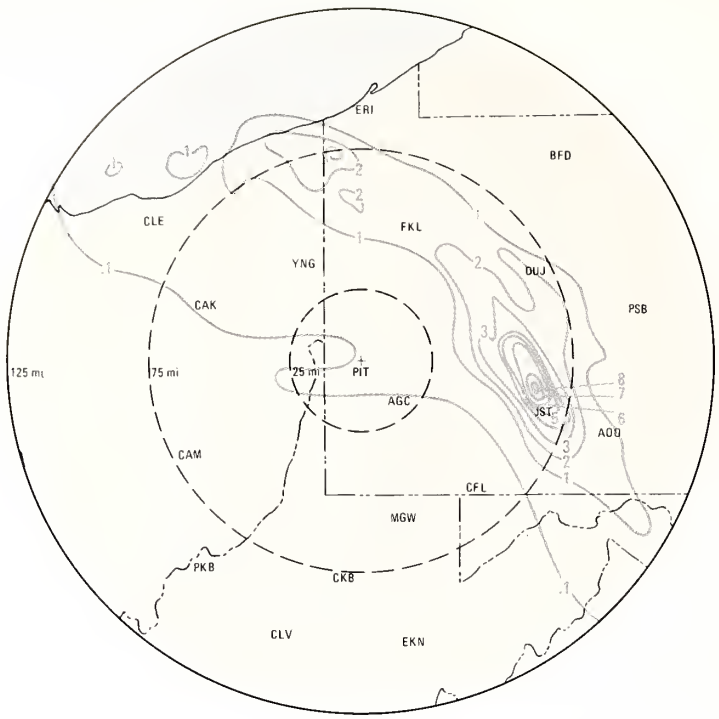

Figure 13. Total rainfall in inches (1200 GMT, July 19 to 1200 GMT, July 20, 1977) from D/RADEX.

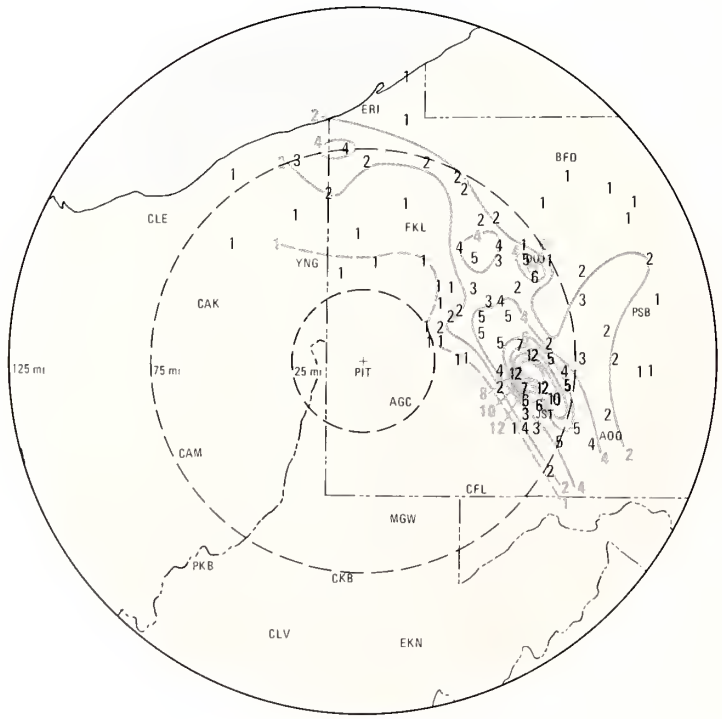

Figure 14a. Total observed rainfall in inches (1200 GMT, July 19 to 1200 GMT, July 20, 1977) for western Pennsylvania.

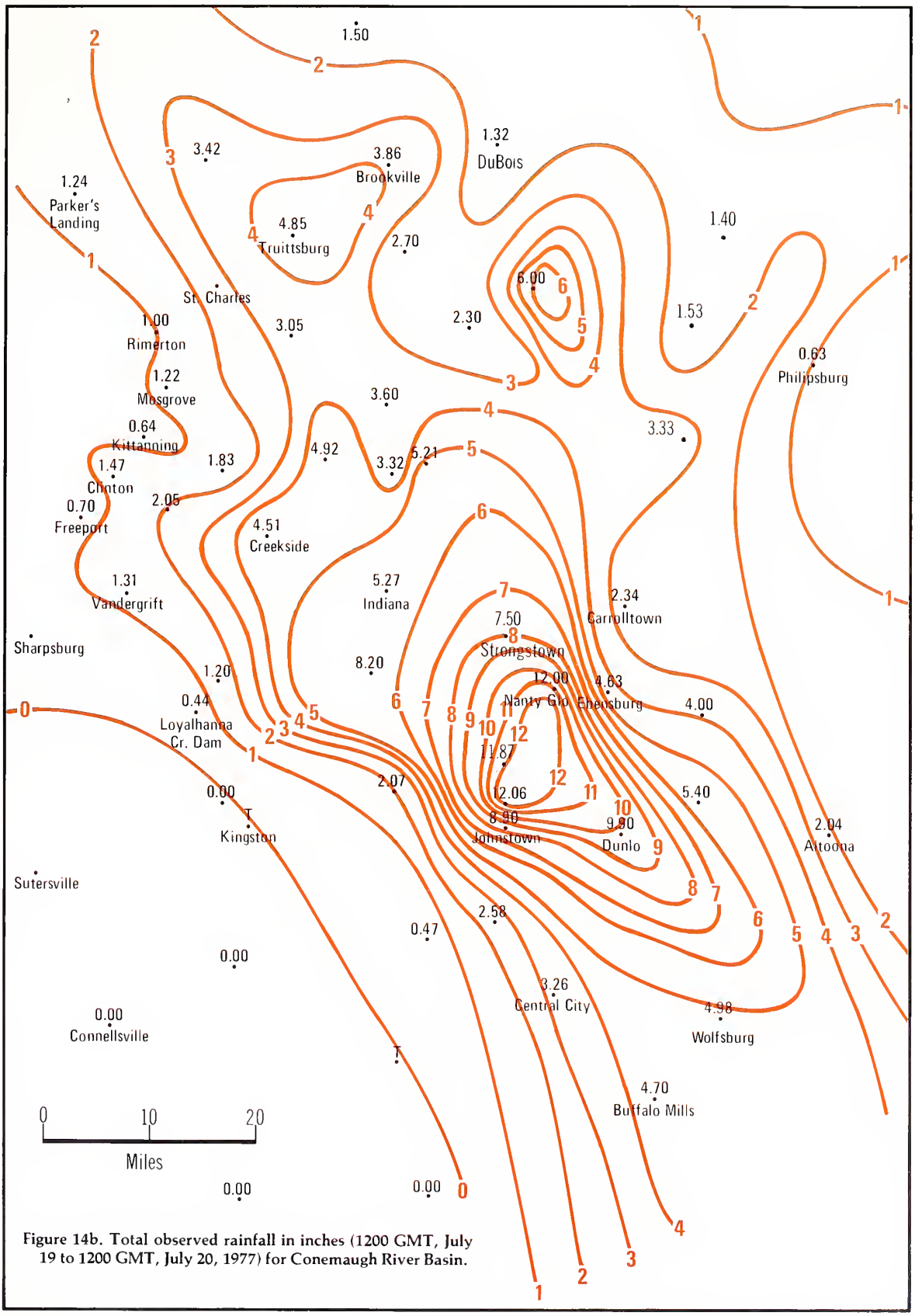

Figure 14b. Total observed rainfall in inches (1200 GMT, July 19 to 1200 GMT, July 20, 1977) for Conemaugh River Basin.

5. DISCUSSION AND SUMMARY

The July 19–20, 1977, flash floods in southwest Pennsylvania resulted when large-scale and mesoscale processes combined to focus excessive convective rains over a relatively small area. Circulation patterns associated with the large surface high off the Atlantic coast and the long-wave, upper-tropospheric ridge over the eastern United States provided a conditionally unstable atmosphere with abundant moisture over a large area of the Ohio Valley and central Appalachian Mountain region. Dynamic processes associated with a slowly moving short-wave trough destabilized the atmosphere and acted to trigger and maintain organized convection during the morning and afternoon of July 19.

In response to the convective activity during the afternoon and early evening, mesoscale pressure systems and low-level baroclinic zones were generated. In western Pennsylvania the boundary separating the rain-cooled air generated by previous thunderstorm activity became quasi-stationary nearly perpendicular to the warm, moist, low-level flow streaming in from Ohio. As this unstable air ascended over the rain-cooled air, new thunderstorms were triggered which then moved southeastward parallel to the outflow boundary. Each thunderstorm cell reinforced the temperature gradients along the outflow boundary, and maintained the triggering mechanism in a quasi-stationary position. The storms moved upslope into the western portions of the Appalachian mountains releasing maximum rainfalls in the hills to the north and east of Johnstown. This process continued for several hours, subjecting the region to a series of storms.

The quasi-stationary nature of the storm was eventually terminated as the short-wave trough moved into eastern Pennsylvania. Advection of somewhat drier mid-tropospheric air and development of weak subsidence with the trough passage over western Pennsylvania eventually suppressed development of new cells.

The meteorological conditions leading to the flood-producing rains around Johnstown are present during most significant flash floods (Maddox et al., 1978b). These storms appear to have several important characteristics: (1) very moist and conditionally unstable conditions with surface to 500 mb precipitable water substantially above normal; (2) a weak short-wave trough (meso-α scale) moving through a large-scale ridge which provides lifting and air mass destabilization; (3) weak wind shear through much of the cloud layer which contributes to high precipitation efficiencies; (4) frontal boundaries, topography, or cool outflow boundaries produced by earlier or existing convection which trigger additional storms and focus heavy rains over a relatively small region; (5) several cells which typically move over the same area, and (6) the tendency for flash-flood producing rainfall to occur at night.

6. REFERENCES

Fujita, T., H. Newstein, and M. Tepper, 1956. Meso-analysis—an important scale in the analysis of weather data. Res. Pap. 39, U. S. Weather Bureau, Wash., D. C., 83 pp.

Greene, D. R., and R. E. Saffle, 1978. Radar analysis of the 1977 Johnstown flash flood. Preprints, Conf. on Flash Floods: Hydrometeorological Aspects, Am. Meteor. Soc., Los Angeles, Calif., 176–180.

Lott, G. A., 1976. Precipitable water over the United States, Vol. 1: Monthly Means. NOAA Tech. Rep., NWS 20, 173 pp.

Maddox, R. A., and C. F. Chappell, 1978. Meteorological aspects of twenty significant flash flood events. Preprints, Conf. on Flash Floods: Hydrometeorological Aspects, Am. Meteor. Soc., Los Angeles, Calif., 1–9.

Maddox, R. A., L. R. Hoxit, C. F. Chappell, and F. Caracena, 1978a. Comparison of meteorological aspects of the Big Thompson and Rapid City floods. *Mon. Wea. Rev.*, 106:375–389.

Maddox, R. A., C. F. Chappell, and L. R. Hoxit, 1978b. Synoptic and meso-α scale aspects of flash flood events. Accepted for publication in *Bull. Am. Meteor. Soc.*

Magor, B. W., 1959. Mesoanalysis: some operational analysis techniques utilized in tornado forecasting. *Bull. Am. Meteor. Soc.*, 40:499–511.

Maurwitz, J. D., 1972. Precipitation efficiency of thunderstorms on the high plains. *J. Rech. Atmos.* (Dessens Memorial Issue), 6:367–370.

Mogil, H. M., and H. S. Groper, 1976. On the short range prediction of localized excessive convective rainfall. Preprints, Conf. on Hydrometeorology, Am. Meteor. Soc., Ft. Worth, Tex., 9–12.

NOAA, 1977. Johnstown, Pennsylvania, flash flood of July 19–20, 1977. Natural Disaster Survey Report 77–1, U. S. Dept. of Commerce, Rockville, Md., 60 pp.

Scofield, R. A., and V. J. Oliver, 1977a. A scheme for estimating convective rainfall from satellite imagery. NOAA-NESS Technical Memorandum 86, U. S. Dept. of Commerce, Washington, D. C., 47 pp.

Scofield, R. A., and V. J. Oliver, 1977b. Using satellite imagery to estimate rainfall from two types of convective systems. Preprints, Tenth Tech. Conf. on Hurricanes and Tropical Meteorology, Am. Meteor. Soc., Boston, Mass., 204–211.

APPENDIX A
UPPER-AIR ANALYSES AND COMPARABLE GOES-1 VISIBLE IMAGERY

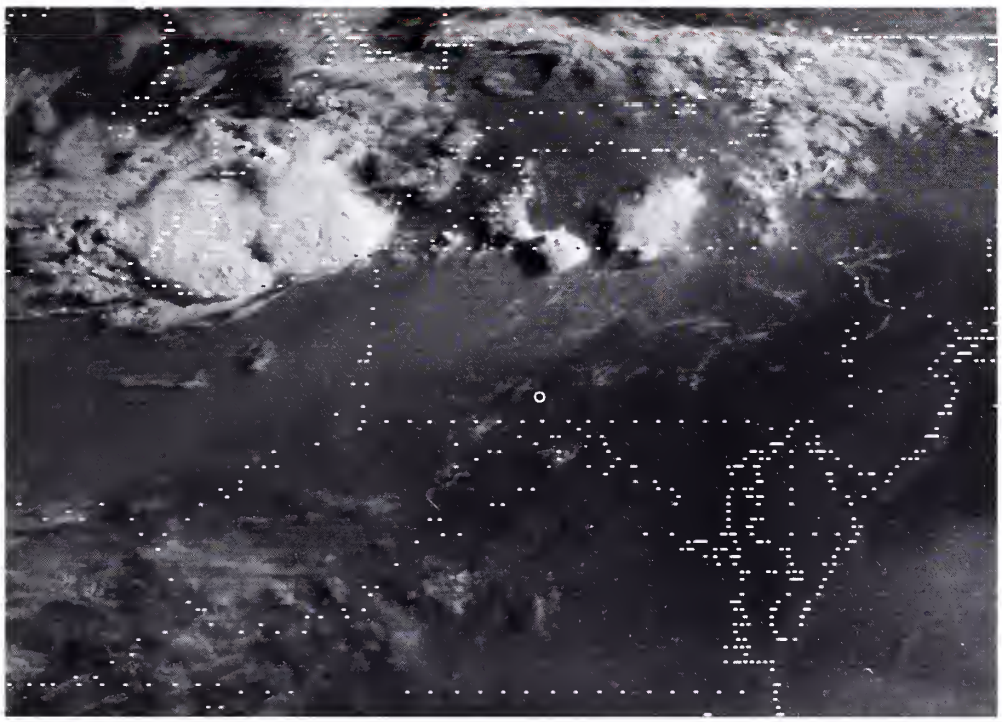

Figure A1a. GOES-1 visible imagery (1 km resolution) for 1200 GMT, July 19, 1977.

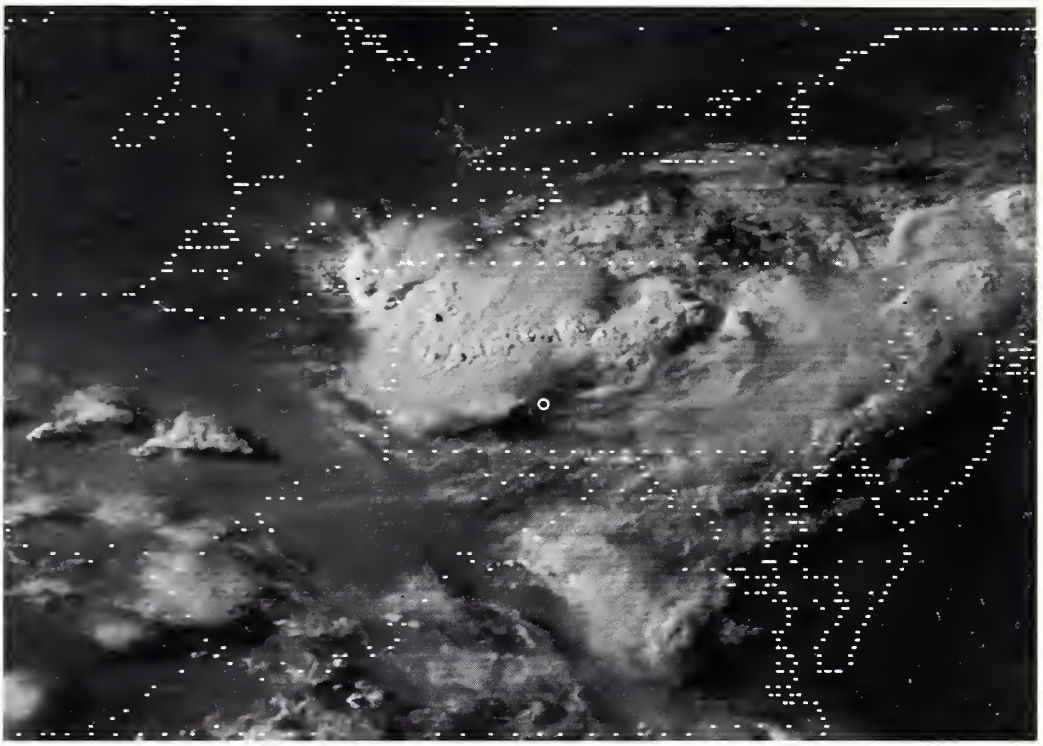

Figure A1b. Visible imagery for 2300 GMT, July 19, 1977.

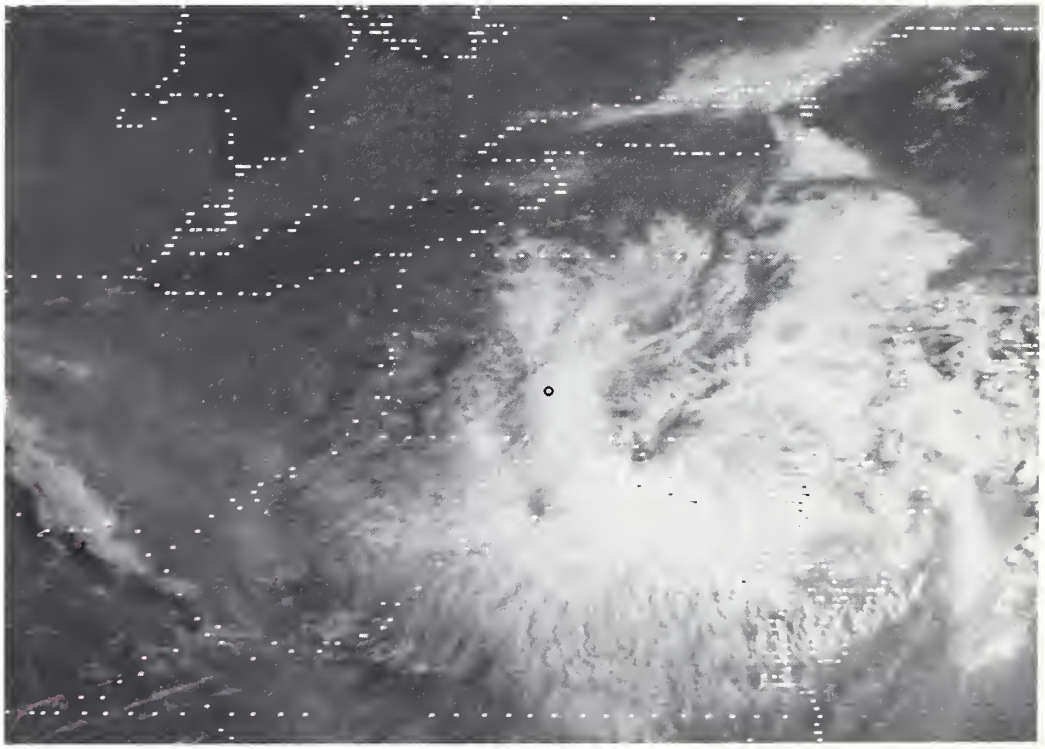

Figure A1c. Visible imagery for 1200 GMT, July 20, 1977.

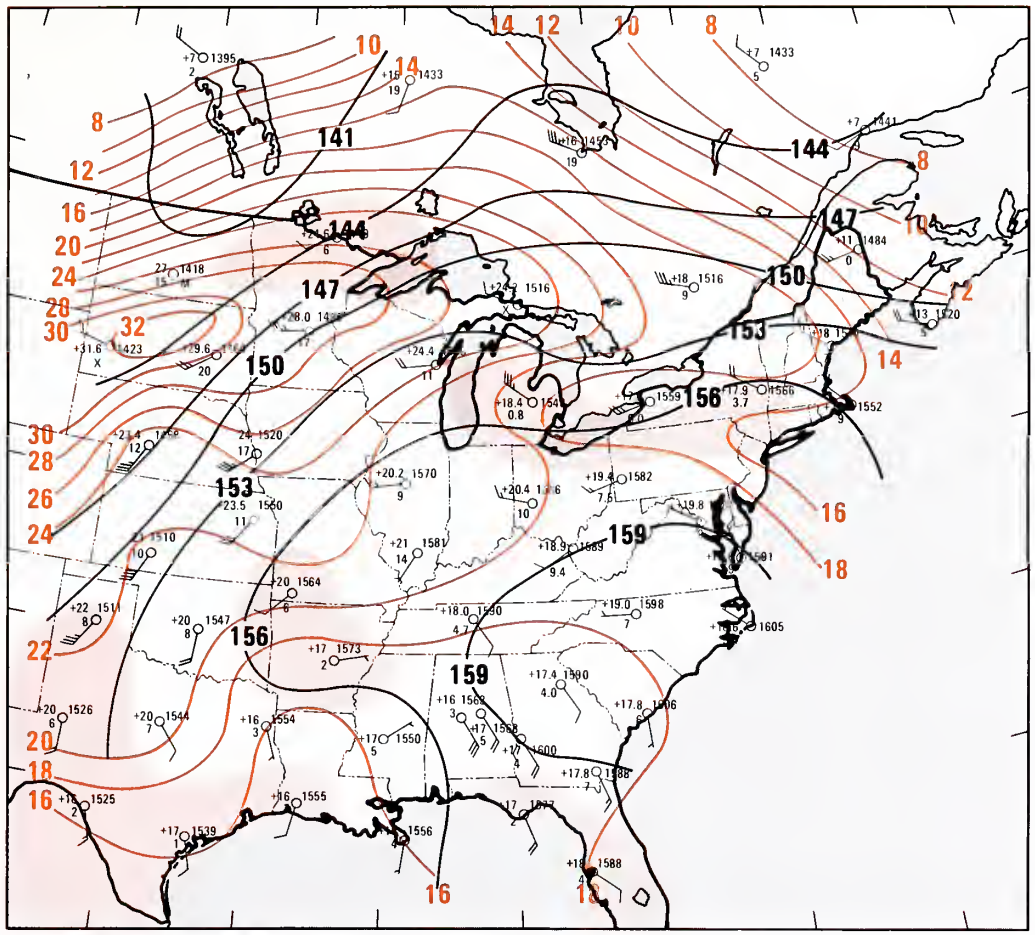

Figure A2a. 850 mb analysis for 1200 GMT, July 19, 1977. Height centers, trough lines, and height contours at 30-m intervals (156=1560 m) are in black. Isotherms for 2°C intervals are in orange; moist regions with dew point temperatures ≥14°C are shaded orange.

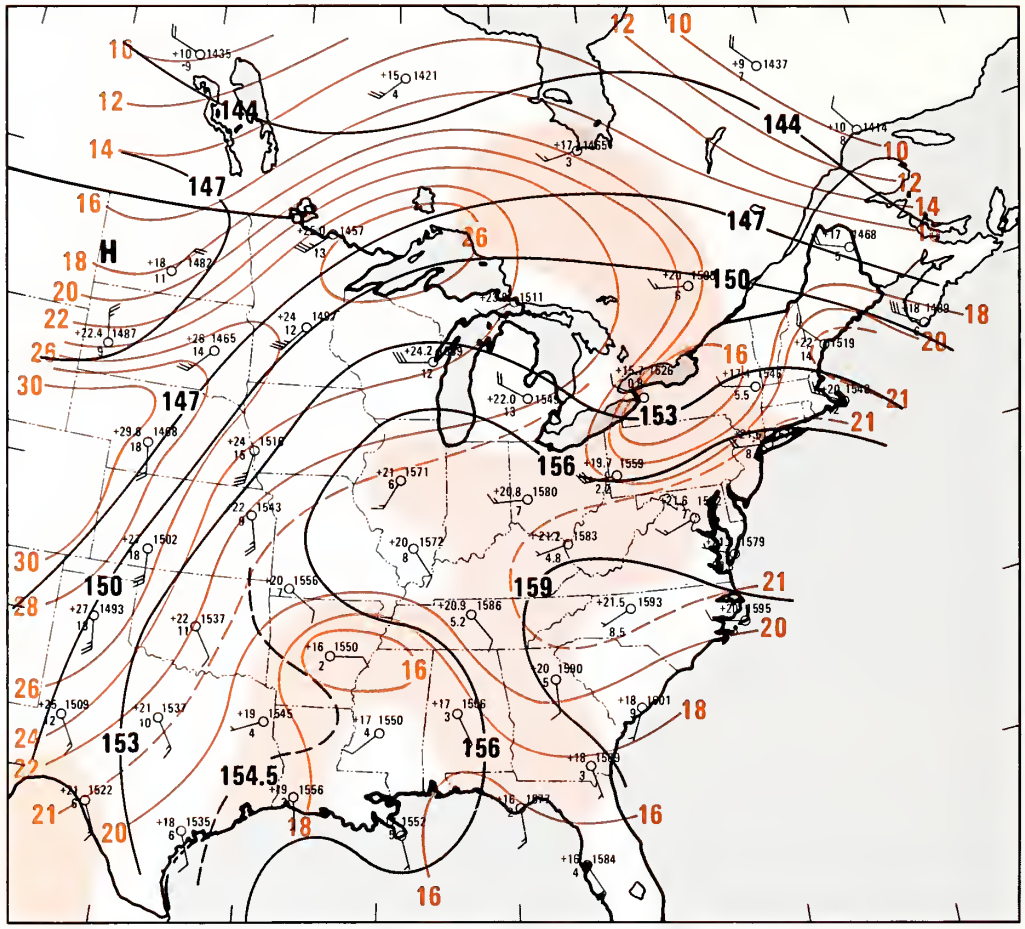

Figure A2b. 850 mb analysis for 0000 GMT, July 20, 1977.

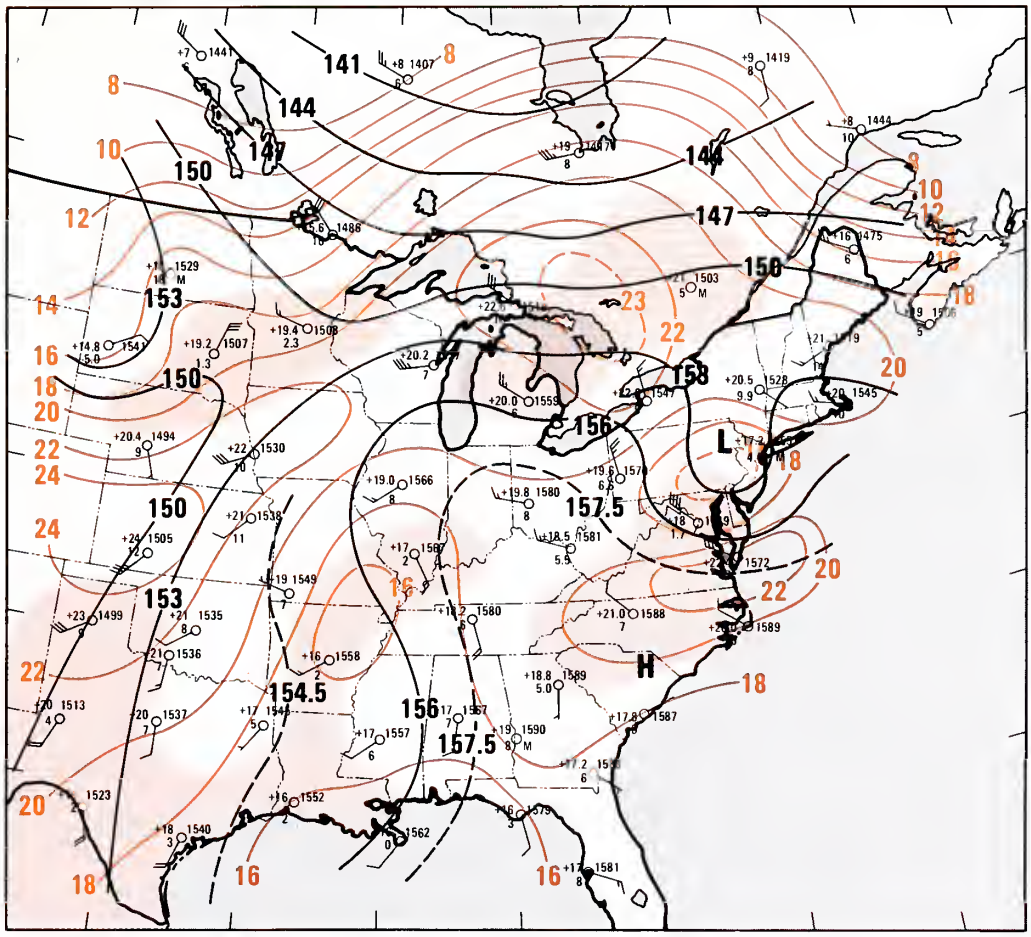

Figure A2c. 850 mb analysis for 1200 GMT, July 20, 1977.

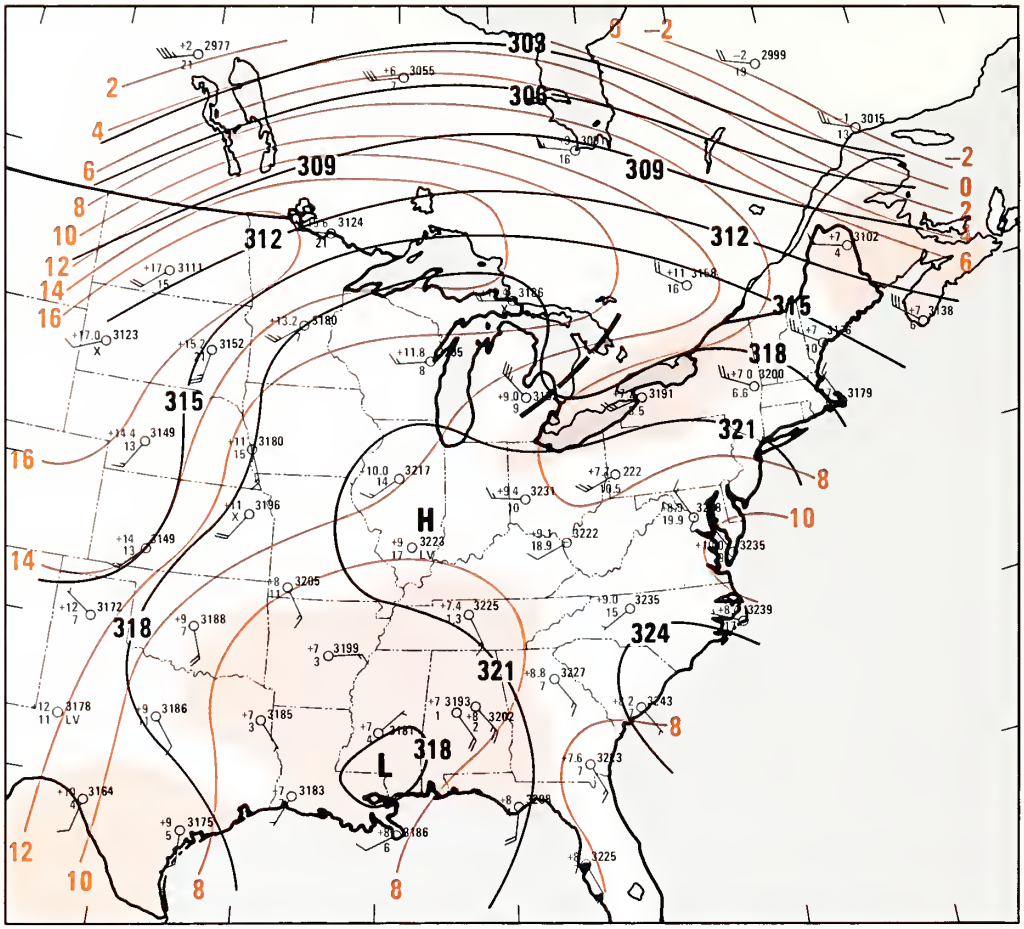

Figure A3a. 700 mb analysis for 1200 GMT, July 19, 1977. Height centers, trough lines, and height contours at 30-m intervals (321 = 3210 m) are in black. Isotherms for 2 °C intervals are in orange; moist regions with $T-T_d \leq 6$ °C are shaded orange.

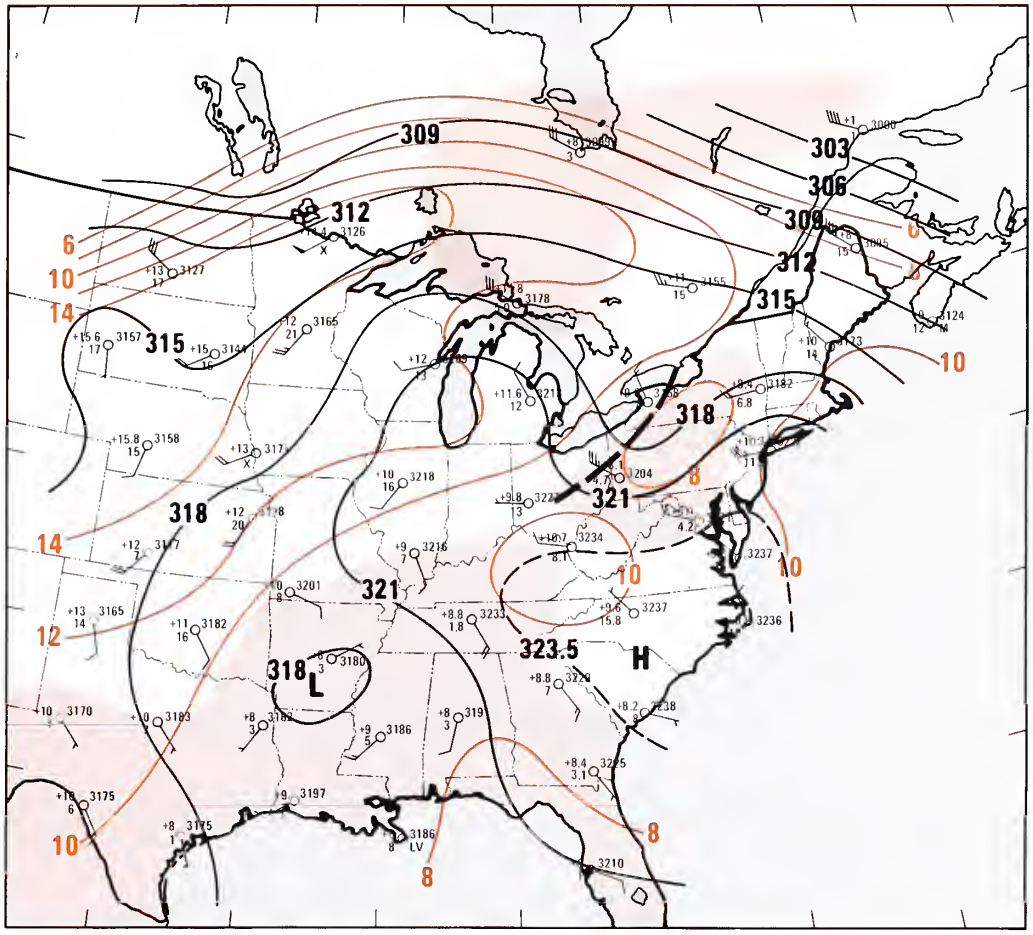

Figure A3b. 700 mb analysis for 0000 GMT, July 20, 1977.

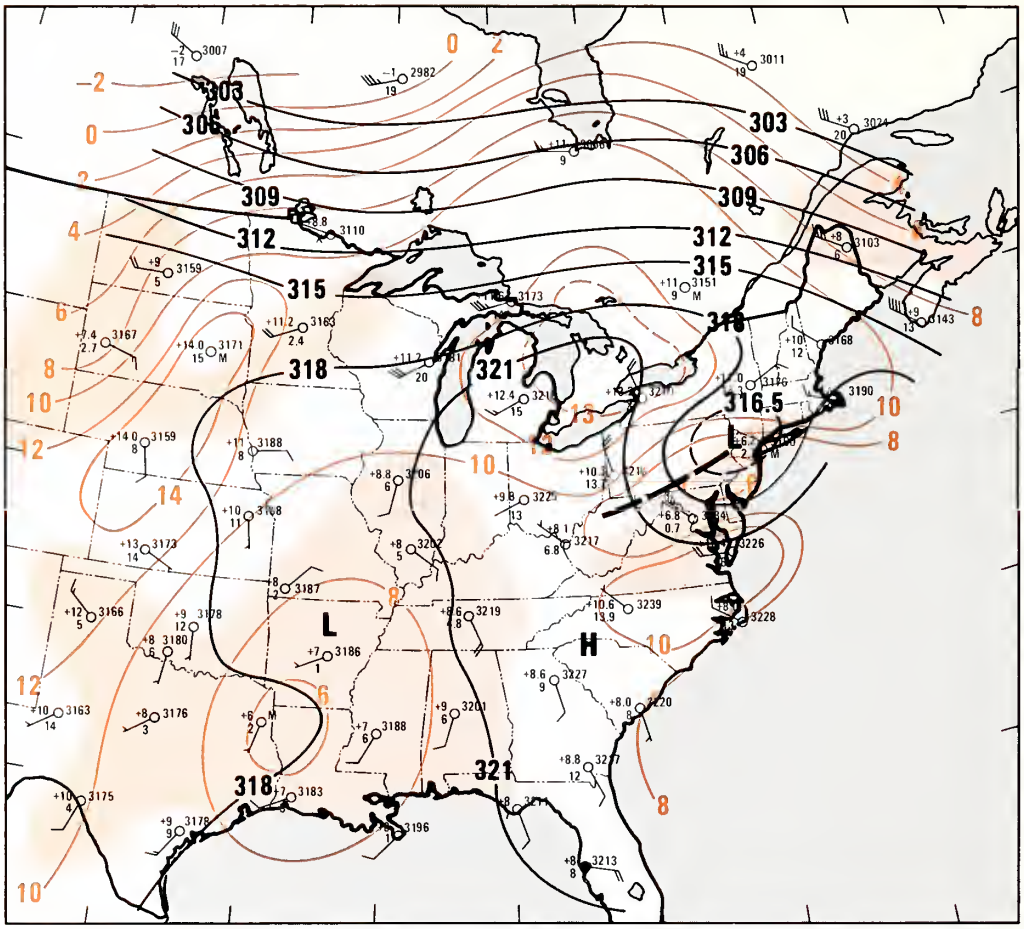

Figure A3c. 700 mb analysis for 1200 GMT, July 20, 1977.

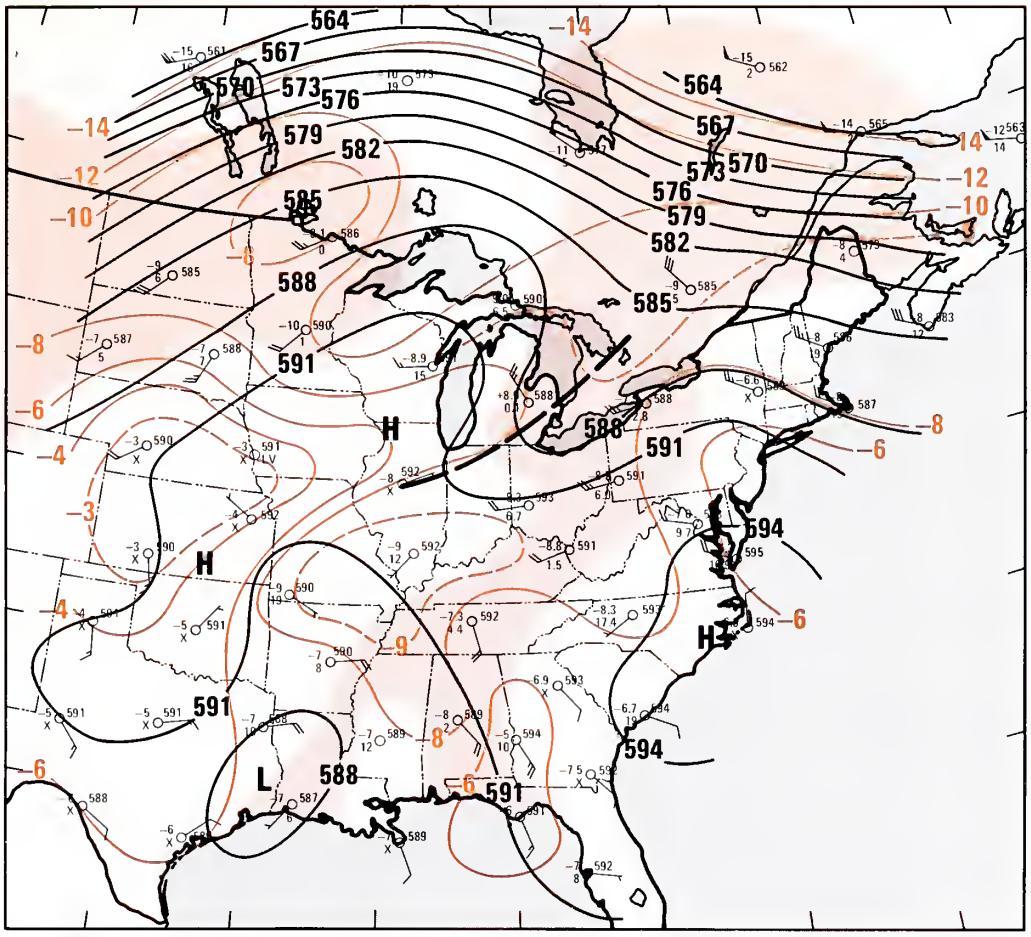

Figure A4a. 500 mb analysis for 1200 GMT, July 19, 1977. Height centers, trough lines, and height contours at 30-m intervals (591 = 5910 m) are shown in black. Isotherms for 2 °C intervals are in orange; moist regions with $T-T_d \leq 6$ °C are shaded orange.

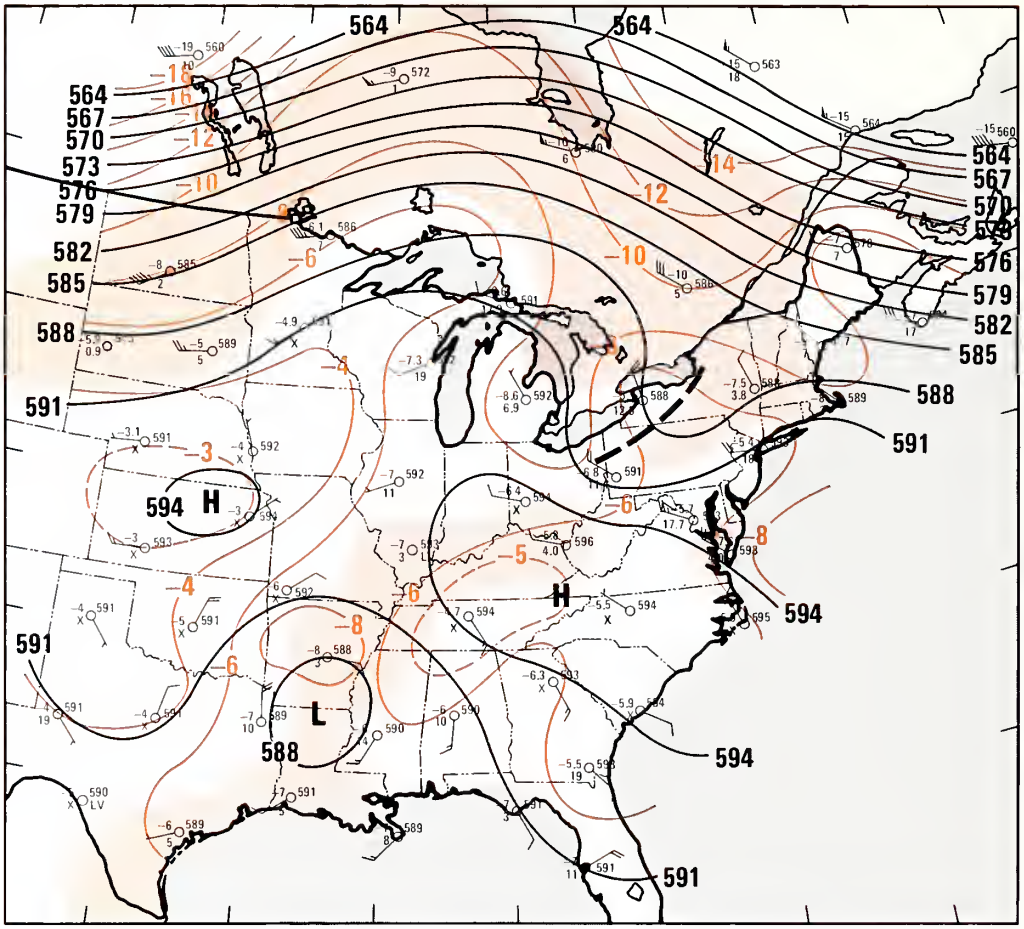

Figure A4b. 500 mb analysis for 0000 GMT, July 20, 1977.

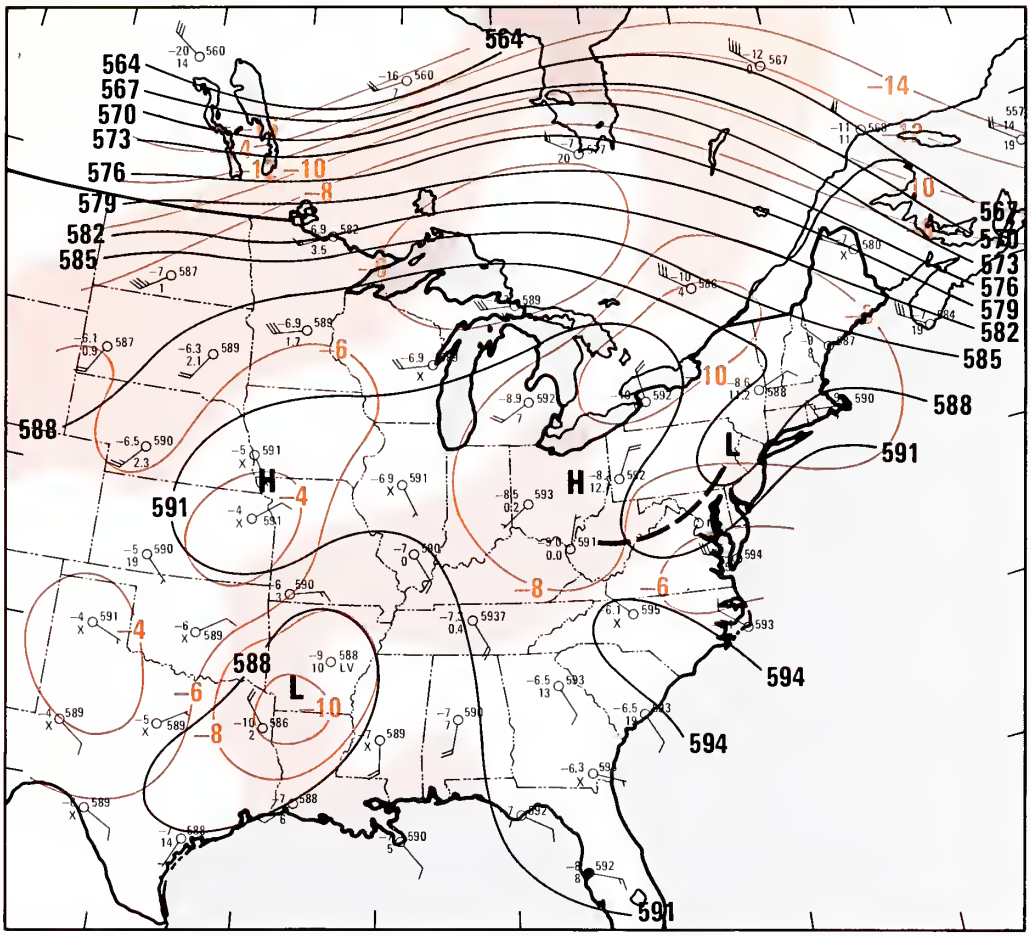

Figure A4c. 500 mb analysis for 1200 GMT, July 20, 1977.

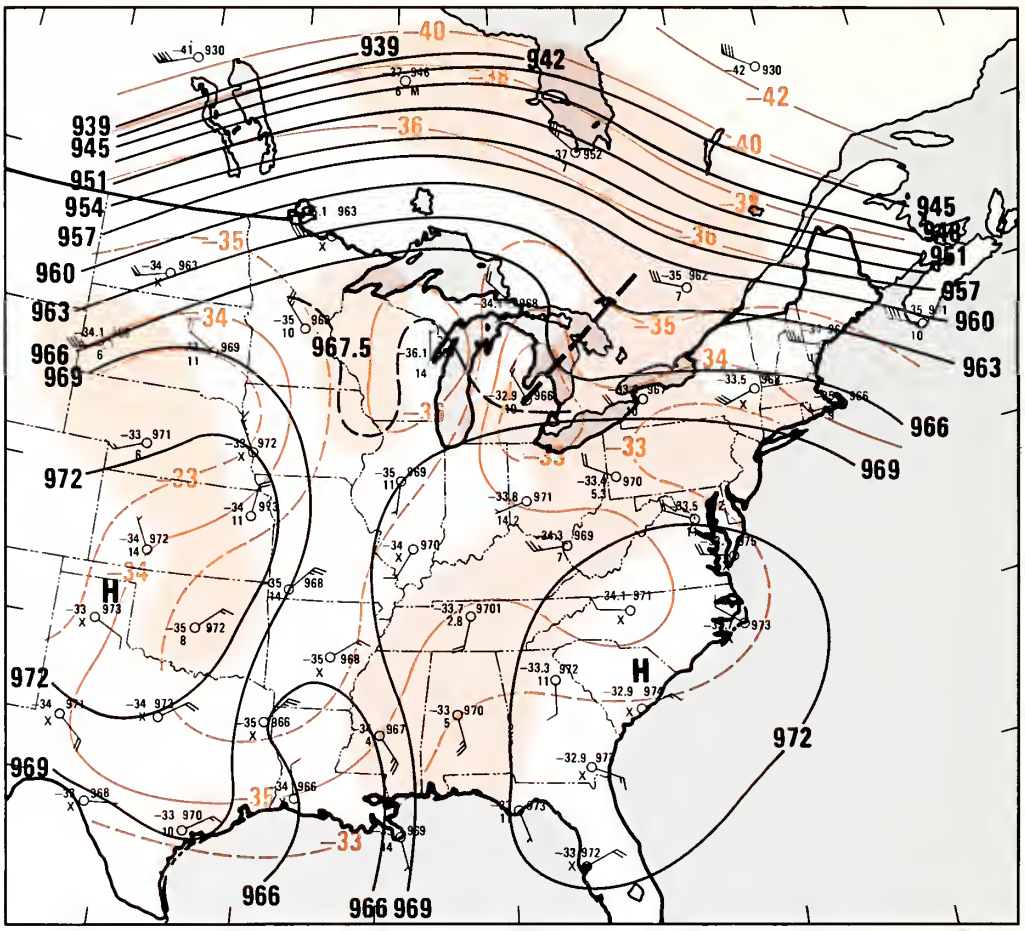

Figure A5a. 300 mb analysis for 1200 GMT, July 19, 1977. Height centers, trough lines, and height contours at 30-m intervals (966 = 9660 m) are in black. Isotherms for 2°C intervals are in orange; moist regions with $T-T_d \leq 10°C$ are shaded orange.

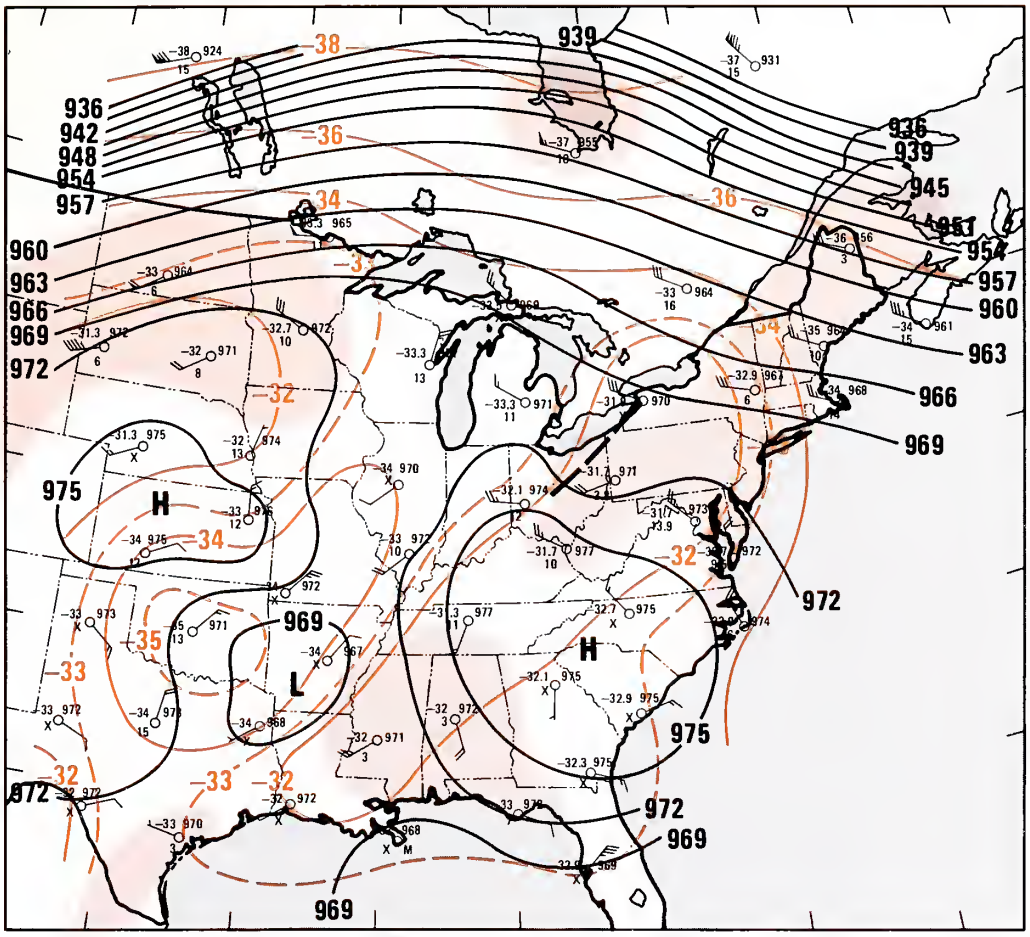

Figure A5b. 300 mb analysis for 0000 GMT, July 19, 1977.

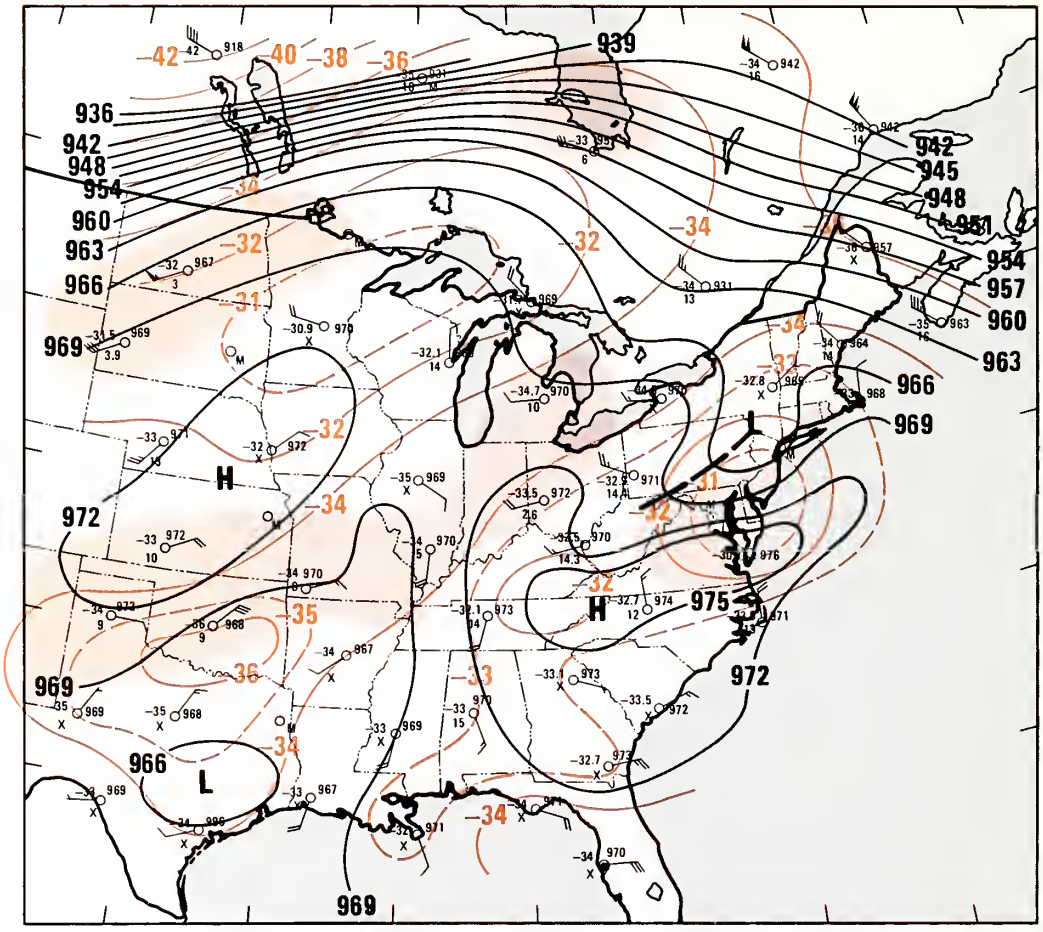

Figure A5c. 300 mb analysis for 1200 GMT, July 20, 1977.

Appendix B

D/RADEX RAINFALL ESTIMATES

Douglas R. Greene

Office of Hydrology, National Weather Service, NOAA
Silver Spring, Maryland

Robert E. Saffle
Techniques Development Laboratory
National Weather Service, NOAA
Silver Spring, Maryland

1. INTRODUCTION

Timely radar data are a key element in a flash flood warning system. This section describes the National Weather Service (NWS) D/RADEX system and techniques used to derive the areal radar rainfall patterns presented in this report.

Any forecaster who has observed the morphology of rainfall patterns on radar can attest to its value in forecasting the onset and/or ending of precipitation. Two steps are involved in using radar as a forecasting tool. The first step is interpreting radar echoes in terms of concurrent weather; this procedure is often called "now-casting." The second step concerns predicting future behavior or movement of the echoes and the weather phenomena associated with them (Greene, 1975). Within the NWS most radar data are given to the user as qualitative videoscope displays. At most stations, these highly perishable data are reduced manually by field forecasters for interpretation, short-range forecasting, and warnings. Techniques for reducing these data manually frequently are impractical because the large quantities of radar data are too difficult to assimilate, and the visual extrapolation of radar data is often difficult because of rapid changes in small-scale echo characteristics. To study these problems in the real-time application of radar data, the NWS began in 1971 the Digitized Radar Experiment (D/RADEX).

2. D/RADEX

D/RADEX comprises four NWS WSR-57 weather radars located in midwestern United States (Kansas City, Mo.; Monett, Mo.; Oklahoma City, Okla.; Stephenville, Tex.) and a special test site at Pittsburgh, Pa. Each of these 10-cm radars is equipped with a video integrator and processor (VIP), a data processing system consisting of a Data General Nova 1200 minicomputer, and peripheral devices. The integrator output of each of 115 1-nmi-range bins is quantitized into one of 10 levels (digits 0 through 9) representing returned power bands varying in width from 4.5 to 6.5 dB. These raw data are collected in a 2-degree by 1-nmi format corresponding directly to the radar reception process.

For transmission and display, these instantaneous intensity values (each digit corresponds to given reflectivity or decibel term which in turn is related to precipitation intensity) are normally transformed to a Cartesian format. The exact configuration of the automated system and the derived and output products has continued to change as we have learned more about the system, improved output and display products, and employed efficient data compression techniques. As a result of six years of operational testing, a sophisticated data processing software package has been developed and implemented into the operational D/RADEX system. A complete description of this software is given by Saffle (1976).

3. RADAR PRECIPITATION ESTIMATES

The amount of power returned to a radar from a hydrometeor target is related to the intensity of precipitation. Quantitative precipitation estimates from weather radar measurements are obtained by using an empirical relationship between rainfall rate, R (mm/h), and the radar reflectivity factor Z (mm^6/m^3). To develop the Z-R relationship, the radar reflectivity factor and returned power are related through the radar equation

$$\overline{P_r} = \frac{C|K|^2}{r^2} Z. \qquad (1)$$

In this simplified form $\overline{P_r}$ is the average power returned to the radar receiver from a volume of precipitation particles, $|K|^2$ is the dielectric factor, C is a constant determined from the characteristics of the radar, and r is the range to the precipitation target. If Rayleigh scattering is assumed (valid when the drop diameter d is small in comparison to the radar wavelength),

$$Z = \Sigma\, d_i^6. \qquad (2)$$

The most commonly used relationship is the one proposed by Marshall and Palmer (1948),

$$Z = 200\, R^{1.6}. \qquad (3)$$

Other investigators have developed similar relationships having different coefficients and exponents. The difference in these relationships can probably be attributed to errors in radar calibration, beam filling errors, and variations of in-cloud drop-size distribution due to meteorological factors. Because of changes of in-cloud drop-size distribution

during the life cycle of storms and in different cloud forms, the best of these relationships fit only average conditions (Greene, 1975).

Early experience in D/RADEX indicated that rainfall rates obtained through applying the Marshall-Palmer equation must be increased by a factor of 2.25 to be consistent with observed convective rainfall rates (Greene and Clark, 1974). The equation resulting from applying this factor to Equation 3 is

$$Z = 55\,R^{1.6}. \qquad (4)$$

In the NWS, rainfall is currently measured and forecast in inches; therefore in D/RADEX rainfall estimates obtained by use of Equation 4 must be converted from mm/h to in/h.

Further experience in D/RADEX showed that Equation 4 overestimated rainfall at higher signal return levels, i.e., D/RADEX digital levels of 8 and 9. These higher reflectivity values are frequently isolated and often attributed to hail shafts. Therefore, for operational applications D/RADEX rainfall estimation rates were modified to the ones given in the table. This table was developed by applying Equation 4 to the midpoint power returned values for D/RADEX levels 1 to 7 and by fixing levels 8 and 9 to a value of 7.09 in/h.

Ideally, different radar-rainfall relationships should be used for different synoptic events and different precipitation forms (i.e., frozen vs. liquid). To accomplish this, sophisticated real-time identification and classification techniques requiring three-dimensional radar data would be necessary (Greene, 1975). This approach would be possible in the D/RADEX type system since it can collect a complete scan of three-dimensional digital data inside a radius of 125 nmi within a period of less than 5 min (see Saffle, 1976).

Table B1. Rainfall rates for D/RADEX levels.

D/RADEX Level	Rainfall Rate (in/h)	
	Range	Midpoint value assigned
1	.045- .11	.07
2	.11 - .23	.16
3	.23 - .45	.34
4	.45 -1.13	.68
5	1.13 -2.25	1.58
6	2.25 -4.50	3.15
7	4.50 -7.09	7.09
8	7.09	7.09
9	7.09	7.09

NWS is now investigating the development of "decision-tree" procedures to accomplish precipitation typing.

In practice, areal rainfall estimates are computed over a 3-nmi by 5-nmi rectangular grid covering the 125-nmi radar umbrella. One 3-nmi by 5-nmi grid box may contain several 2-degree by 1-nmi data bins depending on the range from the radar. To obtain rainfall amounts each digit representing the intensity level from the 2-degree by 1-nmi bin falling within a given 3-nmi by 5-nmi grid box is converted to rainfall rate by using the table, and all these values are averaged to obtain the rainfall rate for the grid box. These grid values are then averaged with those for the previous observation to yield an average hourly rainfall rate for each grid box for the time period covered by the two observations. The average rates are multiplied by the fraction of an hour represented by the time period to get an average rainfall accumulation over each grid box. These short period accumulations are summed over various longer periods to satisfy different user requirements.

The D/RADEX system at the Pittsburgh, Pa., Weather Service Meteorological Observatory was operational the night of July 19–20, 1977, during the disastrous Johnstown flash flood. Figures 11a through 11p present hourly rainfall estimates, and Figure 14a presents the 24-h rainfall for the Johnstown event derived by the Pittsburgh D/RADEX system. A more detailed discussion of the radar analysis of the Johnstown flash flood can be found in Greene and Saffle (1978) and Saffle and Greene (1978).

4. APPENDIX B REFERENCES

Greene, D. R., and R. E. Saffle, 1978. Radar analysis of the 1977 Johnstown flash flood. Preprints, Conf. on Flash Floods: Hydrometeorological Aspects, Los Angeles, Calif., Am. Meteor. Soc., 176–180.

Greene, D. R., 1975. Operational use of digital radar in rainfall measurement and prediction. Proc. Symp. on Weather Radar and Water Management, Chester, England, Water Research Centre and Royal Radar Establishment, 55 pp.

Greene, D. R., and R. A. Clark, 1974. The operational use of digital radar data for flash flood monitoring. Symp. on Flash Floods, Tercentenary of Scientific Hydrology, IAHS–AISH Publ. No. 112, 100–105.

Marshall, J. S., and W. M. Palmer, 1948. The distribution of raindrops with size. *J. Meteor.*, 5:165–166.

Saffle, R. E., and D. R. Greene, 1978. The role of radar in the flash flood watch warning system: Johnstown examined. Preprints, 18th Conf. on Radar Meteorology, Atlanta, Ga., Am. Meteor. Soc., 468–473.

Saffle, R. E., 1976. D/RADEX products and field operation. Preprints, 17th Conf. on Radar Meteorology, Seattle, Wash., Am. Meteor. Soc., 555–559.

Appendix C

USING SATELLITE IMAGERY TO ESTIMATE CONVECTIVE RAINFALL

Roderick A. Scofield

Applications Division
National Environmental Satellite Service, NOAA
Washington, D. C.

A technique for computing rainfall estimates from satellite imagery is discussed herein. Scofield and Oliver (1977a) developed a timely technique using GOES infrared (IR) and visible pictures, which gives half-hourly or hourly rainfall estimates from convective systems. The Scofield/Oliver scheme is presented in the form of a decision tree. The scheme was designed for deep convective systems occurring in moist tropical air masses with high summer tropopauses.

The Scofield/Oliver technique is divided into three main parts: (1) separating the active portion of the convective system from the inactive portion, (2) making an initial estimate using enhanced IR alone, and (3) using successive pairs of high-resolution visible and enhanced IR pictures to pick out additional indications of heavier rainfall. Such indications include overshooting tops, merging thunderstorms, merging convective cloud lines, and rapidly expanding thunderstorm anvils.

When the thunderstorm anvil reaches high levels, such as the clouds in the Johnstown rainstorm, the picture geometry results in the tops being displaced from their true location away from the satellite subpoint. A system that gives the amount of displacement towards the subpoint has been described (NOAA, 1977). In this report, the above principle was used to make all the high cloud tops associated with the Johnstown rainstorm comparable (in location) with the radar and observed rainfall data.

The Scofield/Oliver system was designed to estimate rainfall at a point by comparing two consecutive pictures. In this report, we modified the scheme to give area rainfall. Using results and suggestions from our previous studies on tropical storm Dottie and a severe thunderstorm over Chicago (1977b), the point rainfall scheme was modified as follows.

Four basic steps are followed when estimating half-hourly area rainfall amounts from convective systems:

1. Locate the isohyet that separates the active area of significant rainfall (>0.05 inch/half hour) from the inactive area of little or no rainfall. The clues in Step 3 of the decision tree aid in separating the active area from the inactive area; the isoline separating these two areas is the 0.05-inch/half-hour isohyet. (Steps 3, 4, and 5 are explained in detail in Scofield and Oliver, 1977a.)

2. Locate the clouds associated with the heaviest rainfall and compute the rainfall there. Signatures in the imagery associated with heavier rainfall areas are very cold tops, rapidly expanding thunderstorm anvils, overshooting tops, thunderstorm mergers, and merging convective cloud lines. Isohyet values are obtained from Steps 4 and 5 of the decision tree. After the rainfall values are determined, the shape of these isohyets are drawn according to the following guidelines:

   a. Isohyets of ≥ 0.25 inch/half hour associated with cold, expanding thunderstorm anvils are concentrated in 10 mi or less

Figure C1. D/RADEX intensity values for 0036 GMT superimposed on enhanced infrared imagery (MB curve), 0030 GMT, July 20, 1977.

width. High-resolution visible imagery is the best product for pinpointing the area of heaviest rainfall.

b. Isohyets associated with overshooting tops cover an area about 5 mi in diameter or less.

c. Isohyets associated with mergers cover a larger area than that for single cells.

d. Isohyets must take into account the half-hourly movement of the thunderstorms.

3. Draw additional isohyets at 0.50-in intervals to supplement the 0.05-in isohyet and the isohyet associated with the area of heaviest rainfall. As noted above, the heavy rain is usually spread over an area less than 10 mi wide.

4. Displace the estimate to properly adjust the apparent satellite cloud position to the actual cloud position (NOAA, 1977).

This modified Scofield/Oliver technique was used to produce all the satellite-derived isohyetal analyses in this report. To demonstrate the modified technique, rainfall estimates were produced for two half-hour periods, 0000 to 0030 and 0030 to 0100 GMT. The scheme is most accurate when both visible and IR data are used in the analyses but only IR data were available.

In the figures Johnstown is indicated by JST. The "stars" on these pictures represent those stations that produced hourly rainfall observations during the Johnstown rainstorm.

The largest concentration of heavy rain was located by superimposing D/RADEX "VIP" intensity values for 0036 GMT, 20 July, on the 0300 GMT enhanced IR picture in Fig. C1. These intensity values represented the maximum VIP echo within the 125-nmi D/RADEX range and for a grid box of 3 nmi east-west by 5 nmi north-south.

The Johnstown storm occurred in a weak vertical wind shear environment. A thunderstorm anvil in such an environment characteristically expands radially from the active cells. As a result, that portion of the thunderstorm shown by the G's in Fig. C2 possesses a fairly uniform temperature gradient around the thunderstorm anvil. For this reason, the heaviest rainfall was expected near the center of the thunderstorm system where the tops were the highest (coldest). In this instance, the coldest tops (Fig. C2) were located just south of the cloud system center. In Fig. C1, D/RADEX intensity values of 3 (1.5 in of rain per hour) or greater were clustered near the

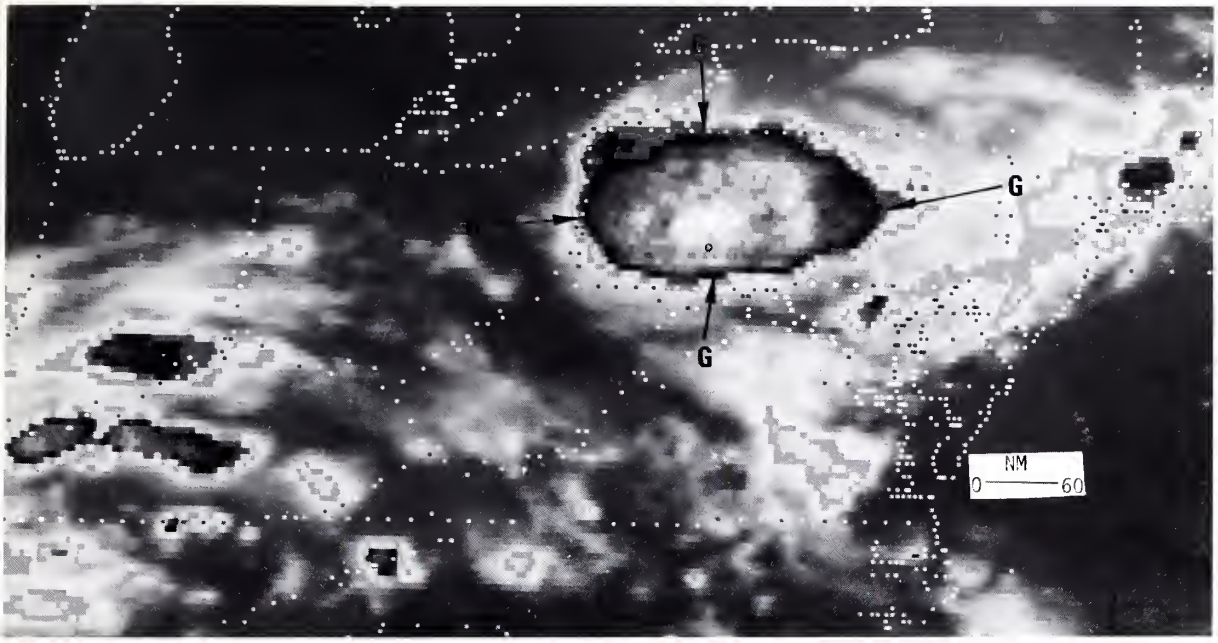

Figure C2. Enhanced infrared imagery (MB curve), 0030 GMT, July 20, 1977 (large-scale coverage).

coldest tops between C and D. By 0030 GMT, the heaviest rainfall was observed in this cluster just north of Johnstown (JST).

Half-hour rainfall estimates were produced using the IR pictures in Figs. C3, C4, and C7.

In the pictures between 0000 GMT and 0030 GMT, the following features are observed. At 0030 GMT (Fig. C4), a rapidly expanding thunderstorm ($>1/3°$ but $\leq 2/3°$ latitude) embedded within the anvil is encircled by a dashed line between C and D. Within this expanding thunderstorm are two high tops at O and T. The D/RADEX "Tops Map" at 0036 GMT in Fig. C5 shows the tops at O and T to be the highest, ranging from 50,000 to 55,000 ft. Other slowly growing ($<1/3°$ latitude) high tops are observed at I, L, K, and Z. These features are evaluated in the 0000 to 0030 estimated isohyetal analysis in Fig. C6. Isohyets of 0.05, 0.25, 0.50, 1.00, and 1.25 inches are shown.

From comparing the pictures between 0030 GMT (Fig. C4) and 0100 GMT (Fig. C7), the following features are observed. The thunderstorms that rapidly expanded at 0030 GMT, indicated by a dashed line between C and D, diminish in size by 0100 GMT; however, the portion of the storm encircled by a dashed line remains quite cold in Fig. C7. Other high tops at 0100 GMT that either expanded or persisted between 0030 and 0100 GMT are located at I, S, R, E, P, U, and V. These features are evaluated in the 0030 to 0100 GMT estimated isohyetal analysis in Fig. C8. The half-inch isohyets in Fig. C8 are due to high tops that appeared to persist over the same area for the 30-min period. However, the half-inch estimate at R is a high top that rapidly expanded $>1/3°$ but $\leq 2/3°$ latitude during the 30-min period.

In these enhanced IR pictures between 0000 and 0100 GMT, overshooting tops were indicated by a patchwork pattern of cold and warm spots in the anvil, which had little or no continuity in the 30-min interval pictures.

Results and conclusions from using the Scofield/Oliver technique on the Johnstown rainstorm are documented in detail by Scofield (1978).

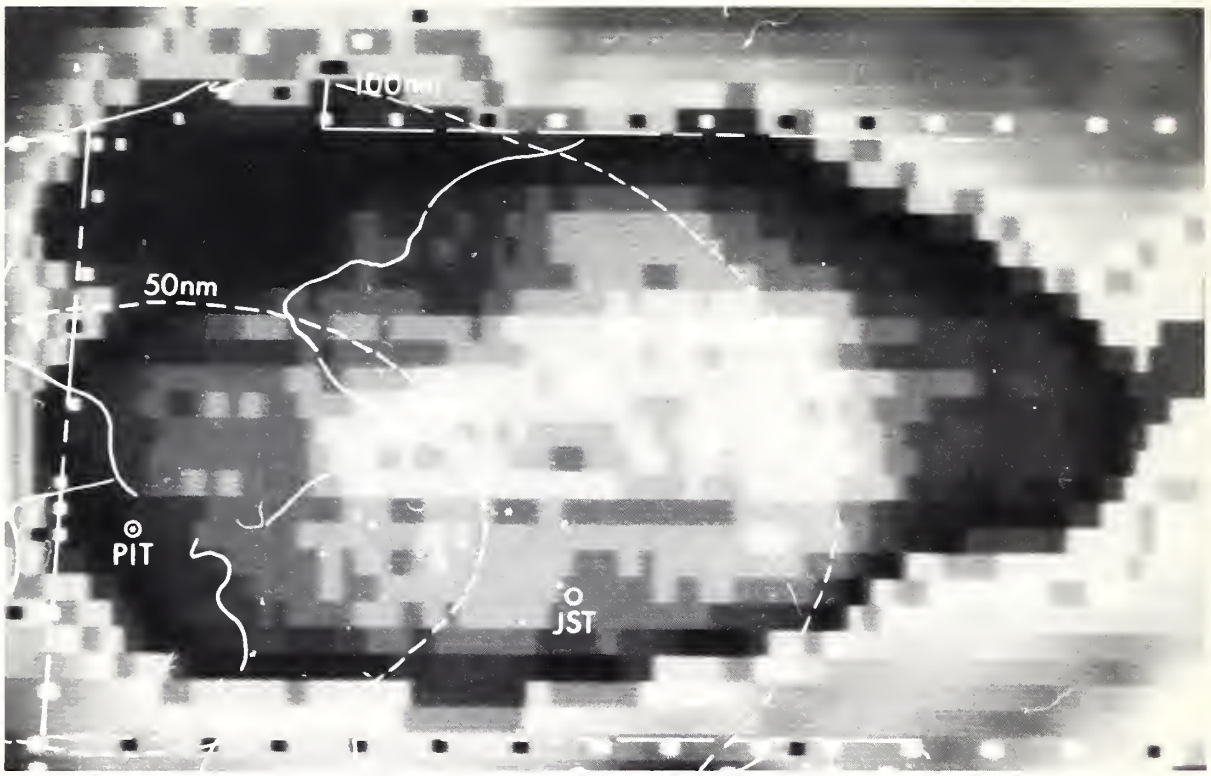

Figure C3. Enhanced infrared imagery (MB curve), 0000 GMT, July 20, 1977.

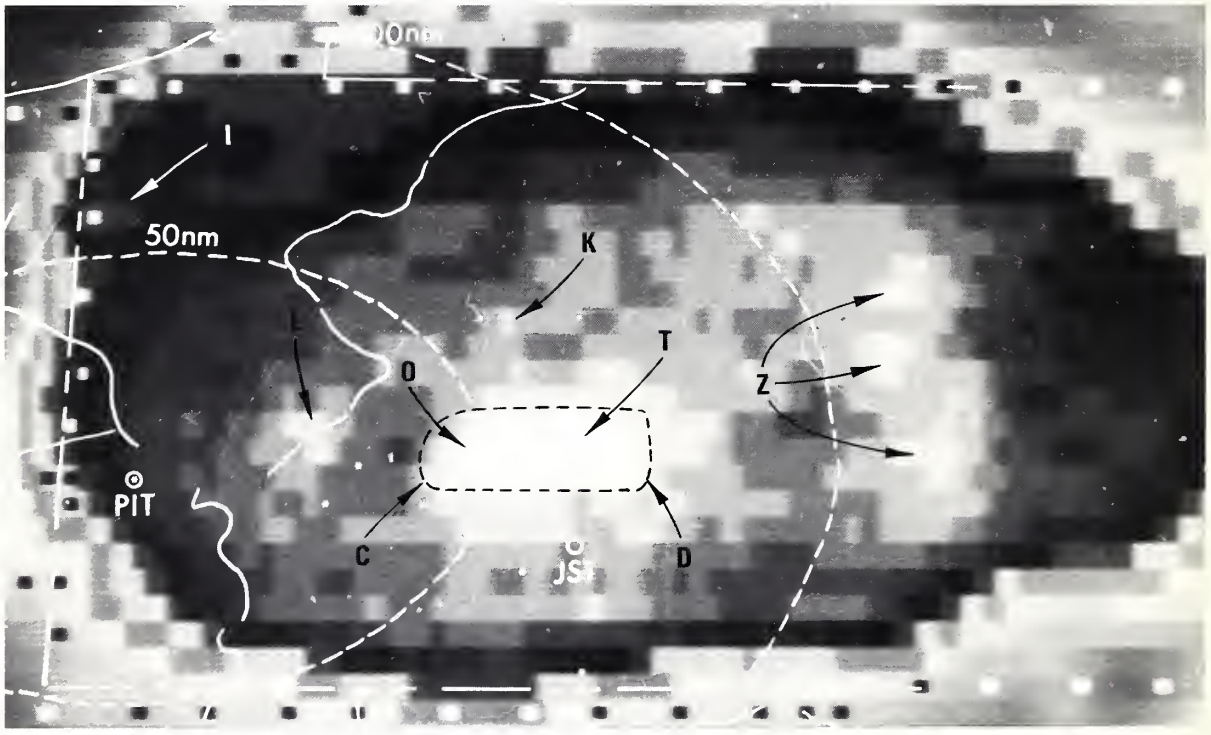

Figure C4. Enhanced infrared imagery (MB curve), 0030 GMT, July 20, 1977.

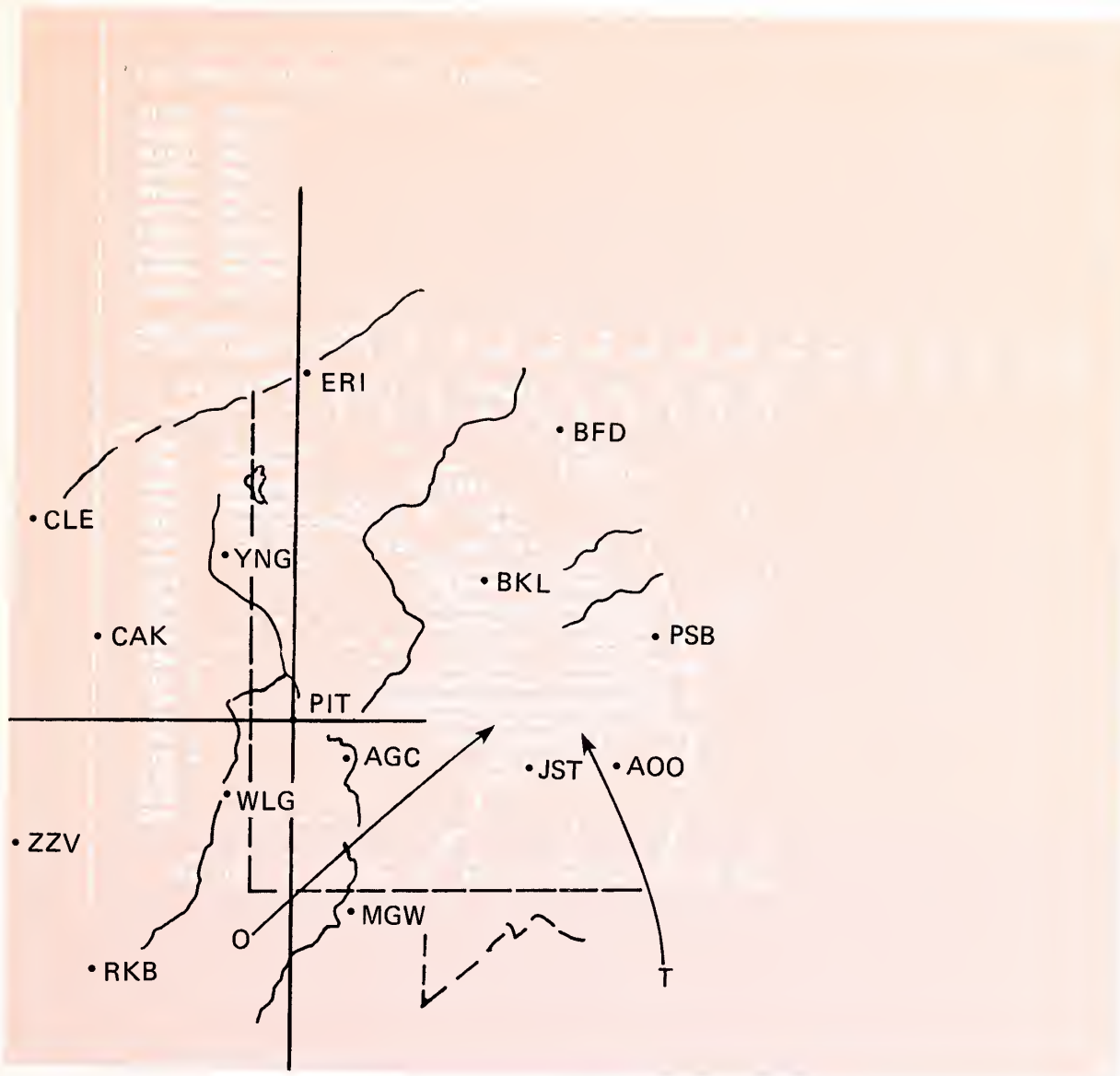

Figure C5. D/RADEX tops map, 0036 GMT, July 20, 1977.

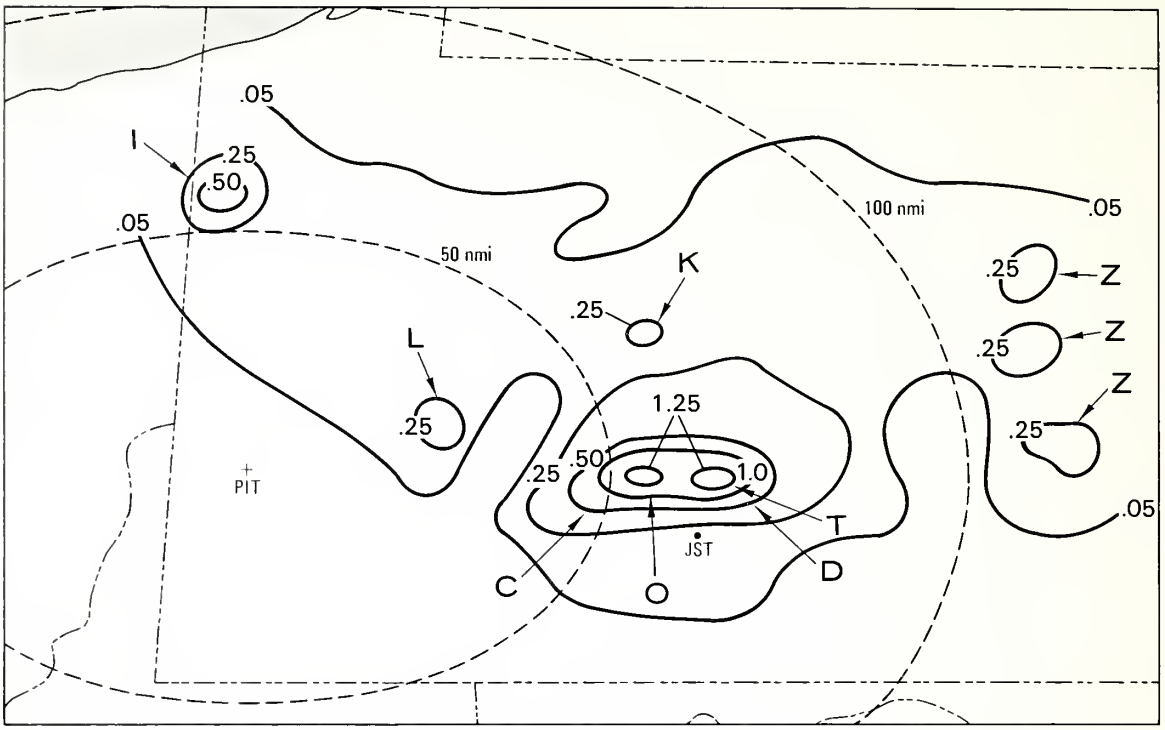

Figure C6. Satellite-derived isohyet analysis in inches, 0000 to 0030 GMT, July 20, 1977.

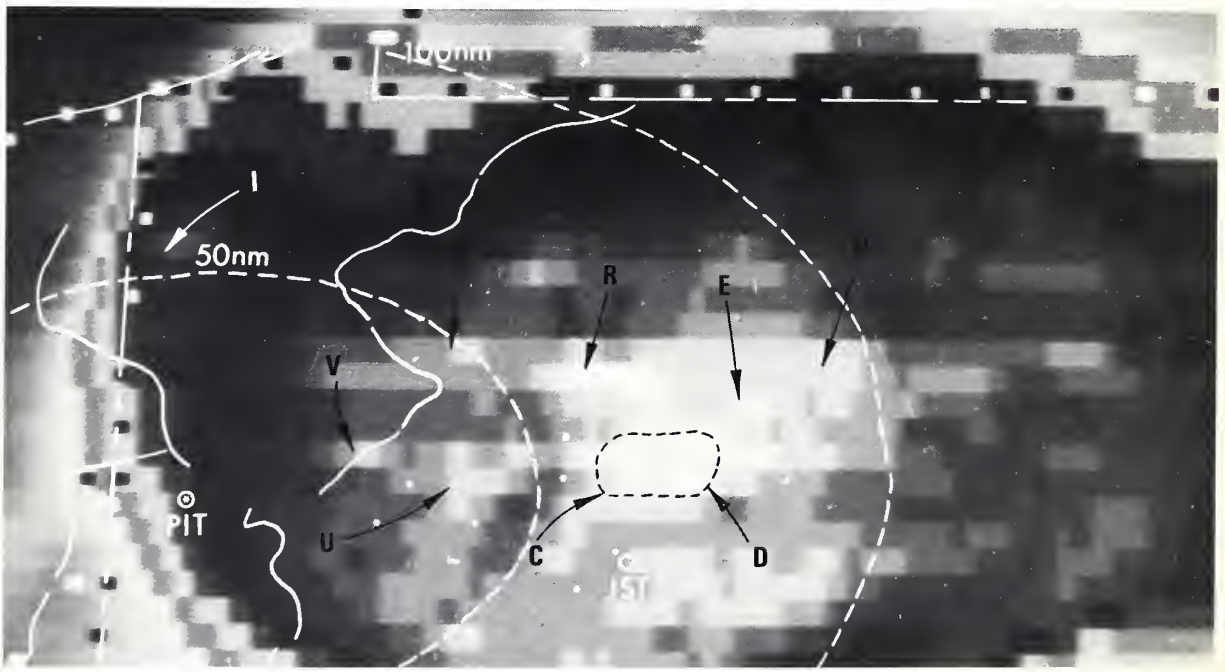

Figure C7. Enhanced infrared imagery (MB curve), 0100 GMT, July 20, 1977.

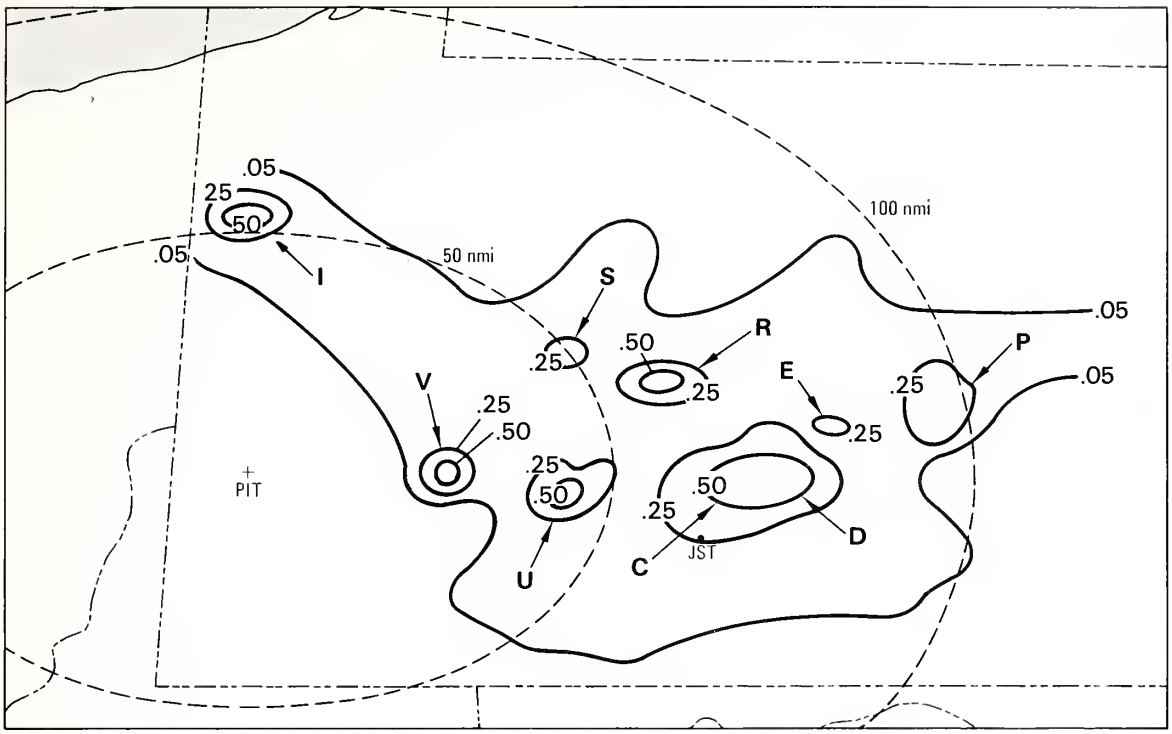

Figure C8. Satellite-derived isohyet analysis in inches, 0030 to 0100 GMT, July 20, 1977.

APPENDIX C REFERENCES

NOAA, 1977. Displacement error of satellite cloud tops. NWS Central Region Tech. Attach. No. 77-G4, 3 pp.

Scofield, Roderick A., and V. J. Oliver, 1977a. A scheme for estimating convective rainfall from satellite imagery. NOAA-NESS Tech. Memorandum 86, U.S. Depart. of Commerce, Washington, D.C., 47 pp.

Scofield, Roderick A., and V. J. Oliver, 1977b. Using satellite imagery to estimate rainfall from two types of convective systems. Preprints, Tenth Tech. Conf. on Hurricanes and Tropical Meteorology, Am. Meteor. Soc., Boston, Mass., 204-211.

Scofield, Roderick A., 1978. Using satellite imagery to estimate rainfall during the Johnstown rainstorm. Preprints, Conf. on Flash Floods: Hydrometeorological Aspects, Am. Meteor. Soc., Boston, Mass., 181-189.

PENN STATE UNIVERSITY LIBRARIES
A00007202194l